



## LADEE Reverse Engineering Study

### Final Report

Team 30

P. Code	Surname	Name
11071875	Bacconnier	Marc
10790352	Cocomazzi	Marco
10767560	Colombo	Andrea
10773170	Coppola	Riccardo
10797598	Domenichelli	Eleonora
11093867	Pezzi	Francesco

Space System Engineering and Operations

Prof: M. Lavagna

L. Bianchi, M. Bussolino

*M.Sc Space Engineering  
A.Y. 2024-2025*

Change log	
Issue	Comments
§ 2.2	Added information on the orbital parameters. Added tables in figures 3 and 4; figure 5 revised.
§ 3.2.2	Added or rewritten information with clarification and comments.
§ 3.2.3	Modified line 1. Clarified analysis of the Pressure Regulated to Blow-down switch referring to what, how and why it is performed.
§ 3.3.1	Further clarified assumption to mathematical model, separation between OCS and RCS mode and margins. Furthermore, a tidier look at formula has been achieved.
§ 3.3.2	Increased justification and strengthened hypothesis over mathematical formulation. Modified formulas for $M_{gas}$ .
§ 3.3.3	Sentence moved from elsewhere. Corrected some formulations.
§ 3.4	Organized numerical results in 3 groups: input miscellaneous data, relative to values retrieved from literature; Mass Data, relative to the Masses data and results of the subsystem; and Volume Data, relative to volumes of the subsystem, thus referring to tanks, and their masses. Added critical comments on results, referring to true mission values.
§ 3.5	Moved Mass budget in this section. Minor changes in the text.
§ 6.1.1	Minor information removal.
§ 6.1.2	Minor information removal.
§ 6.2.1	Switched section position with Sec. 6.2.2. Clarifying sentence for introducing table 23. Reorganized the overall paragraph, highlighting the rationale of each different section.
§ 6.3.2	Rewritten section to remove detailed subsystem consumption list, focusing instead on the meaning of reported values and worst-case scenarios.
§ 6.3.3	Added explicit steady-state assumption at the beginning of the analysis for clarity. Added justification for neglecting Earth radiation and clarified solar flux assumptions for Moon orbit. Expanded hot case explanation: added clear description of flux balance, view factors, and reasons for infeasible radiator area. Clarified radiator modelling assumptions using LADEE architecture. Expanded cold case explanation: clarified why SSM during eclipse is the true cold case, detailed power balance methodology, and heater sizing approach. Added explicit numerical results for predicted cold-case temperature and heater power requirement, noting infeasibility and reasons.

Change log	
<i>Issue</i>	<i>Comments</i>
§ 6.3.4	<p>Rewritten introduction to justify the transition to a multi-node analysis for increased accuracy. Added explicit geometrical modelling assumptions. Detailed the transient thermal balance equation with clear definitions for each additional term, including net internal radiative exchange with view factors and conductive coupling between adjacent nodes. Clarified that incident angles are dynamically updated during simulation to capture Sun, Moon, and deep space orientations, including eclipses, for each face.</p> <p>Expanded the hot case section with a clear explanation of the simulation methodology, the spacecraft's rotational assumptions, and interpretation of periodic thermal profiles across orbits. Described radiator modelling: iterative sizing process, explicit value of implemented radiator area, rationale for decoupling radiators from lateral faces per LADEE architecture. Added explicit numerical results for maximum and minimum temperatures recorded during the hot case.</p> <p>Expanded the cold case section with clear numerical results for the minimum and maximum temperatures, the required heater power, and its infeasibility due to power constraints.</p>

## Contents

<b>1 Mission Objectives and Premises</b>	<b>1</b>
1.1 Mission High Level Goals . . . . .	1
1.2 Functional Analysis and Requirements . . . . .	1
1.2.1 Functional Analysis . . . . .	1
1.3 Mission Requirements . . . . .	2
1.3.1 Mission Scientific Requirements . . . . .	2
1.3.2 Mission Requirements . . . . .	2
1.3.3 Mission Important Aspects . . . . .	3
1.4 Mission Phases . . . . .	3
1.5 Conceptual Operations . . . . .	4
1.6 On Board Scientific Instrumentation . . . . .	4
1.6.1 Payloads - Goals correlation . . . . .	5
1.6.2 Payloads - ConOps/Phases correlation . . . . .	5
1.7 Preliminary Mission Analysis . . . . .	5
1.7.1 LEOP and Transfer phases . . . . .	6
1.7.2 Lunar Orbit Acquisition phase (LOA) . . . . .	6
1.7.3 Commissioning and Science phases . . . . .	6
1.7.4 Disposal phase . . . . .	6
<b>2 Mission Analysis</b>	<b>7</b>
2.1 Trajectory design and functionalities . . . . .	7
2.2 Costs reconstruction . . . . .	7
<b>3 Propulsion Subsystem (PS)</b>	<b>9</b>
3.1 Propulsion system functionalities and phases . . . . .	9
3.2 Subsystem Architecture . . . . .	9
3.2.1 Thruster selection and configuration . . . . .	9
3.2.2 Pressurant, Oxidizer, Fuel and Tanks description . . . . .	9
3.2.3 Subsystem architecture . . . . .	10
3.3 Subsystem Sizing . . . . .	11
3.3.1 Mission masses and volumes . . . . .	11
3.3.2 Pressurant sizing . . . . .	12
3.3.3 Tank sizing . . . . .	12
3.4 Sizing Results . . . . .	13
3.5 Mass and Power budget . . . . .	13
<b>4 Telemetry &amp; Telecommand (TMTC)</b>	<b>14</b>
4.1 Subsystem Architecture . . . . .	14
4.2 Ground Segment Network Selection . . . . .	14
4.3 Design Rationale . . . . .	15
4.3.1 Antennas Configuration . . . . .	15
4.3.2 Ground Stations . . . . .	15
4.3.3 Frequency and Band . . . . .	16
4.4 Communications during Phases . . . . .	16
4.5 Communications during Modes . . . . .	17
4.6 Subsystem sizing . . . . .	17
4.7 Sizing results . . . . .	19
4.8 Power budget . . . . .	19

<b>5 Attitude Orbit Control System (AOCS)</b>	<b>20</b>
5.1 Subsystem architecture . . . . .	20
5.1.1 Sensors . . . . .	20
5.1.2 Actuators . . . . .	20
5.2 Attitude Orbit Control System (AOCS) architecture rationale . . . . .	21
5.2.1 Sensors rationale . . . . .	21
5.2.2 Actuators rationale . . . . .	21
5.3 Attitude Orbit Control System (AOCS) Modes . . . . .	21
5.4 Sensors and Actuators per Mode . . . . .	22
5.5 Pointing Budget . . . . .	23
5.6 Subsystem sizing . . . . .	24
5.6.1 Disturbances Evaluation . . . . .	24
5.6.2 Reaction Wheels sizing: slew . . . . .	25
5.6.3 Thruster sizing: slew . . . . .	25
5.6.4 Slew manoeuvres: Data and Results . . . . .	25
5.6.5 Propellant Mass Sizing: Desaturation with Thrusters . . . . .	25
5.7 AOCS Mass, Power and Data budgets . . . . .	26
<b>6 Thermal Control Subsystem (TCS)</b>	<b>27</b>
6.1 Subsystem Architecture . . . . .	27
6.1.1 LADEE Thermal Passive Control . . . . .	27
6.1.2 LADEE Thermal Active Control . . . . .	27
6.2 Subsystem Design Rationale . . . . .	28
6.2.1 Thermal Control Subsystem (TCS) Architecture Rationale . . . . .	28
6.2.2 Thermal Control and Mission Environment per Phase . . . . .	28
6.2.3 Thermal Control per Mode . . . . .	29
6.3 Subsystem Sizing . . . . .	29
6.3.1 Identification of Survival Thermal Ranges . . . . .	29
6.3.2 Internal Power Dissipated per Mode . . . . .	29
6.3.3 Mono-nodal analysis . . . . .	30
6.3.4 Multi-node analysis . . . . .	30
6.4 Mass, Power and Data budget . . . . .	32
<b>7 Electric Power Subsystem (EPS)</b>	<b>33</b>
7.1 Architecture . . . . .	33
7.2 Subsystem Rationale . . . . .	34
7.3 Power per Phase and Mode . . . . .	34
7.4 Operational Profiles and Available Sources . . . . .	35
7.5 Subsystem Sizing . . . . .	35
7.5.1 Average Power per Mode . . . . .	35
7.5.2 Solar Panels Sizing . . . . .	36
7.5.3 Battery Sizing . . . . .	37
7.6 Sizing results . . . . .	38
7.7 Mass, Power and Data budgets . . . . .	38
<b>8 On Board Data Handling (OBDH)</b>	<b>39</b>
8.1 OBDH Architecture and Rationale . . . . .	39
8.2 OBDH Sizing . . . . .	41

<b>9 LADEE Structure</b>	<b>44</b>
9.1 Primary Structure . . . . .	44
9.2 Secondary structure . . . . .	44
9.3 Tertiary structure . . . . .	45
9.4 Subsystem mass . . . . .	45
9.5 Launcher interface and limitations . . . . .	45
<b>10 LADEE Configuration</b>	<b>46</b>
10.1 External Components Configuration . . . . .	46
10.2 Internal Components Configuration . . . . .	47
<b>11 Mass Budget</b>	<b>48</b>
11.1 Values found in literature . . . . .	48
11.2 Values computed from reverse engineering . . . . .	49
11.3 Comments . . . . .	50

## Acronyms

**ΔHM** Delta-H Mode

**ΔVM** Delta-V Mode

**ADC** Analog to Digital Converter

**AKE** Absolute Knowledge Error

**AMOAB** Analog Multi Operations Avionics Board

**AOCS** Attitude Orbit Control System

**APE** Absolute Performance Error

**BC** Battery Cell

**BD** Blowdown

**BOL** Beginning of Life

**C&DH** Command and Data Handling

**COM** Center of Mass

**COTS** Commercial Off-The-Shelf

**CPU** Central Processing Unit

**CSS** Coarse Sun Sensor

**DACs** Digital-to-Analog Converters

**DET** Direct Energy Transfer

**DMOAB** Digital Multi Operations Avionics Board

**DoD** Depth of Discharge

**DSN** Deep Space Network

**ECSS** European Cooperation for Space Standardization

**EEPROM** Electrically Erasable PROM

**EOL** End of Life

**EPS** Electric Power Subsystem

**ESAD** Electronic Safe and Arm Devices

**FDV** Feed and drain valves

**FIFO** First In First Out

**FOV** Field of View

**FPC** Fine Pointing Control

**FPGA** Field Programmable Gate Array

**FSW** Flight Software

**GG** Gravity Gradient

**HiPAT** High Performance Apogee Thruster

**IAU** Integrated Avionics Unit

**IMU** Inertial Measurement Unit

**IR** Infrared

**LADEE** Lunar Atmosphere and Dust Environment Explorer

**LDEX** Lunar Dust Experiment

**LEOP** Launch and Early Orbit Phase

**LGA** Low Gain Antenna

**LLCD** Lunar Laser Communication Demonstration

**LOA** Lunar Orbit Acquisition

**LOI1** Lunar Orbit Insertion 1

**LOI2** Lunar Orbit Insertion 2

**LOI3** Lunar Orbit Insertion 3

**LV** Latch valves

**MCSB** Modular Common Spacecraft Bus

**MEMS** Micro-Electro Mechanical System

**MGA** Medium Gain Antenna

**MLI** Multi-Layer Insulation

**MMH** Monomethylhydrazine  $CH_6N_2$

**MOAB** Multi Operations Avionics Board

**NASA** National Aeronautics and Space Administration

**NEN** Near Earth Network

**NMS** Neutral Mass Spectrometer

**NOM** Nominal Operating Mode

**NTO** Dinitrogen Tetroxide  $N_2O_4$

**OBC** On Board Computer

**OBDH** On Board Data Handling

**OCS** Orbit Control System

**OF** Oxidizer to Fuel Ratio

**OLM3** Orbit Lowering Manoeuvre 3

**OLM4** Orbit Lowering Manoeuvre 4

**OMMs** Orbit Maintenance Manoeuvres

**P/L** Payload

**PAF** Payload Attach Fitting

**PAM** Payload Adapter Module

**PAPI** Power-switching and Pyro Integration

**PCI** Peripheral Component Interconnect

**PM1** Perigee Manoeuvre 1

**PM2** Perigee Manoeuvre 2

**PMD** Propellant Management Device

**PMs** Perigee Manoeuvres

**PR** Pressure Regulated

**PROM** Programmable ROM

**PS** Propulsion Subsystem

**PT** Pressure Transducers

**PV** Pyro valves

**RAM** Random Acces Memory

**RCS** Reaction Control System

**RF** Radio Frequency

**RRM** Rate-Reduction Mode

**RW** Reaction Wheel

**RWs** Reaction Wheels

**S/C** Spacecraft

**SA** Solar Array

**SACI** Solar Array and Charge control Interface

**SBC** Single Board Computer

**SCaN** Space Communication and Navigation

**SECDED** Single-Error Correct Double-Error Detect

**SN** Space Network

**SNR** Signal to Noise Ratio

**SPG** Single Point Ground

**SRAM** Static Random Acces Memory (RAM)

**SRP** Solar Radiation Pressure

**SSM** Sun Safe Mode

**STA** Star Tracker Assembly

**SW** Software

**TCM** Telecom Mode

**TCM1** Trajectory Correction Manoeuvre 1

**TCS** Thermal Control Subsystem

**TDRSS** Tracking & Data Relay Satellite System

**TEC** Thermoelectric Cooler

**TMTTC** Telemetry & Telecommand

**TPC** Thermal and Power Conditioning Mode

**TS** Temperature Sensor

**ULGA** Upper Low Gain Antenna

**USN** Universal Space Network

**UVS** Ultraviolet Visible Spectrometer

**VDU** Valve Driver Unit

# 1 Mission Objectives and Premises

LADEE was a NASA mission designed to meet the objectives presented in Concept 8 of the Scientific Context for Exploration of the Moon (SCEM) to study the lunar atmosphere and dust prior to significant human activities [1].

## 1.1 Mission High Level Goals

According to the introduction proposed above, the team retrieved information on the formal objectives of the mission from different sources [1] [2] [3], and reported them in Table 1:

Mission High Level Goals:
Determine the composition of the lunar atmosphere and investigate the processes that control its distribution and variability, including sources, sinks, and surface interactions
Characterize the lunar exospheric dust environment and measure any spatial and temporal variability and impacts on the lunar atmosphere
Demonstrate that Lunar Laser Communications Demonstration (LLCD) can operate at high data rates from lunar distances
Create a low-cost reusable spacecraft architecture that can meet the needs of certain planetary science missions
Demonstrate the capability of the Minotaur V as a launch vehicle for planetary missions

Table 1: Mission High Level Goals

## 1.2 Functional Analysis and Requirements

### 1.2.1 Functional Analysis

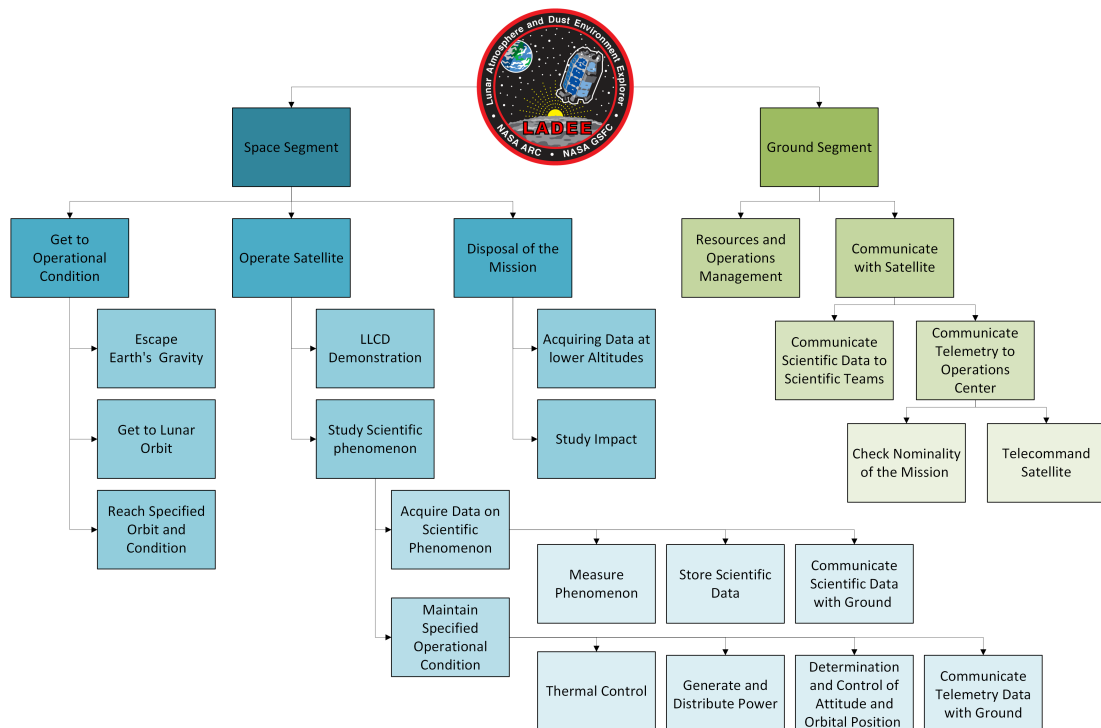


Figure 1: Functional Tree Analysis of LADEE Mission

Considering the mission objectives and most important features, the team was able to build a Functional Tree Analysis, presented in Figure 1. The purpose of the diagram is to ensure a holistic view of the functionalities of the mission.

In the Tree it is possible to identify the strong separation of a Space Segment, composed of the Satellite and Launcher, and a Ground Segment, referring to any operation or functionality conducted from Earth, up to the project management of the resources and finances, highlighted in the *Resources and Operations Management*.

The Space Segment shows more in depth analysed child technical functions, where each of the lowest levels can be especially linked to a very restricted number of subsystems of the spacecraft.

### 1.3 Mission Requirements

#### 1.3.1 Mission Scientific Requirements

The Scientific requirements of the mission are presented in Table 2. These requirements drove the choice of the instrumentation discussed in section 1.6:

Scientific Requirements
<i>Measure the relevant spatial and temporal variations of Ar, He, Na, and K. [...]</i>
<i>Detect or establish new limits for selected other species for which previous detections have been attempted. [...]</i>
<i>Perform a survey for the presence of other species beyond those listed above, or positive ambient ions of these species and other atoms or compounds, within a mass range of 2 – 150 Da and a sensitivity of several particles/cc</i>
<i>Detect or set new limits for the spatial and size distribution of atmospheric dust over an altitude range from 3 km up to 50 km, with a height resolution of 3 km, at a minimum detectable density of <math>10^{-4}</math> grains/cc, for grains from 100 nanometres to at least 1 micrometer in radius. [...]</i>

Table 2: Scientific Requirements retrieved from [4]

The first three requirements focus on establishing boundaries for analysing both gasses previously identified in past missions and potential new gasses within a specific mass range, which includes volatiles and refractory elements, while excluding heavier molecules unlikely to be present in the tenuous lunar exosphere. The fourth requirement sets specific thresholds for dust analysis, using constraints derived from previous mission data, to resolve uncertainties about the lunar dust environment and its sources.

#### 1.3.2 Mission Requirements

The team considered some of the requirements as more meaningful to the significance of the mission, here reported:

Requirement ID	Requirement
LFD02	<i>The trans-lunar trajectory shall be consistent with the capabilities of the Minotaur V launching from the Wallops Flight Facility [...]</i>
LFD09	<i>The LADEE lunar orbit shall be retrograde with an inclination of 155°-180°</i>
LFD11	<i>The lunar Science orbit shall result in a minimum of 600 sunrise terminator crossings with altitudes of 50 km or less</i>
LFD15	<i>The Science Phase Orbit shall have apoapsis altitudes below 150 km</i>
LFD16	<i>The Science Phase Orbit design shall maintain an altitude that can accommodate at least 4 days of decay time before impact with the lunar surface</i>

Table 3: Requirements retrieved from [5]

### 1.3.3 Mission Important Aspects

The team determined that there's no such a parameter which would size much of the mission on its own, and thus no driver was considered. However, the team recognized some of the most important aspects of the mission, which affect many subsystems:

- Due to the use of Minotaur V as the designated launcher, the first requirement, **LFD02**, necessitates the design of a trajectory compatible with its capabilities. This requirement highlights the Minotaur V's inability to provide a sufficient single impulse to insert LADEE into lunar orbit. Furthermore, given the launcher's uncertain performance, the trajectory must account for potential variations.
- Requirements **LFD09**, **LFDD11** and **LFD15** derive from the need for scientific instruments that analyse the Lunar exosphere to have a close approach to dust and particles. This imposes the need for a low altitude orbit, with special interest in sunrise terminator crossings, where the scientific phenomena are amplified and more frequent. **LFD09** imposes a retrograde orbit. This is related to instrumentation discussed in sec. 1.7.3.
- Furthermore, it is important to note that, although the mission design was intended to rely on high-TRL technologies, the LADEE mission featured several firsts. As with **LFD02**, LADEE was the first mission to launch from Wallops Flight Facility, the first and only mission to use the Minotaur V launcher, and the first mission to utilize the MCSB platform. This seems contradictory, but the team came to the conclusion that all these firsts were related to the relatively low budget of the mission. As in fact, Minotaur V predecessor, Minotaur IV, had already performed successfully some launches and was a low-cost LEO launcher. MCSB (Modular Common Spacecraft Bus) was again on a first mission but was already flight tested and built to be flown in many different missions, using modularity to minimize costs.
- Furthermore, from the team's perspective **radiation and thermal control** and **telecommunications** are critical factors. The absence of atmosphere and low surface albedo pose the satellite under serious variations in temperature and the effect of external radiations. Eclipses will instead cause interruptions in continuous communications with Earth.

### 1.4 Mission Phases

As proposed in Ref.[3], the mission is structured into distinct phases, each designed to ensure a transition from launch to the achievement of scientific objectives:

1. **Pre-Launch Phase:** the spacecraft is integrated with the launch vehicle, undergoing final system checks and configuration. All pre-flight procedures are completed to ensure mission readiness before liftoff.
2. **Launch and Early Orbit Phase (LEOP):** the mission begins with the launch, placing the spacecraft into an initial trajectory. Following separation, the spacecraft activates its systems, verifies their status, and transitions from a protective mode to operational pointing. This phase includes initial tracking and determination of the achieved trajectory.
3. **Transfer Phase:** the spacecraft follows a trajectory leading to the Moon, with planned manoeuvres to adjust its path and optimize arrival conditions. During this phase, periodic checks ensure all onboard systems are functioning correctly, and any necessary adjustments are performed.
4. **Lunar Orbit Acquisition (LOA) Phase:** upon arrival at the Moon, the spacecraft executes a sequence of manoeuvres to gradually be captured by Moon and establish an orbit suitable for the following phase.

5. **Commissioning Phase:** the spacecraft undergoes an extensive system verification process. This includes checks of power, thermal, and attitude control systems, as well as verification of operational capabilities. Functional tests of the payload and communication systems are conducted to confirm readiness for scientific operations. Additionally, this phase includes the demonstration of the Lunar Laser Communications Demonstration (LLCD), a key mission objective aimed at testing high-data-rate optical communication.
6. **Science Phase:** the spacecraft carries out its primary mission objectives, collecting and transmitting data while maintaining its operational orbit. Routine maintenance, health checks, and necessary orbit adjustments are performed to support continuous data collection.
7. **Disposal Phase:** a controlled deorbit sequence is executed to ensure a predictable conclusion. Post-mission activities include final data transmission, system shutdown procedures, and documentation of mission results.

It is worth noting that an Extended Science Phase was later introduced due to efficient propellant usage, allowing additional low-altitude observations. However, since this phase was not part of the original mission design, it has not been included in the classification above.

## 1.5 Conceptual Operations

Figure 2 shows the Conceptual Operations of the mission, depicting the relationship between phases, modes and operations along a timeline.

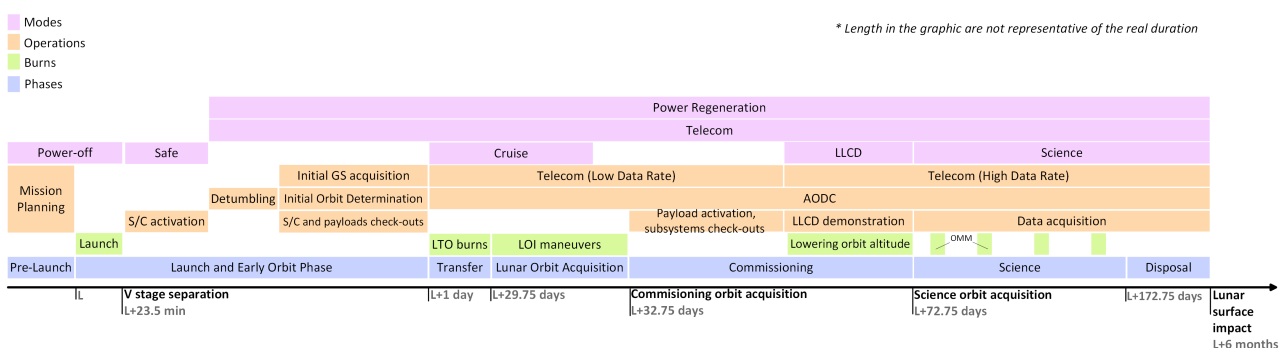


Figure 2: ConOps of the LADEE mission

The team decided to focus on understanding the general concept of the mission without providing an in-depth analysis of specific solutions, which will be thoroughly explored in later sections.

It is worth noting that while different modes appear overlapped in the graph, in the actual mission they will alternate. As proposed in Ref. [6], different modes are repeated during the day. For instance, during the science phase, a possible alternation can be instruments mode, Telecom mode with Earth-pointing configuration, power regeneration, followed by a return to science mode.

## 1.6 On Board Scientific Instrumentation

The LADEE's science payload suite was equipped with four different instruments, each of which had a specific and crucial role for the mission success in terms of goal achievement.

- **Neutral Mass Spectrometer (NMS):** The NMS is able to measure the mass distribution of neutral species in the lunar exosphere with a mass between 2-150 Daltons. It operates ionizing exospheric gases through electron impact and then determining their masses at unit mass resolution with a quadrupole mass filter. It can also work in a non-ionizing mode to detect ambient ions.

- **Ultraviolet Visible Spectrometer (UVS):** The UVS is a point spectrograph operating in the wavelength range of 230–810 nm. It employs two optical apertures to observe the exosphere at altitudes and local times above the surface. It also takes solar occultation measurements in the lunar sunrise terminator. The two optical elements are a spectrometer with command/telemetry I/O and data handling, optical fibers, an integrated thermal and mechanical structure, and one deployment door aperture. It complemented the NMS, as the two instruments analysed different gases.
- **Lunar Dust Experiment (LDEX):** LDEX is a dust detector by impact ionization capable of detecting micron and submicron size particles. When a dust particle hits a big hemispherical target, it forms an electron and ion cloud pair. These are focused and accelerated by an electric field before detection using a micro-channel plate.
- **Lunar Laser Communication Demonstration (LLCD):** LLCD was a technology demonstration that proved the utility of high-bandwidth optical communication from distant space. It encompassed the Lunar Laser Space Terminal and White Sands, NM-based Lunar Laser Ground Terminals.

#### 1.6.1 Payloads - Goals correlation

The instruments were designed to fulfil the mission goals proposed for the mission as shown in Table 4.

Mission Goals	Payloads
Determine the composition of the lunar atmosphere and investigate the processes that control its distribution and variability, including sources, sinks, and surface interactions;	NMS - UVS
Characterize the lunar exospheric dust environment and measure any spatial and temporal variability and impacts on the lunar atmosphere.	UVS - LDEX
Demonstrate that Lunar Laser Com Demonstration (LLCD) LLCD can operate at high data rates from lunar distances.	LLCD

Table 4: Payload and Goals

#### 1.6.2 Payloads - ConOps/Phases correlation

To properly achieve the mission goals the operations of the instrumentation is specified for each of the mission phases. The activities of each payload are summarized in Table 5.

Payload	LEOP and Transfer	LOA	Commissioning	Science
UVS	-	-	<i>Checkout</i>	<i>Operating</i>
NMS	-	-	<i>Checkout</i>	<i>Operating</i>
LDEX	-	-	<i>Checkout</i>	<i>Operating</i>
LLCD	<i>Checkout</i>	-	<i>Demonstration</i>	-

Table 5: Payload operations and Phases

The three primary instruments on board operate during the science phase, when the spacecraft is in the operational orbit. Because of particular attitude and energy constraints UVS and NMS can't operate at the same instants, so an operations plan is defined to alternate their activities on a "per-orbit" basis, actuating at each revolution around the Moon only one of the two payloads.

### 1.7 Preliminary Mission Analysis

This section provides an overview of the trajectory design and the correlations between the mission analysis choices and each of the phases of the mission.

### 1.7.1 LEOP and Transfer phases

Launch transfers LADEE from the Wallops Flight Facility in a Low Earth Orbit, with the aim of activating the spacecraft and performing a first check-out of the instrumentation and with the high-level goal to demonstrate the effectiveness of the Minotaur V launcher, as presented in section 1.1.

Successively, the trajectory design objective is to reach the Moon and be captured by its gravity with reduced burn losses and with enough flexibility to compensate the potentially large dispersions of the launch vehicle. Hence, a phasing loop trajectory consisting of three Perigee Manoeuvres (PMs) is preferred to a direct transfer. With this approach, the apogee can be raised to lunar distance and the intersection of the orbits is phased with the arrival of the Moon, with the second and third loops potentially resizable in response to a wide range of insertion orbits.

### 1.7.2 Lunar Orbit Acquisition phase (LOA)

The successive manoeuvres consist in three Lunar Orbit Insertion (LOI) burns to allow capture into a lunar orbit with limited  $\Delta v$  budget, with a similar reasoning as the Perigee Manoeuvres design. The three burns lower incrementally the apogee until the achievement of the desired commissioning orbit.

### 1.7.3 Commissioning and Science phases

The commissioning orbit is designed to satisfy two important goals: the demonstration of the LLCD technology and a basic check-out of the science payload. The orbit is designed to have an altitude around 250 km, high enough to guarantee reduced gravitational perturbations caused by the Moon, ensuring the stability of the spacecraft while minimizing orbit maintenance manoeuvres, which would complicate the operations in the commissioning phase.

A scientific orbit is also designed to provide correct and meaningful measurements of the lunar exosphere composition and dust environment. Some of the scientific requirements imposed for this objective are the LFD11 and LFD15 presented in table 3, which limit the altitude of the scientific orbit. Furthermore, as expressed in requirement LFD09, the orbit is chosen to be retrograde to minimize the effects of contamination of the measurements due to spacecraft out-gassing on the NMS at the sunrise terminator, a key region of the exosphere. The inclination requirement between 155°-180° ensures to cover similar ground tracks to increase the statistical significance of the measurements and to maintain a bounded thermal environment for the instruments.

Hence, the commissioning orbit is designed to be a circular retrograde orbit of 250 km altitude and 157° inclination, while the scientific orbit must maintain the apoapsis altitude at or below 150 km and the periapsis altitude at or below 50 km [7]. These characteristics lead to the necessity of propulsive Orbit Maintenance Manoeuvres (OMMs) to maintain the desired scientific operational conditions.

### 1.7.4 Disposal phase

The design of the scientific orbit allows also to execute the disposal by naturally lowering LADEE's altitude, once that the onboard propellant is almost completely consumed. This phase ends with the impact of the spacecraft on the lunar surface, without any specific target point. The impact provided valuable data to study the landing of future missions.

## 2 Mission Analysis

In this section, the team will correlate the trajectory design with functionalities of the mission and  $\Delta v$  budget per each manoeuvre.

### 2.1 Trajectory design and functionalities

Table 6 summarizes the main functionalities of the mission and the design of the trajectories made to achieve them.

Trajectory Feature	Functionality
Phasing loops for lunar transfer	Save fuel and compensate the uncertain launcher performance
Small lunar orbits	Allow more flexibility in the operational timeline
Higher altitude commissioning orbit	Perform commissioning without maintenance manoeuvres
Low altitude scientific orbit	Satisfy the scientific requirements for proper measurements
Retrograde scientific orbit	Preserve measurements from out-gassing of the NMS

Table 6: Orbit design and functionalities

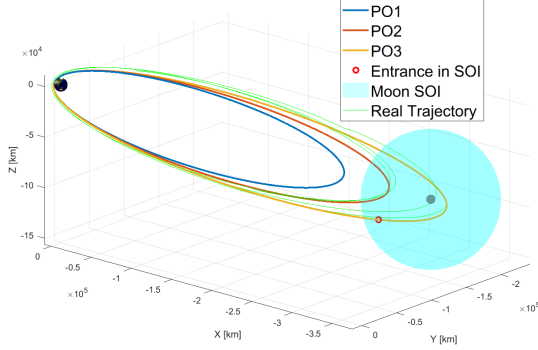
### 2.2 Costs reconstruction

The team proceeded by analysing the  $\Delta v$  reported for the manoeuvres of the real mission [5], comparing them with the cost budget calculated from a simplified simulation of the trajectories. The reconstructed manoeuvres are based on Keplerian orbits, which work accurately under the assumption of a two-body system. The reconstruction focuses on the trajectory changing burns executed by LADEE after its injection by the Minotaur V launcher, hence excluding a small Trajectory Correction Manoeuvre 1 (TCM1). Since these manoeuvres have a deterministic nature, an usual margin of 5% is applied to the total cost.

Manoeuvre	Real cost [m/s]	Reconstruction [m/s]
PM1	16.76	17.13
PM2	17.49	16.15
LOI1	330.50	455.96
LOI2	291.05	293.00
LOI3	244.23	238.49
OLM3	35.43	42.16
OLM4	33.89	31.91
OMMs	101.09	111.42
Total	1070.44	1123.96
Total with margin (+5%)	1123.96	1266.53

Table 7: Real and Reconstructed mission costs

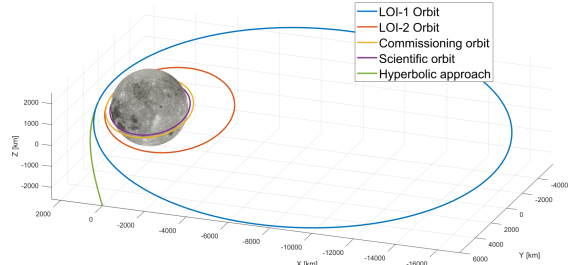
The numerical modelling of the mission is split in two sections. The first part contains the three geocentric phasing orbits used to reach the Moon. After injection the spacecraft is on an elliptical orbit with apogee altitude of 274600 km, then executes burns PM1 and PM2 at the pericentre to increase the apogee up to lunar distance. The reconstruction provides quite accurate results in terms of  $\Delta v$ , meaning that the orbits are precisely described by the Keplerian framework. **The orbital elements and graphical results, compared with actual orbits coming from ephemerides, are reported in figure 3.** The transition between the first and the second part is modelled with the patched conics approach, which leads to some approximation errors because orbits in the Earth and Moon system can be modelled precisely only with a three-body approach. The team decided to use this method anyway to avoid an excessive complexity in the calculations. For this reason Lunar Orbit Insertion 1 (LOI1) is the burn with the greatest variation with respect to the real data, as it is the manoeuvre that executes the transfer from the last phasing orbit to the first lunar orbit. The order of magnitude is still consistent.



	<b>PO1</b>	<b>PO2</b>	<b>PO3</b>
$a$ [km]	143771	166136	194757
$e$ [-]	0.9543	0.9604	0.9663
$i$ [deg]	37.65	37.65	37.65
$\Omega$ [deg]	230	230	230
$\omega$ [deg]	155	155	155

Figure 3: Phasing orbits and orbital parameters of lunar transfer

The second phase consists of the selenocentric segment of the mission. After lunar capture is completed, perigee burns LOI2 and LOI3 lower the orbits until the achievement of the commissioning orbit, circular with 250 km of altitude. A shift between the periapsis of LOI1 and LOI2 can be observed, achieved naturally exploiting the Moon's gravitational perturbations. Finally, OLM3 and OLM4 reduce respectively the perigee and apogee, obtaining the scientific orbit. Similarly to the first part, the model follows quite accurately the real mission costs, because inside the sphere of influence of the Moon the system can be approximated as a two-body problem. Graphical results and orbital elements are reported in figure 4. The elements are defined in a Moon-Centred Inertial frame. Among these, the argument of perigee and the right ascension of the ascending node were not found in literature, so, they were arbitrarily set to zero, as their values do not affect the  $\Delta v$  results due to the manoeuvres being nominally coplanar and co-apsidal.



	<b>LOI1</b>	<b>LOI2</b>	<b>COMM</b>	<b>SCIEN</b>
$a$ [km]	9751	2953	1988	1813
$e$ [-]	0.7512	0.3268	0	0.0138
$i$ [deg]	157	157	157	157
$\Omega$ [deg]	-	-	-	-
$\omega$ [deg]	-	-	-	-

Figure 4: Lunar orbit evolution and corresponding orbital parameters

Finally, a series of Orbit Maintenance Manoeuvres (OMMs) were performed during the Science Phase. GMAT [8] was used during the modelling of OMMs, allowing the inclusion of the harmonics model for the Lunar gravitational field, as well as influence of Earth and SRP, obtaining very similar results. In Fig.5, a time-based comparison of pericentre and apocentre with real data [5] is presented. Both parameters were kept within specific limits.

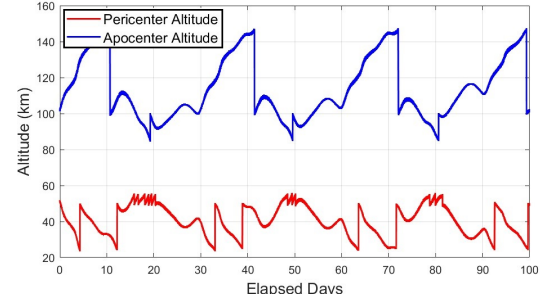
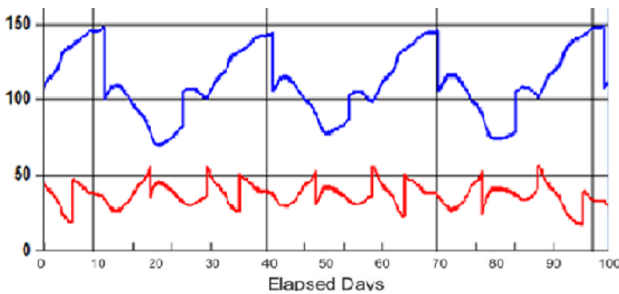


Figure 5: Comparison between real and modelled altitude

### 3 Propulsion Subsystem (PS)

#### 3.1 Propulsion system functionalities and phases

The LADEE propulsion system, as previously explained, was designed to perform orbital manoeuvres and maintain the specified attitude and orbit control during the Science Phase. These two functions were somewhat distinct, as they imposed different quantitative requirements on the propulsion subsystem. Based on this distinction, it can be inferred that the Orbit Control System (OCS) was responsible for executing orbital manoeuvres to place LADEE into its designated lunar orbit. Meanwhile, the Reaction Control System (RCS) was primarily used for stabilization during orbit maintenance, attitude control manoeuvres and desaturating the Reaction Wheels (RWs), which served as the primary active attitude control mechanism. Table 8 lists the  $\Delta V$  associated with each of the previously identified mission phases; Launch and Early Orbit Phase and Disposal are missing because no manoeuvres were performed by the Spacecraft (S/C) during these phases.

Phase	$\Delta V$ [m/s]	Thruster
Transfer	34.25	OCS
Lunar Orbit Acquisition	865.78	OCS
Commissioning	69.32	OCS
Science	154.96	RCS

Table 8: Delta-V distribution across mission phases [7]

As expected, the majority of the total  $\Delta V$  is linked to OCS burns, while RCS is mainly responsible of Orbit Maintenance Manoeuvres during Science phase.

#### 3.2 Subsystem Architecture

##### 3.2.1 Thruster selection and configuration

The OCS featured one 455 N High Performance Apogee Thruster (HiPAT), able to complete the orbital manoeuvres requested in Mission Analysis. It is mounted along body axis -Z so that, by controlling the attitude of the satellite, strong impulsive manoeuvres could be performed without creating any momentum on the spacecraft [9].

The RCS consisted of four 22 N thrusters, angled 45 degrees from the Z-axis [9]. This configuration enabled LADEE to achieve full three-axis attitude control and perform RWs desaturation [10]. Additionally, it minimized the risk of exhaust gases impacting the spacecraft's external surfaces, thereby reducing surface contamination. Furthermore, due to the nature of the Modular Common Spacecraft Bus (MCSB), the propulsion module is positioned at the spacecraft lower end, ensuring that the tanks and thrusters are as close as possible. This minimizes the required cabling space along the spacecraft and reduces complexity and pressure losses.

##### 3.2.2 Pressurant, Oxidizer, Fuel and Tanks description

The selected fuel and oxidizer were Monomethylhydrazine  $CH_6N_2$  (MMH) and Dinitrogen Tetroxide  $N_2O_4$  (NTO) which form an hypergolic couple, eliminating the need for an ignition system and enhancing reliability [11]. Additionally, they are both cost-effective and good-performing, **with a strong heritage**. Furthermore, it is important to notice that MMH has been chosen over **classical hydrazine**.

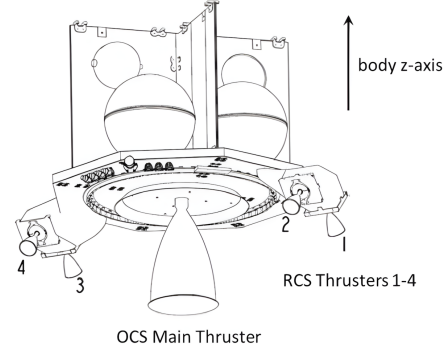


Figure 6: LADEE thruster layout [9]  
The diagram shows a cross-section of the LADEE spacecraft's lower end, focusing on the propulsion module. The OCS Main Thruster is at the bottom center. Four RCS Thrusters (labeled 1, 2, 3, 4) are arranged in a square pattern around the main thrust vector. An arrow labeled "body z-axis" indicates the orientation of the body axis. Internal components like tanks and cables are visible within the module.

due to its lower melting point, -2°C for hydrazine and -52°C for MMH, allowing for wider survival temperature range.

Helium was selected as pressurant due to its good gas dynamic properties and low mass cost.

The system had a total of six tanks, two each for fuel, oxidizer and pressurant. This approach offers several advantages. Firstly, it allows for greater flexibility in the subsystem configuration. This has been exploited with a symmetrical positioning of the tanks which minimizes centre of mass excursions and inertia variations [12]. Secondly, having redundant tanks enhances reliability, reducing the risk of mission failure due to a single tank malfunction. All tanks were manufactured from a titanium alloy (Ti-6Al-4V) chosen for its performance, low mass, cost-effectiveness, and corrosion resistance [12]. This last aspect can be identified as a driver for the choice of the material due to the high reactivity of hydrazines against tank walls. Tanks were also equipped with a Propellant Management Device (PMD) to guarantee operations in a microgravity environment [13].

### 3.2.3 Subsystem architecture

In Figure 7 is represented the team's reconstruction of LADEE's propulsion subsystem architecture:

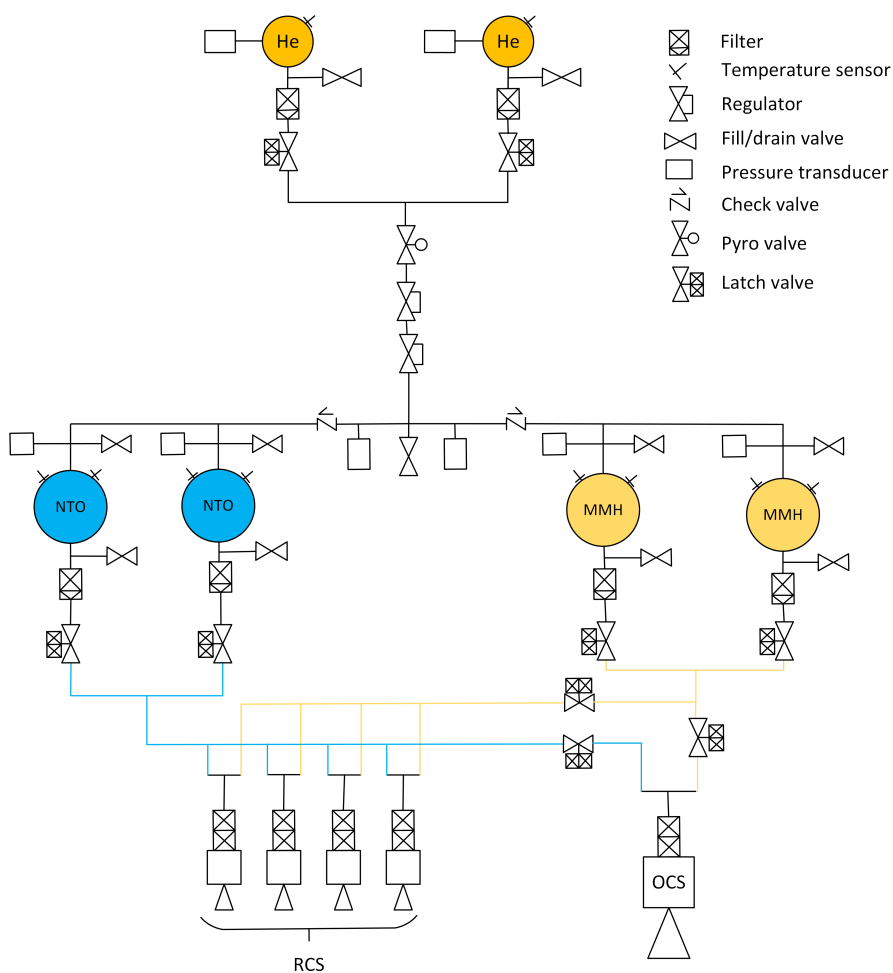


Figure 7: Reproduction of LADEE's propulsion system architecture

Some of the most important aspects to be highlighted are:

**Redundancies:** The team considered that further redundancy in feeding lines could have been ideal, although no confirmation of this hypothesis has been found. In fact, if either the OCS or the RCS had experienced partial or complete failure, that wouldn't have allowed LADEE to reach the Moon in the first case, or to maintain orbit or attitude in lunar orbit in case of RCS failure, jeopardizing in both

cases the mission's success. For the same reason, the team considered the presence and redundancy of some valves and sensors, as can be seen in the series of two regulators.

**Pressure Regulated (PR) and Blowdown (BD) system:** The propulsion system was designed to operate in a PR configuration during OCS operations, up to the achievement of the Lunar Science Orbit, and then switch to a BD mode during RCS operations [9]. This architecture is fully aligned with the logic introduced in Sec. 3.1, as it guarantees constant thrust and mass flow rate during the most critical orbital manoeuvres, reducing trajectory dispersions and improving manoeuvre precision. Once high accuracy is no longer essential, the system transitions to the simpler and more reliable blowdown mode, ideal for small correction manoeuvres such as attitude control or momentum unloading. This approach required the inclusion of a regulating pressure valve to maintain the specified pressure in the propellant tanks during the PR phase, and a pyrotechnic isolation valve to seal off the pressurant volume after switching to blowdown mode.

### 3.3 Subsystem Sizing

#### 3.3.1 Mission masses and volumes

Considering the actual  $\Delta V$  of the mission [7], the team was able to reconstruct the sizing of mass and volume of propellant needed, specifying the amount of oxidizer and fuel. For good engineering practice, the team considered margins over certain parameters, which are highlighted with an overline.

First, the total  $\Delta V$  retrieved from Mission Analysis was divided into two subsets of manoeuvres: those executed prior to achieving the Lunar Science Orbit and those performed afterward [7]. It is reasonable to assume that the former subset was accomplished solely by the OCS, while the latter was provided exclusively by the RCS. Although the RCS was engaged concurrently during OCS burns for attitude stabilization, its contribution to the net  $\Delta V$  in this phase is negligible due to the short firing durations and smaller thrust contribution. These two subsets of manoeuvres are denoted as  $\Delta V_{OCS}$  and  $\Delta V_{RCS}$  [7], each executed by the respective propulsion systems characterized by specific impulses  $I_{sp,OCS}$  and  $I_{sp,RCS}$  [7, 14]. These parameters serve as inputs to the rocket equation to estimate the propellant mass requirements for each control system. It's important to note that the "dry mass" for OCS manoeuvres is the dry mass  $\overline{M}_{dry}$  plus the propellant mass for RCS,  $M_{prop,RCS}$ , as this last can be considered inert mass as it's not expelled during OCS manoeuvres.

$$\begin{cases} \overline{M}_{dry} = M_{dry}(1 + 20\%) \\ MR_{RCS} = e^{\frac{\Delta V_{RCS}}{I_{sp,RCS} \cdot 90}} \\ MR_{OCS} = e^{\frac{\Delta V_{OCS}}{I_{sp,OCS} \cdot 90}} \end{cases} \Rightarrow \begin{cases} M_{prop,RCS} = (MR_{RCS} - 1) \overline{M}_{dry} \\ M_{prop,OCS} = (MR_{OCS} - 1) (\overline{M}_{dry} + M_{prop,RCS}) \\ M_{prop} = M_{prop,RCS} + M_{prop,OCS} \end{cases}$$

Therefore, applying margins over the propellant mass, namely 3% for residuals, 2% for ullage and 0.5% for loading uncertainties, it is possible to compute the masses of fuel and oxidizer. The Oxidizer to Fuel Ratio (OF) was assumed such that it would grant identical volumes for the two liquids, which is coherent with LADEE PS architecture, as shown in Fig. 6:

$$\begin{cases} \overline{M}_{prop} = M_{prop} \cdot (1 + 3\% + 2\% + 0.5\%) \\ OF = \frac{\rho_{NTO}}{\rho_{MMH}} \end{cases} \Rightarrow \begin{cases} M_{MMH} = \frac{\overline{M}_{prop}}{(1+OF)} \\ M_{NTO} = \overline{M}_{prop} - M_{MMH} \end{cases}$$

Based on these estimations, the required volumes of oxidizer and fuel can be derived, enabling the sizing of the corresponding propellant tanks, which is addressed in the following sections.

$$\begin{cases} V_{NTO} = \frac{M_{NTO}}{\rho_{NTO}} \\ V_{MMH} = \frac{M_{MMH}}{\rho_{MMH}} \end{cases} \Rightarrow V_{prop} = V_{NTO} + V_{MMH} \Rightarrow \begin{cases} \overline{V}_{prop} = V_{prop} \cdot (1 + 10\%) \\ \overline{V}_{NTO} = V_{NTO} \cdot (1 + 10\%) \\ \overline{V}_{MMH} = V_{MMH} \cdot (1 + 10\%) \end{cases}$$

### 3.3.2 Pressurant sizing

As already defined, the system worked during OCS operations as a Pressure Regulated (PR) system and during RCS operations as a Blowdown (BD) system [7]. To switch between operating modes the system isolated the pressurant tanks from the propellant tanks, probably through the use of a pyrotechnic valve as proposed in section 3.2.3. This left a certain quantity of helium unused at  $P_{gas,f}$  in the pressurant tanks for the remainder of the mission [7]. The remaining gas flowed instead in propellant tanks, pressurizing them during BD system operations, which end as the pressure reaches  $P_{prop,f}$ . As Mission Analysis required multiple firings, often relatively small, with long interval of inactivity it is possible to assume almost isothermal gas expansion [15], from which the balance of mass yields:

$$\begin{aligned} M_{gas} &= \frac{P_{gas,initial} V_{gas}}{RT_{gas}} = \frac{P_{gas,final} V_{gas}}{RT_{gas}} + \frac{P_{prop,f} \bar{V}_{prop}}{RT_{prop}} \\ \Rightarrow M_{gas} &= \frac{P_{prop,f} \bar{V}_{prop}}{RT_{gas} \left( 1 - \frac{P_{gas,final}}{P_{gas,initial}} \right)} \end{aligned}$$

Where it's assumed that the entirety of the spacecraft is at the same temperature, thus  $T_{gas}$  and  $T_{prop}$  are both assumed to be equal to  $T_{SC}$ . Margins are applied over the gas mass and, consequently, the gas volume must be recomputed to correctly size gas tank:

$$\begin{cases} \bar{M}_{gas} = M_{gas} \cdot (1 + 20\%) \\ \bar{V}_{gas} = \frac{\bar{M}_{gas} RT_{gas}}{P_{gas,initial}} \end{cases}$$

### 3.3.3 Tank sizing

This section proposes the reverse-engineering of LADEE's tanks' dimensions. As is common in space-craft design, identical tanks were assumed for the oxidizer and fuel, while different sizing was applied to the pressurant tanks. All tanks were spherical in shape [7, 13], with two tanks allocated for each fluid. It is possible to compute the radius  $r$  and the thickness  $t$  of the two types of tanks as follows:

$$\begin{cases} r_{tank,prop} = r_{tank,NTO} = r_{tank,MMH} = \left[ \frac{3}{4\pi} \left( \frac{\bar{V}_{NTO}}{2} \right) \right]^{\frac{1}{3}} = \left[ \frac{3}{4\pi} \left( \frac{\bar{V}_{MMH}}{2} \right) \right]^{\frac{1}{3}} \\ r_{tank,gas} = \left[ \frac{3}{4\pi} \left( \frac{\bar{V}_{gas}}{2} \right) \right]^{\frac{1}{3}} \\ \\ \begin{cases} t_{tank,prop} = t_{tank,NTO} = t_{tank,MMH} = \frac{P_{prop,i} r_{tank,prop}}{2\sigma} \\ t_{tank,gas} = \frac{P_{gas,i} r_{tank,gas}}{2\sigma} \end{cases} \end{cases}$$

Given the geometry, it is possible to compute the masses of the tanks:

$$\begin{cases} M_{tank,prop} = \rho_{tank} \frac{4}{3}\pi [(r_{tank,prop} + t_{tank,prop})^3 - (r_{tank,prop})^3] \\ M_{tank,gas} = \rho_{tank} \frac{4}{3}\pi [(r_{tank,gas} + t_{tank,gas})^3 - (r_{tank,gas})^3] \end{cases}$$

### 3.4 Sizing Results

$P_{\text{gas},i}$	248.2 bar [7]
$P_{\text{gas},f}$	23.8 bar [7]
$\Delta V$	1134.6 m/s [7]
$\rho_{\text{fuel}}$	875 kg/m <sup>3</sup> [16]
$\rho_{\text{ox}}$	1442.46 kg/m <sup>3</sup> [17]
$P_{\text{prop},i}$	17.24 bar [7]
$P_{\text{prop},f}$	11.03 bar [7]
$T_{\text{SC}}$	293 K
$R$	2077.3 J/(kg·K)
$I_{\text{sp,RCS}}$	305 s [14]
$I_{\text{sp,OCS}}$	320 s [14]

Table 9: Input Data

$M_{\text{dry}}$	240.70 kg [7]
$M_{\text{dry}}$	288.84 kg
$M_{\text{RCS}}$	1.0535
$M_{\text{ROCS}}$	1.3658
$M_{\text{prop, RCS}}$	15.45 kg
$M_{\text{prop, OCS}}$	111.32 kg
$\bar{M}_{\text{prop}}$	133.74 kg
O/F	1.6485
$M_{\text{MMH}}$	83.24 kg
$M_{\text{NTO}}$	50.50 kg
$\bar{M}_{\text{gas}}$	0.30 kg

Table 10: Mass Data

$\bar{V}_{\text{prop}}$	1269.63 cm <sup>3</sup>
$\bar{V}_{\text{gas}}$	74.89 cm <sup>3</sup>
$\bar{V}_{\text{MMH}}/\bar{V}_{\text{NTO}}$	634.81 cm <sup>3</sup>
$\sigma$	880 MPa
$\rho_{\text{tank}}$	4500 kg/m <sup>3</sup>
$r_{\text{tank, prop}}$	19.64 cm
$r_{\text{tank, gas}}$	9.63 cm
$t_{\text{tank, prop}}$	0.19 mm
$t_{\text{tank, gas}}$	1.36 mm
$M_{\text{tank, prop}}$	4 · 0.42 kg
$M_{\text{tank, gas}}$	2 · 0.72 kg

Table 11: Volume Data

It is possible to note that, as expected from division presented in Sec. 3.1, most of the propellant Mass (around 88 %) is devoted to OCS manoeuvres. The Masses of propellant, and particularly, of oxidizer and fuel show little variations with respect to true mission values respectively 134.8 kg of which 51.2 kg of fuel and 82.1 kg of oxidizer [7]. Relative to pressurant mass a little overestimation of around 7% is achieved with respect to the 0.28 kg in the real mission [7]. However, this is probably due to the remaining propellant inside the tanks which results in a bigger  $P_{\text{prop},f}$  from reports [7]. Furthermore, the tank masses appear to be significantly underestimated, with the propellant tanks and pressurant tanks weighing approximately 2.45 kg and 1.5 kg each on the real mission. This underestimation is likely due to the additional weight introduced by the PMD and the safety margins applied to the wall thickness, whose increase has a cubic effect on the overall tank mass.

### 3.5 Mass and Power budget

In the end, the team performed a reverse engineering of the Mass and Power budget. The mass of the subsystem is computed considering the more massive components margined to account for harness:

$$\begin{aligned} M_{\text{PS}} &\approx M_{\text{OCS}} + 4M_{\text{RCS}} + 4M_{\text{tank,prop}} + 2M_{\text{tank,gas}} \\ &= 5.2 \text{ kg} + 4 \cdot 0.965 \text{ kg} + 4 \cdot 0.42 \text{ kg} + 2 \cdot 0.72 \text{ kg} = 12.18 \text{ kg} \\ \bar{M}_{\text{PS}} &= M_{\text{PS}} \cdot (1 + 20\%) = 14.63 \text{ kg} \end{aligned}$$

The propulsion system being analysed is chemical, and since hypergolic propellants do not require ignition, it doesn't use direct power to generate thrust. As a result, the only components that consume power are the valves and sensors. Therefore, the total power budget has been estimated by summing all different contributions considered in the architecture shown in Fig. 7.

	OCS	RCS	PT	TS	FDV	LV	PV	Total
Power [W]	9.8	11	0.3	0.025	1	2	1	88.45
Quantity	1	4	8	10	11	10	1	-

Table 12: Power budget

The values presented in Tab. 12 were primarily sourced from the datasheet [14] [18], with the exceptions being those that were unavailable, which were obtained from similar missions and components or estimated. Two types of components were not considered in the calculation, the pressure regulators and check valves, which are typically mechanical parts and do not absorb any power. Comparing the power budget with similar missions and with the overall power budget of 295W the absorbed power appears to be reasonable and consistent. It should also be noted that the two types of thrusters are never operated simultaneously, therefore the actual absorbed power is generally lower than the computed value.

## 4 Telemetry & Telecommand (TMTC)

### 4.1 Subsystem Architecture

The LADEE TMTC subsystem was designed to support communication and telecommand functionalities across the whole mission. It primarily consisted of:

- Two custom-made **omnidirectional Low Gain Antennas (LGAs)** which were mounted on opposite sides of the satellite with a tilt angle of  $67.5^\circ$ , as can be seen in Figure 8a. This configuration maximized the receiving opportunities, although it didn't guarantee complete coverage of the celestial sphere due to interferences.
- One custom-made **Medium Gain Antenna (MGA)** which was equipped with a circular plate to increase directivity. It was positioned nearby the Upper Low Gain Antenna (ULGA), probably for ease of assembly, both on the radiator deck. This thermally controlled the temperature of the two antennas and other instruments on it.
- The **Lunar Laser Communication Demonstration (LLCD)**, carried out onboard LADEE. Although it enabled communication between the spacecraft and ground stations, it served solely as a technology demonstration and did not impact the nominal operations of the science mission. Therefore, it will not be discussed further in this section.
- The **RF transfer switch** onboard LADEE allowed dynamic control over the spacecraft's communication system. While the receiver was always active to ensure continuous command reception from Earth, the switch enabled LADEE to transmit using different configurations or modes depending on the operational needs.
- A combination of **diplexer**, **splitter**, and **coupler** was used connected to LADEE's LGAs and enabled the use of the antennas for simultaneous reception and low-rate transmission [19].
- **Bandpass filter** to suppress potential random noises to the MGA in transmission.
- A newly designed **S-Band Transponder** which incorporated the receiver and the transmitter/telemetry/ telecommand interface.

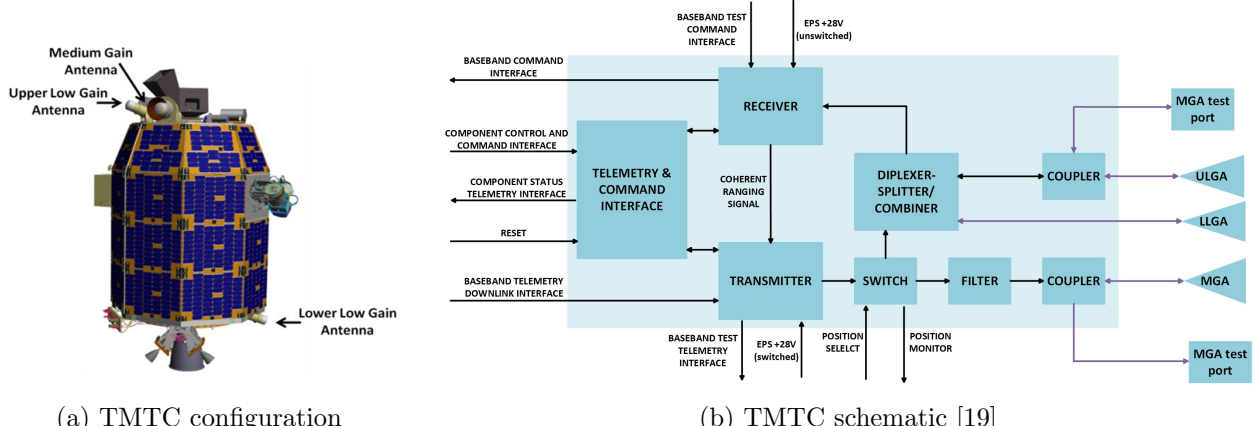


Figure 8: Subsystem overview

### 4.2 Ground Segment Network Selection

The forefront of LADEE's Ground Segment, responsible for data exchange between spacecraft and ground, used all three of NASA's Space Communication and Navigation (SCaN) networks [3], [20]:

- **Deep Space Network (DSN)**: seven S-band enabled, 34-m antennas from the facilities in Canberra (AU), Madrid (ES) and Goldstone (CA) were the primary assets for telemetry, command and tracking throughout the mission.

- **Near Earth Network (NEN)**: two antennas, a 9-m one located in Santiago (CL) and an 18-m one at the White Sands (NM) facility, complemented the DSN, primarily for tracking services including Doppler, ranging and auto-track angle measurements.
- **Space Network (SN)**: this network, via Tracking & Data Relay Satellite System (TDRSS), was employed to guarantee telemetry and command coverage mainly during Perigee Manoeuvres.
- **Universal Space Network (USN)**: even if not part of NASA's SCaN, two antennas of this network, located in South Africa and Western Australia, were used to enhance global tracking coverage.

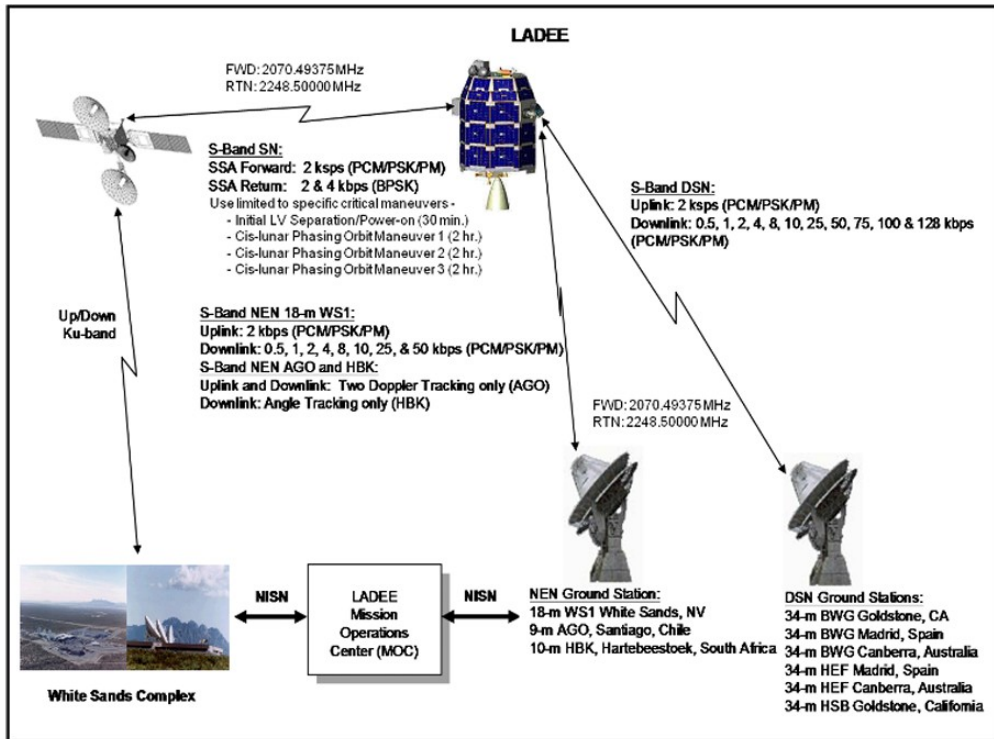


Figure 9: TMT architecture [19]

### 4.3 Design Rationale

#### 4.3.1 Antennas Configuration

The MGA was dedicated exclusively to transmission, while the two LGAs operated primarily in receive-only mode during nominal conditions, with the capability for low-rate transmission when needed [19]. This setup is easily justified: during nominal operations, the spacecraft maintained sufficient pointing accuracy to support high data rate communication via the MGA. In scenarios where accurate pointing could not be guaranteed, such as during safe mode, the omnidirectional ensured data transmission. For reception, the quasi-omnidirectional nature of the LGAs was designed to ensure reliable uplink communications and telecommand capability regardless of the spacecraft's attitude or orbital position.

#### 4.3.2 Ground Stations

The DSN is made up of three sites that are spread equidistantly across the world; this strategic placement enables constant communication with distant spacecrafts. The DSN antennas were chosen over the designed-for NEN ones due to higher power and sensitivity, but also to maintain a cost-effective mission operations staffing schedule over the lunar month. Due to the need for flexibility in trajectory design and the simultaneous classification of Perigee Manoeuvres (PMs) as high-criticality, telemetry and command coverage were required. However, such coverage could not be reliably provided by the DSN. This led to relying on the SN. Both NEN and SN were used for initial acquisition, PMs support and to supplement communications coverage while LADEE was out of view of DSN.

#### 4.3.3 Frequency and Band

LADEE utilized S-band, with uplink frequency of 2070.49 MHz and downlink of 2248.5 MHz [19]. The main drivers for the selection of the S-band for the LADEE mission were the cost minimization and limitation of the spacecraft-mounted antennas' dimensions. In addition to its extensive heritage, which renders it a low technological risk for the mission, the S-band allows the use of compact antennas while providing satisfactory transmission performances and data rates. Furthermore, it guarantees low atmospheric attenuation and limited susceptibility to weather-related phenomena.

#### 4.4 Communications during Phases

In the following lines, a possible correlation between TMTC and different mission phases is presented:

Mission Phase	GS	TMTC Notes
<b>Launch and LEOP</b>	TDRSS used for early contact during LV separation; DSN (GLD, CAN, MAD) for TT&C; NEN (AGO, WS1) and USN (HBK, AUWA01) provided tracking support.	TDRSS link was used during critical LV separation and initial power-on (see Fig 9). This ensured near real-time monitoring before ground station handover. Low data rate expected for remaining part of the phase, primarily driven by initial downlink of telemetry and spacecraft status.
<b>Transfer</b>	TDRSS used during PMs due to limited ground visibility; DSN (GLD, CAN, MAD) for routine communications; NEN (AGO, WS1) and USN (HBK, AUWA01) supported tracking.	Highly critical during PMs, for which ground station coverage could not always be guaranteed. To ensure TMTC coverage, especially during burns, NASA's TDRSS was employed. Low data rate with the relay satellite in both forward and return links, as reported in Figure 9, compatible with the omnidirectional LGAs for telemetry and commands. Away from burns, higher telemetry volumes were needed [21], favouring the use of the MGA to maximize data return.
<b>Lunar Orbit Acquisition (LOI)</b>	DSN only (GLD, CAN, MAD): redundancy planned due to LOI-1 criticality.	The LOI1 burn was mission-critical and required real-time telemetry and ground coverage. To meet this need, the manoeuvre was placed in Earth view despite a suboptimal $\Delta V$ . High telemetry data rate was likely required before the burn to enable precise execution. Data volume remained high throughout the rest of the phase as well.
<b>Commissioning</b>	DSN (GLD, CAN, MAD) for daily OD contacts; NEN (AGO, WS1) backup in case of DSN conflicts.	Involved full system verification, including payload checks. The MGA remained in use, and a very high data volume was transmitted, also due to the activation and testing of LLCD, which significantly increased downlink capacity [21].
<b>Science Phase</b>	DSN (GLD, MAD, CAN); NEN (WS1).	Onboard autonomy was increased, reducing the need for uplink, thanks to preplanned science state transitions. Downloaded data volume increased during this phase due to acquisition of science data, which were transmitted nightly in two 1-hour DSN sessions via the MGA at 128 kbps. Additional unattended DSN/NEN contacts used LGAs for health and status updates [3]. Tracking intensified around OMMs.

Mission Phase	GS	TMTC Notes
Disposal	No documentation: Likely same of Science Phase.	The final phase required continued downlink of science and spacecraft data until the impact with the lunar surface. Uplink was still relevant to communicate the final trajectory updates and ensure proper targeting of the disposal manoeuvre.

Table 13: Ground stations and TMTC configuration across LADEE mission phases

As evident from the discussion above, both uplink and downlink data volumes were closely correlated with the mission phase and its associated level of autonomy. Phases with limited autonomy, such as Transfer and LOI, required increased focus on downlink telemetry and uplink commanding. Differently, during more autonomous phases like Science, communication was primarily driven by the transmission of collected data.

#### 4.5 Communications during Modes

In the following lines, a possible correlation between TMTC and different operating modes is presented:

- **Safe Mode:** Attitude is automatically adjusted to maximize solar exposure via the Sun Safe Mode Controller [22]. As a result, precise pointing of the Medium Gain Antenna (MGA) cannot be guaranteed. Communications therefore rely on omnidirectional Low Gain Antennas (LGA), enabling a robust link regardless of orientation. Although the data rate is low, the downlink remains sufficient for essential telemetry and to receive recovery commands from ground.
- **Telecom Mode:** segments of daily orbital timeline were reserved for communication [23], distinct from science activities. These communication windows involve Earth-pointing configurations, with two main attitude profiles employed [3]: *COMM (Orbit Normal)*, where the +Z axis is aligned with the positive orbit normal vector, and *COMM (Anti-Orbit Normal)*, where the +Z axis is aligned with the negative orbit normal vector. In both cases, the MGA maintains Earth-pointing to ensure efficient telemetry download, command uplink, and transmission of stored data. The adoption of two distinct COMM configurations may have been intended to provide flexibility in transitioning to or from adjacent operational modes, while still preserving effective Earth-pointing for communication purposes.

#### 4.6 Subsystem sizing

The reverse sizing of the TMTC computes  $E_b/N_0$  and Signal to Noise Ratio (SNR) using the link budget equation (5) under the most complex operational condition, verifying communication with the DSN at maximum bit error rates:  $10^{-7}$  for downlink and  $10^{-5}$  for uplink. The corresponding minimum  $E_b/N_0$  values are then obtained from reference diagrams [24]. Both downlink and uplink were sized only for communication with the DSN ground antennas because this was the configuration mainly used during the lunar science mission, which represents the worst case regarding signal loss. Therefore, the sizing is realized assuming the satellite to be at maximum lunar distance  $d = 4.050 \cdot 10^8 \text{ m}$  [25]. The net datarates in downlink were variable, but during most operations they were set to 8 kbits/s for the omni antennas and 128 kbits/s for the medium gain antennas, while uplink datarate was 8 kbits/s through the omnis [7]. The frequencies of communication are discussed in Sec. 4.3.3. Diameter of the MGA is 18 cm, while for the 2 omni LGAs is 7.9 cm [26]. LADEE uses BPSK modulation for the uplink mode, as described in [19]. The downlink modulation is not specified; therefore, it is assumed to be the same. With regard to encoding, no literature was found specifying the scheme used. For the sake of an assumption of worst case, convolutional encoding is used since it has the higher overhead factor. This is supported by the transponder description, in which the capacity to perform this type of encoding is mentioned [27]. The gross datarate is retrieved from the net datarate, encoding scheme and modulation scheme as follows.

$$R_{\text{gross}} = R_{\text{net}} \frac{\alpha_{\text{enc}}}{\alpha_{\text{mod}}} \quad [\text{kbits/s}] \quad (1)$$

Where  $\alpha_{\text{enc}} = 2$  [28] and  $\alpha_{\text{mod}} = 1$  [29]. The bandwidth is then computed from formula  $B = (1+\alpha)R_{\text{gross}}$ , where the roll-off factor  $\alpha$  typically varies between 0 and 1, so it was reasonably assumed to be 0.5. The contact strategy consisted of two contact windows every day between 5 p.m. and 12 a.m. Pacific time [3]. During the science phase, the average duration of the lunar contact windows was around 1 h 7 min 31 sec [9], which means that the average data volume transferred per contact was 129.63 MB for downlink through the medium gain antenna. The radio transmitted 5 W of power through the antennas in downlink [7], while the uplink power is assumed to be 250 W, according to the capabilities of all the DSN antennas [30]. No specific info was found on the type of amplifier used in the mission, so a solid state amplifier (SSA) is assumed as it is compliant with the light mass of the spacecraft and power needed. Its efficiency is set to 0.3, according to data in literature [24], leading to an input power required for the downlink of 16.67W. The efficiency of the MGA is  $\mu_{\text{par}} = 0.55$  [24] while for the omnidirectional antenna no values were found so it was set to  $\mu_{\text{par}} = 0.4$  since it should be lower than the parabolic one. The gains and the beamwidths can be computed as follows.

$$G = 10 \log_{10} \left( \frac{\pi^2 D^2 \mu_{\text{par}}}{\lambda^2} \right) \quad [\text{dB}] \quad (2) \qquad \theta = 70 \frac{\lambda}{D} \quad [\text{deg}] \quad (3)$$

The losses considered in the reverse sizing are free space losses, cable losses, pointing losses and atmospheric losses:

- Free space losses are computed through the analytical formula  $L_s = 20 \log_{10} \left( \frac{\lambda}{4\pi d} \right)$ .
- Cable losses typically vary between -3 dB and -1 dB; hence they are reasonably set to -2 dB.
- Pointing losses in downlink are computed from the formula:  $L_p = -12(e_{\text{down}}/\theta_{rx})$ , where the relative pointing errors are retrieved from accuracy requirements found in literature. During the science phase, the required accuracy is  $0.09^\circ$ , while during the lunar transfer, below 50,000 km, the requirement is  $0.2^\circ$  [20]. During the sizing, the condition considered is the first one, as it represents the worst-case scenario from a loss point of view. In fact, in this condition, even if the pointing losses are slightly lower, the space losses increase considerably as the distance increases from around 50,000 km to lunar distance. In the uplink case, the spacecraft uses the omnis as receivers, and therefore the pointing error  $e_{\text{up}}$  is associated mainly with the transmission. This value was found in literature to be around  $0.1^\circ$  [31], considering only systematic errors. The assumption introduced of perfect omnidirectional antennas result in an unrealistic value for the pointing losses if the formula above is used. For this reason, the following formula was chosen:  $L_p = -12(e_{\text{up}}/\theta_{tx})$ . The assumption to utilize the  $\theta_{tx}$  as a reference is justified by the fact that the dominant source of pointing error is attributed to the ground antenna.
- Atmospheric losses for S-band communications are set approximately to -0.04 dB, based on frequency-mapped diagrams [24]. This value applies to zenith conditions only. However, even at lower elevations, atmospheric losses remain a minor part of total losses, which are dominated by the free space component.

The  $E_b/N_0$  is retrieved from the link budget equation as follows:

$$\frac{E_b}{N_0} = P_{\text{tx}} + G_{\text{tx}} + G_{\text{rx}} + L_c + L_s + L_a + L_p - 10 \log_{10}(R_{\text{gross}}) - N_0 \quad [\text{dB}] \quad (4)$$

Where  $N_0 = 10 \log_{10}(k T_e)$  is the noise power spectral density, which is a function of the Boltzmann constant  $k$  and the equivalent noise temperature  $T_e$ , whose value is around 38 K for the DSN 34-m antennas [32], in downlink mode. In the uplink mode, since the antenna is omnidirectional, the actual noise temperature should account for disturbances from all bodies within its field of view. However,

for simplicity in calculations, only Earth is considered, and hence  $T_e$  is set at 290 K, the standard Earth temperature. The SNR is computed similarly as follows:

$$SNR = P_{tx} + G_{tx} + G_{rx} + L_c + L_s + L_a + L_p - P_{noise} \quad [\text{dB}] \quad (5)$$

Where  $P_{noise} = 10 \log_{10}(k T_e B)$  is the noise power caused by random thermal motion of electrons in antenna equipment and external environment.

#### 4.7 Sizing results

In this section, the results of the reverse sizing are presented. The limit values of  $E_b/N_0$  and SNR are computed as mentioned in the previous section, with an additional margin of 3dB.

	<b>Downlink MGA</b>	<b>Downlink omnidirectional</b>	<b>Uplink</b>	<b>Unit</b>
$R_{Gross}$	256	16	16	kbps
B	384	24	24	kHz
$E_b/N_{0min}$	$4.5 + 3$	$4.5 + 3$	$5 + 3$	dB
$SNR_{min}$	$3.2391 + 3$	$3.2391 + 3$	$2.7391 + 3$	dB
$P_{tx}$	6.9897	6.9897	23.979	dB
$G_{tx}$	9.9475	1.4116	54.775	dB
$\theta_{tx}$	51.886	118.22	0.2983	deg
$G_{rx}$	55.472	55.472	0.6952	dB
$\theta_{rx}$	0.2747	0.2747	128.39	deg
$L_{point}$	-1.2882	-1.5903	-1.3485	dB
$L_{space}$	-211.63	-211.63	-210.91	dB
$E_b/N_0$	16.171	19.374	27.063	dB
$SNR$	14.414	17.617	25.302	dB

Table 14: Numerical results

Results of the reverse sizing show that the communication is achieved with  $E_b/N_0$  and SNR well over the minimum value requested. It is important to note that even though this is a preliminary analysis, the conditions that were considered correspond to the worst case scenario on the TMTC point of view. Therefore, the results presented in Table 14 are considered satisfactory. The gains for the MGA and the two LGAs are compliant with values found in literature [26]. It can be observed that the final values of  $E_b/N_0$  and  $SNR$  in downlink are lower for the MGA compared to the omnidirectional, which is uncommon given the higher gain of the MGA. However, this can be explained by the significant difference in data rate between the two cases.

#### 4.8 Power budget

This section presents the power that the TMTC subsystem needs to operate in nominal configuration. The Space Micro μSTDN is the S band transponder used in the mission, which integrates a telemetry and command unit, a receiver with demodulator, a transmitter with modulator and an encoding/decoding unit [27]. The maximum power requested from the transmitter and receiver sections are 35W and 6W respectively. Other components connected to the transponder are the transfer switch, test couplers, and a diplexer / coupler [19]. Only the switch has a slight power consumption, but no information on the precise value was found. It is reasonably assumed that it may be at least one order of magnitude smaller than the transponder consumption. In reverse sizing, the power budget for the TMTC considers the case of the maximum power needed, which means transmission and reception at the same time, with a margin of 5% to take into account the switch and small cable losses. Hence, the power needed for the TMTC is 43.05W.

## 5 Attitude Orbit Control System (AOCS)

### 5.1 Subsystem architecture

The purpose of the AOCS system is to guarantee controllability of the satellite throughout all its operational life. For this reason, the LADEE is equipped with a 3-axis attitude control system. For attitude determination, LADEE uses a single dual-head Star Tracker Assembly (STA), an Inertial Measurement Unit (IMU), and twelve Coarse Sun Sensor (CSS). Attitude control is achieved through four Reaction Wheel (RW) that include a set of MEMS gyroscopes and four 22 N RCS thrusters [3].

#### 5.1.1 Sensors

- **Coarse Sun Sensor (CSS):** The sensors used are not explicitly detailed in the literature; however, based on similar missions, the following data are plausible. These sensors typically achieve an accuracy of better than  $5^\circ$ , with Field of View (FOV) around  $\pm 40^\circ$ . As passive elements, they consume no power, weigh less than 45 g, and have typical dimensions of approximately 51 mm x 25 mm x 18 mm [33]. This is consistent with the fact that the LADEE mission employs 12 Sun Sensors, indicating that they must be small and lightweight.
- **Star Tracker Assembly (STA):** The star tracker on LADEE employs specialized wide-field lenses to frequently capture images of nearby stars and accurately determine the spacecraft's orientation [34]. Specific values for LADEE's STA are not available; however, typical values from similar NASA missions can be used. The FOV is typically in the range of  $20^\circ \times 20^\circ$ , with a weight of approximately 2.6 kg and dimensions of 164 mm x 156 mm x 348 mm. The power consumption can reach up to 12.6 W at  $60^\circ\text{C}$ , varying with temperature. Regarding the accuracy, it has a bias accuracy of 8.25 arcsec for pitch/yaw and 11.1 arcsec for roll, a low-frequency error of  $< 3.3$  arcsec for pitch/yaw and  $< 15.6$  arcsec for roll, and a noise equivalent angle of  $< 6$  arcsec for pitch/yaw and  $< 49.4$  arcsec for roll at a  $0.1^\circ/\text{s}$  tracking rate [35].
- **Inertial Measurement Unit (IMU):** The inertial measurement for LADEE is performed using the LN-200S IMU, manufactured by Northrop Grumman [36]. From the datasheet, the sensor contains an accelerometer with bias repeatability of 300 mg, noise of  $35 \text{ mg}/\sqrt{\text{Hz}}$  and scale factor accuracy of 300 ppm and a gyroscope with bias repeatability of  $1^\circ/\text{hr}$ , scale factor stability of 100 ppm and angle random walk of  $< 0.07^\circ/\sqrt{\text{hr}}$ . Its size is a diameter of 8.89 cm, a height of 8.51 cm, and weighs 784 g. Under nominal operating conditions, its power consumption is 12 W [37].
- **MEMS rate sensors:** Mounted on each reaction wheel is also a MEMS gyroscope of the quartz tuning fork variety [38], which is able to measure the angular velocity along the wheel axis. Performances include maximum rate going from 1.3 deg/sec to 450 deg/sec, 0.014 deg/sec ( $1-\Sigma$ ) for max range and a power consumption of 1 W [39].

#### 5.1.2 Actuators

- **Reaction Wheel (RW):** LADEE has four MicroWheel 1000 made by Microsat Systems Canada Inc. [40]. They weigh each less than 1.44 kg and consume less than 9 W of power in steady-state mode, including the MEMS rate sensor. They provide high-precision torque control, less than  $\pm 500$  Nm within 10 seconds, and store up to 1.1 Nms of angular momentum [39].
- **RCS thrusters:** The spacecraft is also equipped with four Reaction Control System (RCS) thrusters designed for small manoeuvres and attitude control. With a mass of 0.965 kg and a power consumption of 11 W each, the thrusters can provide a thrust of up to 27.8 N and a specific impulse of around 305 s [14].

## 5.2 AOCS architecture rationale

The LADEE attitude design is developed to meet the pointing requirements of all instruments, which involve changes in orientation relative to the main nominal attitude known as the RAM attitude [41], explained in section 5.3. These attitude excursions are limited by several flight restrictions designed to protect the instruments from direct Sun exposure and maintain the spacecraft in its thermal and power operating range [42].

### 5.2.1 Sensors rationale

The section of an array of 12 **CSS** is driven by the intrinsic functionality of this type of sensor. In fact, a single Sun sensor can only identify a cone in which the Sun lies, meaning that at least three sensors are needed to determine the Sun's direction [38]. To ensure data availability at any spacecraft orientation, a 12-sensor array is used, with sensors evenly distributed on the spacecraft surface [10]. These sensors are essential for Sun-safe mode, but they cannot retrieve full attitude information since at least two independent directions are required. For this reason, LADEE included a Fine Pointing Control (FPC) system incorporating two **star trackers** to obtain precise attitude determination. Since these are the only sensors capable of providing complete attitude determination, occlusions and interference must be minimized. This is the rationale behind the choice to include two instruments, to increase the FOV and their placement on the upper part of the spacecraft to ensure maximum visibility during nominal operations. The **IMU** together with **MEMS gyros**, is used to determine the spacecraft's angular velocity and acceleration as well as give an estimation of the attitude through propagation during period of star tracker occlusion [3]. The decision to include two types of inertial sensors is motivated by several factors. Primarily, RWs require rate sensors to support slew control [43], making their integration into the Reaction Wheel Assembly essential. In addition, the IMU offers significantly higher precision but consumes approximately ten times more power than rate sensors, as shown in Sec. 5.1.1. Therefore, when high precision is not required, MEMS-based sensors present an alternative for angular velocity estimation.

### 5.2.2 Actuators rationale

LADEE has four **reaction wheels** arranged in a pyramid configuration rather than a three-axis setup, as this provides full control even in the event of a single wheel failure and reduces the required torque to achieve the same control torque. For most of the mission, attitude control is performed using the RWs; however, during main engine burns and reaction wheel momentum desaturation, the spacecraft switches to using **RCS thrusters**. These are configured as four thrusters angled 45° from the Z-axis to ensure full 3-axis control.

## 5.3 AOCS Modes

During the mission, several attitude profiles were planned for the operations of LADEE. This section presents the main modes that influence the attitude of the satellite.

**Nominal Operating Mode (NOM):** it refers to the mode used during the commissioning and science operations, in which precise pointing of the payload is crucial. Some sub-modes can be identified[4] [3]:

- RAM mode: it is the most frequently used operating mode, in which the NMS and Lunar Dust Experiment (LDEX) foresees are pointed along the velocity vector, so that dust grains would strike the instruments. This is possible as the two apertures are aligned such that concurrent measurements can be made. In this mode, the spacecraft rotates about its axis of symmetry once per orbit.
- TILT mode: it is designed to point the NMS field of view downward 30° off the ram, which allows measurements of more energetic sputtered species that would not be detected after a collision with a surface in the mass spectrometer.

- WAKE mode: it is designed to allow instrument background measurements by pointing the NMS 180 degrees away from RAM, providing measurements without atmospheric gas entering the instrument.
- ION mode: in this mode, the spacecraft reorients its axis perpendicular to the orbital plane so that the NMS is pointed towards the ecliptic normal, looking for exospheric ions that have been picked up by the solar wind electric field.
- Limb stare mode: it is the main off-RAM altitude required by Ultraviolet Visible Spectrometer (UVS) operations, unsuitable for NMS measurements. In this mode, the telescope is fixed on a specific grazing altitude just above the lunar limb to detect resonant scattering from exospheric gases and dust [4].

**Sun Safe Mode (SSM):** it allows the spacecraft to remain power positive, thermally safe, and with the payload protected, spinning on the Z-axis and the Sun vector axis, or S-axis. Three different states of Sun safe situation are considered: instrument safing state, controlled roll-yaw state, and eclipse state. Instrument safing state is to manoeuvre the spacecraft so that the instrument is immediately turned away from pointing directly to the Sun. Then the controlled roll-yaw state consists on slowly spinning about Z-axis for thermal regulation, distributing evenly the heat from the Sun, and rotating about the S-axis for momentum management, by allowing lunar gravity gradient to act in opposite directions over time and decrease momentum build-up. Finally, the eclipse state is activated if a minimum number of Sun sensors reads zero current, to minimize the control effort by not holding any specific attitude against external torques. The RW interaction with the spacecraft dynamics is minimized, as the feedback-controlled system simply becomes the rigid-body dynamics of the spacecraft subject to external disturbances [38].

**Telecom Mode (TCM):** in the communication windows two attitude profiles are employed [3]: *COMM (Orbit Normal)*, with the +Z axis aligned with the positive orbit normal vector, and *COMM (Anti-Orbit Normal)*, with the +Z axis aligned with the negative orbit normal vector. In both cases, the MGA maintains Earth-pointing. During the LLCD demonstration the *COMM (Anti-Orbit Normal)* attitude is maintained [3].

**Delta-V Mode ( $\Delta VM$ ):** In this mode, the AOCS manages precise orientation prior to the burns of the OCS. This is possible with the 3-axis control of the RCS. The attitude profiles are customized for each manoeuvre [3].

**Rate-Reduction Mode (RRM):** when the spin rates are excessively high, the RCS thrusters are used to reduce the induced body rates to the point where the reaction wheels can take over. This mode was used upon launch deployment [3].

**Delta-H Mode ( $\Delta HM$ ):** it serves the function of managing the spacecraft's angular momentum by using attitude thrusters RCS to de-saturate the reaction wheels or to null excess body rates. This mode is particularly important for spacecraft such as LADEE, where prolonged science operations and precise attitude control can lead to momentum build-up due to environmental disturbances [44].

**Thermal and Power Conditioning Mode (TPC):** it involves maintaining a stable orientation with the Z-axis aligned with the ecliptic normal, and a fixed rotation around it. This attitude ensures proper solar panel illumination for power generation and supports thermal balance during non-operational periods.

#### 5.4 Sensors and Actuators per Mode

In NOM mode, all sensors are used to achieve the different attitude profiles in lunar orbits and no information that could exclude one in particular was found in the literature. As previously mentioned, the main actuators for attitude control are the RWs. The same is valid for the TCM and the TPC as they are often activated during the science and commissioning phases.

In SSM measurements from coarse Sun sensors are crucial and also pyramid configuration RWs are used. Spin rates are measured through MEMS rate gyros, embedded in each reaction wheel [38].

Without specific information in literature, it is reasonably assumed that the STA and IMU are not involved in this mode, as the control around the Z-axis and the Sun vector requires only knowledge of the Sun direction, while the spinning rates are measured by the MEMS gyros.

In RRM spinning rates are often above the operational limits of CSS and STA, so the only active sensors are the IMU and the MEMS gyros for measuring the spinning rates. It is important to note that the IMU is used more frequently because of its accuracy, but in this mode high precision measurements are often not needed as the rates are just reduced until the other sensors can operate. Hence, the MEMS gyros, even if less precise, are not excluded from being active in this mode. The actuators to reduce the rates are the RCS thrusters.

In  $\Delta VM$  the attitude control is mainly realized with the RCS thrusters, and measurements of the STA and CSS are required to provide precise attitude determination for the orbital manoeuvres. It is reasonably assumed that in this mode the IMU is active to accurately measure the angular rates, while MEMS gyros are just a backup solution as they are less precise.

Similarly, in the  $\Delta HM$  the main actuators are the RCS thrusters, while all the attitude sensors could be active depending on the situation, as no information that could exclude one of them was found.

Modes	Active Equipment					
	CSS	STA	IMU	GYRO	RW	RCS
NOM	X	X	X	X	X	
TCM	X	X	X	X	X	
SSM	X			X	X	X
RRM			X	X		X
$\Delta VM$	X	X	X			X
$\Delta HM$	X	X	X	X		X
TPC	X	X	X	X	X	

Table 15: AOCS equipment used per mode

## 5.5 Pointing Budget

The 3-axis control is dictated by the pointing requirements of different modes. The available data are included in Table 16, with some values assumed based on literature.

MODE	Pointing Direction	Accuracy Required
LDEX RAM	1 Rev/Orbit with +Z along neg. orbit normal	$APE < 5^\circ$
NMS Survey	Same as LDEX RAM but with arbitrary yaw angle	$APE < 2^\circ$
NMS Ion Scan	NMS ecliptic South with Panel 1 to Sun	$APE < 2^\circ$
UVS Limb	UVS Telescope limb with +Z orbit normal	$APE < 0.2^\circ$ $AKE < 0.15^\circ$
COMM (Orbit Normal)	MGA toward Earth with +Z pos. orbit normal	$APE < 2^\circ$
COMM (Anti Orbit Normal)	MGA toward Earth with +Z neg. orbit normal	$APE < 2^\circ$
LLCD Earth	Same as COMM (Anti Orbit Normal)	$APE < 1^\circ$
Delta-V	Custom designed for manoeuvre attitude	$APE < 5^\circ$
Thermal and Power Conditioning	+Z ecliptic normal and fixed rotation about Z-axis	$APE < 2^\circ$

Table 16: Pointing budget for mode

The requirements are primarily driven by the onboard instruments, as they are all body-mounted, meaning that all pointing must be achieved through attitude control [3]. All information regarding instrument requirements are taken from [4]. Regarding communication modes, no specific data on

the required pointing accuracy are available in the literature. However, during tracking, the pointing direction remains the same as in RAM mode, as shown in Table 16. According to the literature, this ensures the possibility of using some instruments during communication, in particular the NMS and LDEX [41]. Therefore, the Absolute Performance Error (APE) is set equal to the most stringent requirement among those specified for these instruments. The same assumption is applied to thermal and power conditioning. In fact, this mode also coincides with RAM, since the condition required to ensure sufficient power generation and maintain the necessary temperature is simply to rotate once per orbit while keeping the Z-axis normal to the orbital plane [45]. All the pointing requires to justify the sensor choice, particularly the star trackers presence for their high precision. No values were found about Absolute Knowledge Error (AKE) other than the one for UVS. As a general rule, it is assumed one order of magnitude greater than the APE of the corresponding mode.

## 5.6 Subsystem sizing

For the sizing of the AOCS, the team approximated the distribution of the satellite's dry mass as a cylinder, resembling that of LADEE. The masses of fuel and oxidizer are modelled as 4 concentrated masses in the estimated position of the respective tanks. From this the team computed the Center of Mass (COM) of the satellite and the inertia of the whole system.

### 5.6.1 Disturbances Evaluation

The team decided to evaluate and compare the disturbances during the Transfer Phase and the Science Phase. For the former, the first Phasing Loop was considered, corresponding to an elliptical orbit with a low perigee altitude (200 km). For the latter, a circular orbit at an altitude of 50 km was modelled. Only these two phases were considered, due to the closer proximity to the primary bodies and the resulting stronger contribution from Gravity Gradient (GG) effects, as well as Atmospheric Drag during the Phasing Loops near Earth.

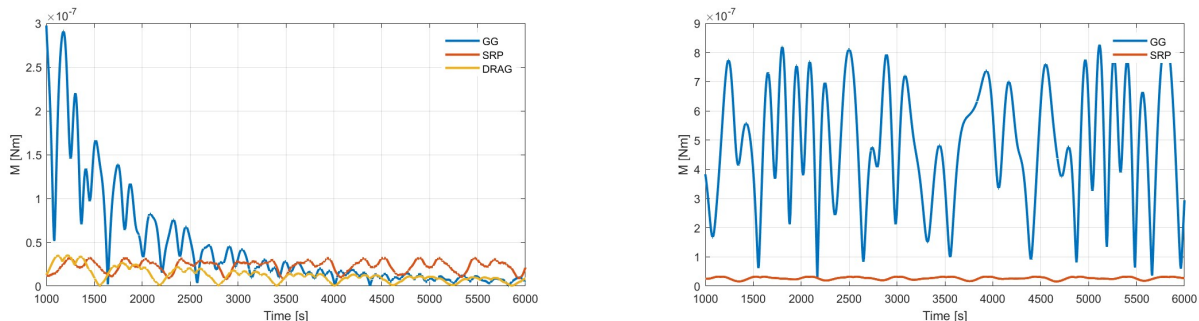


Figure 10: Comparison between perturbations on Earth and Moon

The perturbations were propagated in Simulink, considering the uncontrolled satellite and initialized with angular velocities of approximately 1 deg/s on each axis. It can be observed that the most critical condition during the first phase occurs near the perigee, as expected, with a decrease in both GG and Atmospheric Drag effects as the distance from Earth increases. Conversely, during the Science Phase, both perturbations exhibit a more constant behaviour, with a greater influence of the GG due to the closer proximity to the primary body. The orders of magnitude are reasonable, despite the lunar propagation not accounting for the Moon's highly non-uniform gravitational field [46].

Perturbations due to the magnetic field were neglected at this stage, considering the preliminary nature of the study and the low internally induced magnetic field expected for a spacecraft of such dimensions, evaluated using NASA's estimation [47].

In terms of operational modes, particularly those of medium to long duration, all will be characterized by a nearly constant GG and cyclic SRP, except for the TCM, where the situation will be reversed due to the Earth-Pointing orientation.

The reference condition for RW and Thruster sizing will be the Moon-based scenario. This represents the condition with the highest momentum accumulation in the orbit, and thus the most demanding in terms of desaturation frequency.

### 5.6.2 Reaction Wheels sizing: slew

For RWs sizing, a worst-case slew manoeuvre with  $\theta_{slew,max} = 180^\circ$  was considered. Initially, the team evaluated a minimum-time slew manoeuvre using maximum torque, but this approach brought to early saturation of the RWs. Subsequently, an accelerate-brake manoeuvre was considered, employing a reduced torque to ensure feasibility. However, this resulted in an excessively long manoeuvre time,  $t_{slew}^{acc,brake}$ , reported in table 18. This led the team to consider another angular rate profile consisting of three phases: acceleration, coasting at constant angular rate, and braking. A maximum of 80% of  $h_{slew,max}$  has been considered to avoid complete saturation of RWs, and from this value the maximum slew rate is computed:

$$\dot{\theta}_{slew,max} = \dot{\theta}_{coast} = \frac{\bar{h}_{slew,max}}{I_{max}} = \frac{0.8h_{slew,max}}{I_{max}} \quad (6)$$

From here, time of acceleration, coasting and brake can be computed:

$$t_{acc} = t_{brake} = \frac{\dot{\theta}_{slew,max} I_{max}}{T_{max}}; \quad t_{coast} = \frac{\theta_{slew,max} - 2\theta_{acc}}{\dot{\theta}_{coast}} = (\theta_{slew,max} - \frac{T_{max} t_{acc}^2}{I_{max}}) \frac{1}{\dot{\theta}_{coast}} \quad (7)$$

$$t_{slew} = t_{acc} + t_{coast} + t_{brake} \quad (8)$$

### 5.6.3 Thruster sizing: slew

As described in Section 5.6.2, the team evaluated alternative solutions to achieve a half-rotation of the spacecraft. In particular, a slew manoeuvre using the RCS was considered. An higher slew rate ( $\dot{\theta}_{slew,max}$ ) than the one computed in Sec. 5.6.2 is assumed, as a higher angular velocity can be expected due to the absence of appendages and, consequently, less stringent structural constraints. This approach was regarded by the team as a viable alternative for achieving faster slew manoeuvres.

### 5.6.4 Slew manoeuvres: Data and Results

Parameter	Data Value
Height S/C	2.37 m
Radius S/C	0.925 m
$I_{max}$	290.2 kg m <sup>2</sup>
$I_{min}$	163.2 kg m <sup>2</sup>
Reflectivity	0.3
$\mu_{moon}$	4902 km <sup>3</sup> /s <sup>2</sup>
$a_{orbit,moon}$	1787 km

Table 17: Data Input

Parameter	Data Value
$h_{max,RWs}$	1.1 Nms [48]
$T_{max}$	0.03 Nm [48]
$\dot{\theta}_{slew,max}$	0.1737 deg/s
$t_{slew}^{acc,brake}$	34.54min
$t_{acc}$	29.33 s
$t_{coast}$	1006 s
$t_{slew}$	17.75 min

Table 18: RWs slew

Parameter	Data Value
$F_{thruster}$	22 N
Lever Arm	0.5921 m
$I_s$	305 s
$\dot{\theta}_{slew,max}$	0.5 deg/s
$t_{acc}$	97.21 ms
$t_{coast}$	359.1 s
$t_{slew}$	6.002 min

Table 19: Thrusters slew

### 5.6.5 Propellant Mass Sizing: Desaturation with Thrusters

To guarantee enough time for reaction wheel desaturation the team considered  $t_{desat} = 5$  s:

$$F_{desat} = \frac{\bar{h}_{max}}{n L t_{desat}} \quad (9)$$

The next step is to understand the needed frequency of desaturation. Referring to Sec.[5.6.1] and considering a reference value for the maximum torque along the orbit, the number of orbits after which RW desaturation is required and the total number of desaturations is:

$$h_{dist} = \bar{T}_{max,dist} t_{orbit}; \quad N_{orbit,desat} = \frac{\bar{h}_{max}}{h_{dist}}; \quad N_{tot,desat} = \frac{N_{tot,orbit}}{N_{orbit,desat}} \quad (10)$$

The maximum torque considered is the maximum combination of GG and SRP obtained in the propagation. Both  $h_{max}$  and  $T_{max,dist}$  are overlined as margins were applied. From the number of

desaturations found, the propellant mass can be evaluated, that is already included in the total amount evaluated in Propulsion Subsystem Chapter:

$$M_{prop} = \frac{I_{tot}}{I_{sp90}} = \frac{N_{tot,desat} t_{desat} F_{desat}}{I_{sp90}} \quad (11)$$

$T_{max,dist}$	$\eta$	$t_{orbit}$	$h_{dis,orbit}$	$N_{orbit,desat}$	$N_{tot,orbit}$	$N_{tot,desat}$	$N_{days,desat}$	$M_{prop}$
$8.86e - 7 N\ m$	2	6780.96 s	0.0120 Nm	73.23	1274.15	17.39	5.63	0.0043 kg

Table 20: Desaturation Results

The frequency of desaturation is consistent with what is found in the literature. As stated in [49], desaturation is not a frequent operation and is only required every "few days". Less consistent may be the propellant mass allocated for desaturation. In general, it is expected to be a small value due to high specific impulse of the thrusters.

## 5.7 AOCS Mass, Power and Data budgets

In this section the masses, power and data requested by each AOCS unit are presented. The total power is divided per each mode presented in 5.4, as none of them uses all the equipment at the same time. A few notes must be highlighted. The MEMS gyros are embedded in the RWs, that include their mass. RWs and gyros consume around 9W, while if only the gyros are active the power consumption is 1W. In the  $\Delta HM$ , as mentioned in the sizing, the desaturation is realized with just two of the RCS thrusters, hence a 50% flag is indicated. In this analysis, even if the actuators often execute manoeuvres with a torque smaller than the maximum possible, the power considered is the maximum required by the single units, to size the worst-case scenario on the power consumption point of view.

Equipment	Units	Mass [Kg]	Power [W]	Modes				
				NOM/TCM/TPC	SSM	RRM	$\Delta VM$	$\Delta HM$
<b>CSS</b>	12	0.045	0	X	X		X	X
<b>STA</b>	2	2.6	12.6	X			X	X
<b>IMU</b>	1	0.784	12	X		X	X	X
<b>GYRO</b>	4	-	1	X	X	X		X
<b>RW</b>	4	1.44	9	X	X			
<b>RCS thrusters</b>	4	0.965	11		X	X	X	50%
<b>Total</b>		16.144		73.20	80.00	60.00	81.20	63.20

Table 21: Mass and Power budgets

Table 22 provides essential information that the AOCS must transmit to the ground station. Data selection focuses on critical aspects for the subsystem and the format ensures minimal data overhead, while adhering to established recommended standards from the CCSDS. [50]

Parameter	Type	Data size [bits]	Notes
Attitude	float	4 x 32	Attitude status in terms of quaternions, float type is selected for precision.
Angular Rate	float	3 x 32	S/C rotation rates along body axes.
Control mode ID	uint	1 x 8	Encodes current AOCS mode.
Timestamp	uint	1 x 32	Time tagging each message, crucial for event timeline reconstruction.
Health status	uint	1 x 16	Detailed status of sensors, actuators, subsystems.
<b>Total</b>	-	280	-

Table 22: AOCS Data budget

## 6 Thermal Control Subsystem (TCS)

### 6.1 Subsystem Architecture

The TCS ensures that all subsystems and payload temperatures remain within the required limits. This is realized mainly with passive solutions, but also active elements are employed in specific subsystems and Payloads (P/Ls) components. The equipment of the TCS is presented in the following section.

#### 6.1.1 LADEE Thermal Passive Control

**Radiators:** the main contribution to thermal regulation is realized with passive radiators, present in different subsystems and critical P/Ls. The largest is the radiator panel, on top of the Radiator Assembly, which houses the avionics, batteries, attitude sensors, and two P/Ls [7]. The UVS has radiative surfaces coated with silverized tape facing out from the spacecraft. Also, LDEX features several additional radiating surfaces designed to minimize solar and lunar IR loading.

**Multi-Layer Insulation (MLI):** All three scientific P/Ls of the mission include Dummore's MLI for thermal protection [7] [51]. NMS has MLI consisting of germanium black Kapton on its outer layer. Regarding the UVS, MLI is applied at each of the eight mounting fasteners in contact with the radiator panel. In LDEX the external surfaces of the electronics module are covered with thermal control materials, including MLI and silver-teflon tape [7].

**Body-mounted solar array:** The MCSB design is characterized by body-mounted and fixed solar arrays. The photovoltaic solar cells are produced by Emcore Corporation [52]. The BTJ is the one assumed to be present on LADEE [53].

**Washers:** In the UVS, low thermal conductivity washers made of G-10 material are placed around each mounting fastener, in combination with the MLI, to secure the unit to the radiator deck [7].

**Heat straps:** The NMS has an aluminum heat strap to further sink the electronics located under the sensor housing, ensuring conduction with the main structure [7].

**Coatings:** The NMS thermal control includes 5 mil silver Teflon coating on the external surfaces of the main electronic box. This coating has low absorptivity, around 0.08-0.10 [54].

#### 6.1.2 LADEE Thermal Active Control

**Heaters:** active heaters are applied to increase the temperature of specific parts whenever their minimum limit is not granted by passive elements only. They are used on each instrument, the LLCD optics, the propulsion system and its feeding lines, batteries, transponder and radiator panel. Onboard the spacecraft, the heaters are primarily Kapton foil types, powered by the spacecraft bus and protected by circuit breakers. Heaters are divided into:

Operational heaters: they maintain instruments at their minimum operating temperature in active mission phases, and are controlled by flight software based on temperatures recorded by sensors [7].

Survival heaters: they prevent components from dropping below their survival temperature during inactive periods. They are present in all three scientific payloads and on the radiator module, and are controlled by an independent thermostat [10].

Bake-out and Decontamination heaters: they heat sensitive areas to high temperatures to remove volatile or molecular contaminants before or during the mission. Bake-out heaters are used in the NMS to remove contaminants from internal surfaces during the mission, and in the UVS, they serve for contamination control. Decontamination heaters instead are present in the ion source cover of the NMS to heat the sensor housing to  $+180^{\circ}\text{C}$  in orbit to ensure accurate measurements [7].

**Thermoelectric Coolers (TECs):** they play a limited part in the thermal control. In the UVS, the S7031-1006S FFT-CCD image sensor has integrated TECs to work under proper thermal conditions. The TEC can cool the detector to  $10\text{-}50^{\circ}\text{C}$  colder than the spectrometer heat sink.

## 6.2 Subsystem Design Rationale

### 6.2.1 TCS Architecture Rationale

This subsection explains how the previously introduced TCS components are interconnected with the instruments and subsystems, highlighting the architectural choices adopted to maintain thermal control throughout the mission.

**Radiator panel:** most instruments and electrical components, excluding the NMS and the LLCD, were mounted directly on the radiator deck, allowing centralized passive cooling while local heaters managed component-specific survival requirements [55]. Equipped with its own heaters and oriented toward deep space, the radiator panel enabled effective temperature control through combined passive and active means.

**Payloads:** P/Ls were thermally mounted according to their specific needs. For example, the UVS required significant thermal decoupling achieved through MLI and washers, while the LDEX was equipped with dedicated coolers to support its operational thermal requirements.

**Body-mounted solar panels:** selected to ensure power generation across a wide range of attitudes while avoiding complex deployment mechanisms [7]. This design resulted in high surface absorbance (0.8-0.9) [56], likely mitigated by MLIs or additional insulation layers to decouple external and internal environments. Their emissivity (around 0.8) [56] also enabled fast passive cooling, allowing them to function as radiators when not Sun-facing [57].

**Propulsion subsystem:** equipped with heaters to prevent propellant freezing in tanks and feeding lines. It is reasonable to assume the presence of heat straps connecting the tanks to outer surfaces or the radiator panel, facilitating both electrical grounding to prevent unwanted ignition and efficient thermal control of the propellant tanks.

**Heaters:** operational heaters were controlled by flight software, while survival heaters were commanded by independent thermostats, providing redundancy and ensuring thermal stability even in case of failures. This dual architecture was critical during commissioning to prepare instruments for science operations while maintaining thermal limits across the system.

### 6.2.2 Thermal Control and Mission Environment per Phase

LADEE traversed diverse space environments, each imposing conditions the spacecraft had to endure. This resulted in a range of thermal conditions requiring robust thermal management strategies.

**LEOP, Transfer, and Lunar Orbit Acquisition (LOA) phases:** during these phases, the spacecraft was exposed to solar irradiance, Earth's infrared (IR) emissions and albedo, and heat generated by atmospheric drag, which can be neglected except during Launch and Early Orbit Phase (LEOP) for the low altitudes at perigee. Additionally, when the spacecraft was further away from Earth, it was essential to prevent excessive cooling, as it was in deep space with only a few essential components operating. The solar heat flux is set to a value of  $1367.5 \text{ W/m}^2$ , which is reasonable for an almost constant distance of 1 AU from the Sun [24], with minimal variations in solar activity due to the short duration of the mission. Assuming a mean albedo coefficient for Earth of 0.4, a mean emissivity of 0.8, and an average temperature of 288 K [24] in space, the maximum and minimum heat fluxes at Earth's orbit were calculated, as reported in table 23.

**Commissioning, Science and Disposal phases:** these phases are characterized by low-altitude orbits around the Moon. The absence of atmosphere and low surface albedo induce a lunar Infrared (IR) thermal flux, comparable in magnitude to solar irradiance on the bright side [7]. On the other hand, the cold face of the Moon emits low thermal fluxes, around  $5 \text{ W/m}^2$ . Furthermore, during these phases the spacecraft reached full operational activity, where multiple subsystems worked simultaneously, with an increase in internal heat fluxes with respect to previous phases. This led to the design challenge of extreme thermal gradients during each orbit, ranging from intense heating in sunlight to deep cold during eclipse periods. The solar heat flux in these phases is the same as the previous case, following the same hypothesis. An albedo coefficient of the Moon of 0.136 [24] was considered to

compute  $q_{\text{albedo,Moon}}$ . The infrared emission was calculated assuming a surface emissivity of 0.864 and an average surface temperature of 330 K [24]. In table 23 both the computation for Commissioning and Science-Disposal orbits are proposed.

Phases	$q_{IR,Earth}$	$q_{\text{albedo,Earth}}$	$q_{IR,Moon}$	$q_{\text{albedo,Moon}}$	$q_{Sun}$
<b>LEOP, Transfer, LOA</b>	293.35	514.21	-	-	1367.5 [24]
<b>Commissioning, Science and Disposal</b>	-	-	444 – 548	142.15-175.72	1367.5 [24]

Table 23: Estimated Heat Fluxes along Mission Phases, in  $[W/m^2]$ .

### 6.2.3 Thermal Control per Mode

A fixed rotation around the Z body axis is implemented in **RAM Mode**, **TPC**, and **SSM**. This prevents prolonged solar exposure on the same face of the spacecraft that would result in localized overheating and reduced efficiency of the sun-facing solar panels. The same rotation allowed all external surfaces to periodically face deep space, enabling passive cooling. In contrast to the rotation performed in the modes mentioned, during **TCM**, the spacecraft maintains nearly inertial pointing toward Earth, resulting in sustained solar exposure and increased temperature over the Sun-facing surface. Despite the limited duration of the mode, around 1 hour, this configuration was found to be the sizing condition for the hot case in the thermal analysis [10]. Throughout the mission, heaters maintained non-operating components above survival temperatures, while keeping active ones within functional limits—especially during the **SSM** phase, when only essential systems were powered to reduce energy consumption.

## 6.3 Subsystem Sizing

### 6.3.1 Identification of Survival Thermal Ranges

The team first identified the minimum and maximum operating temperatures needed to ensure each component's survival and functionality, as summarized in the Table 24.

Subsystem	Component	$T_{min}$ [°C]	$T_{max}$ [°C]
<b>Payload</b>	NMS, UVS, LDEX, LLCD [7]	-20 (NMS, UVS, LDEX)	40 (NMS, LLCD)
<b>AOCS</b>	IMU, RWs, CSS, STA [39] [35]	-30 (RWs, STA)	60 (RWs, STA)
<b>TMTC</b>	MGA, LGAs, Transponder [27]	-30 (Transponder)	65 (Transponder)
<b>PS</b>	Tanks [24]	0	40
<b>EPS</b>	Battery [24], PCDU, Solar Panels	10 (Battery)	30 (Battery)
<b>OBDH</b>	OBDH [24]	-20	60
<b>Design</b>	-	-20	50

Table 24: Operating temperature ranges of spacecraft components.

Limiting temperatures are reported for each subsystem, with the critical components indicated in parentheses. Based on this table, the team selected the satellite's minimum and maximum temperature as input for the sizing. It is important to note that the chosen values do not represent the absolute worst-case  $T_{min}$  and  $T_{max}$  values. Instead, a milder range was selected. This approach is justified by the assumption that all components will be individually thermally controlled actively and passively.

### 6.3.2 Internal Power Dissipated per Mode

Table 25 shows the estimated internal power generated by each subsystem in different operational modes. The reported values account for the active components of each subsystem during the specific operational phases, also considering their relevant efficiencies when applicable. The worst-case scenarios for internal power dissipation are found in the Nominal mode, which shows the highest power generation due to active scientific operations and continuous subsystem use, and in the Thermal and Power Conditioning mode, which represents the lower bound for internal heat generation within the analysed mission phases.

Subsystem	NOM	SSM	TCM	DeltaVM	DeltaHM	RRM	TPC
P/L	41	0	0	0	0	0	0
AOCS	42.4	59.2	42.4	78.6	69.4	70	42.4
TTMTC	4.8	4.8	36.9	4.8	4.8	4.8	4.8
OBDH	15	15	15	15	15	15	15
EPS	238.0	238.0	238.0	238.0	238.0	238.0	238.0
PROPELLION	14.7	14.7	14.7	14.7	14.7	14.7	14.7
<b>TOTAL</b>	<b>355.8</b>	331.6	346.9	351.0	341.8	342.4	<b>314.8</b>

Table 25: Internal Power, in [W], dissipated by subsystem across different mission phases.

### 6.3.3 Mono-nodal analysis

The sizing is first conducted in steady state condition considering a mono-nodal sphere with same area as the real spacecraft and considering as heat sources the Sun and the Moon. The contribution of Earth's emitted and reflected radiation is neglected due to the large distance between the spacecraft and the Earth. Additionally, the solar flux is assumed to be equal to that at 1 AU, as the variation in distance between the Moon and Earth is negligible compared to the Sun-Earth distance. The resulting fluxes are reported in Tab 23. The values of  $\alpha_{SC}$  and  $\varepsilon_{SC}$  are both assumed to be 0.8 [58, 59], typical for solar panels, which cover most of the spacecraft's external surface.

**Hot case scenario** As reported in Sec. 6.2.3 the hot case scenario to be analysed is during NOM due to internal dissipation. The maximum hot-case temperature is computed from a power balance between absorbed solar flux, emitted power, and internal dissipation. Solar flux is assumed to irradiate only the spacecraft's cross-sectional area, while the surface not facing the Sun radiates to deep space, which is modelled as a blackbody at 3 K. The view factor with the Moon determines the fraction of the surface exposed to lunar infrared emission. The resulting temperature is 368.20 K, well above the allowable margin. The minimum area of a radiator is therefore evaluated considering body mounted radiators, according to LADEE architecture, with a  $\varepsilon_{rad}$  of 0.85 to be conservative.

$$A_{rad}^{\min} = \frac{Q_{\text{sun}} + Q_{\text{albedo}} + Q_{IR} + Q_{\text{int}} - \sigma \varepsilon_{sc} A_{\text{space}} [(T_{sc}^{\max} - 15K)^4 - T_{\text{space}}^4]}{\sigma (\varepsilon_{rad} - \varepsilon_{sc}) [(T_{sc}^{\max} - 15K)^4 - T_{\text{space}}^4]} \quad (12)$$

The resulting area from this calculation is 188.87 m<sup>2</sup>, which is clearly unfeasible, primarily due to the small difference between the spacecraft and radiator emissivities.

**Cold case scenario** The cold case might seem to be the Thermal and Power Conditioning Mode due to its low internal dissipation Table 25, but since it is activated only to cool down the spacecraft once it becomes too hot, the actual coldest temperatures occur during Sun Safe Mode (SSM), especially during eclipses. Proceeding with the power balance during eclipse, considering therefore only moon emissivity, spacecraft emission, internal generation and radiators emission, a predicted temperature of 137.27 K is computed, significantly below the minimum acceptable survival temperature for key components. The power needed for heaters to increase temperature to margin levels is computed through balance of heat transfer rates in Eq. 13.

$$Q_{heat}^{\min} = \sigma \varepsilon_{sc} A_{\text{space}} [(T_{sc}^{\min} + 15K)^4 - T_{\text{space}}^4] - Q_{\text{int}} - Q_{IR} + Q_{rad} \quad (13)$$

The minimum power needed, considering a margin of 25% (from ECSS), is 57 KW. The value is obviously unfeasible, mainly due to the unrealistic area computed for the radiators.

### 6.3.4 Multi-node analysis

The outcome of a mononodal approach is clearly not coherent with mission requirements, the reason could be based on the strong assumption introduced by the simple model. To further analyse the temperature range experienced with increasing accuracy and to study how the transient behaviour

affects the boundaries, a multi-node approach is proposed. LADEE geometry can be approximated as an elongated octagonal prism. Assuming that the bases can be neglected in the thermal analysis due to the greater height of the structure, eight nodes are considered, one for each lateral face. For each face, the same emissivity is assumed for the external and internal surfaces, ensuring a coherent internal radiative exchange model and simplifying the simulation structure.

The power balance is the following:

$$\rho_i V_i c_{Vi} \frac{\partial T_i}{\partial \tau} = Q_{sun,i} + Q_{IR,i} + Q_{albedo,i} - Q_{ds,i} + Q_{rad,net,i} + Q_{cond_{ik}} + Q_{cond_{is}} + Q_{int,i} \quad (14)$$

The above transient thermal balance equation includes the following additional terms:

- $Q_{rad,net,i}$ : net internal radiative power, defined as the net balance between the power radiated internally by the  $i$ -th face and the power irradiated onto it by the other  $j$  faces, taking into account the relative view factor  $F_{ij}$  between surfaces.
- $Q_{cond_{ik}} = -h_{cik} A_{cik} (T_i - T_k)$ : conductive exchange term between the  $i$ -th face and the adjacent  $k$ -th face, where  $h_{cik}$  represents the equivalent conductive coefficient, incorporating the material's thermal conductivity and the contact characteristics.

Regarding the already introduced contributions  $Q_{sun}$ ,  $Q_{IR}$ ,  $Q_{albedo}$ , and  $Q_{ds}$ , it should be noted that they are also specific to each individual face, hence the subscript  $i$ . Relative incident angles are introduced and updated during the simulation to capture their variability along the orbital motion, considering the relative position of each face with respect to the Sun, the Moon, and deep space over time, including also eclipses. Finally, for the term  $Q_{int}$ , the internally generated power is evenly distributed among all nodes.

**Hot case scenario** By numerically integrating the energy balance equations, the transient temperature profiles of the different nodes over time are obtained. The results are shown below:

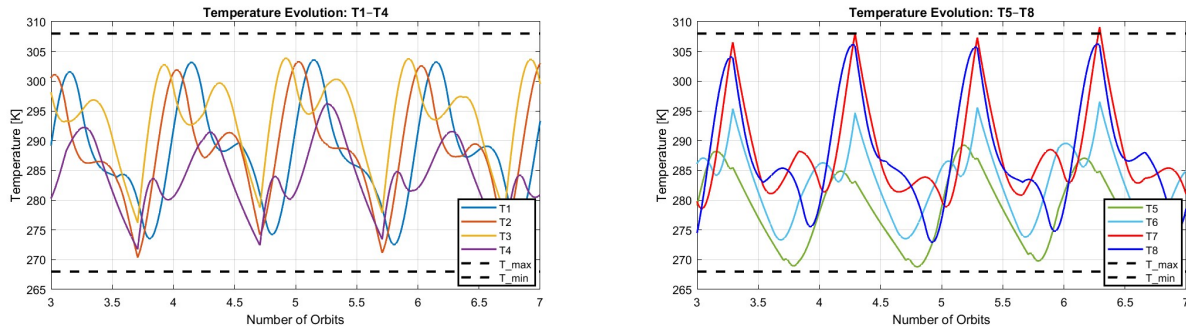


Figure 11: Temperatures during NOM.

The results refer to an extended period covering multiple orbits in the Nominal operational mode. The simulation assumes that the spacecraft completes one rotation per orbit about its Z-axis, consistent with the real configuration [7]. As expected, the temperature profiles exhibit a periodic repetition across successive orbits, with alternating positive and negative gradients driven by the cyclic transitions between eclipse and sunlit phases.

It is important to note that the simulation includes the use of radiators to control the thermal environment of the spacecraft. The radiator surface area was determined through an iterative process, adjusting its value until the node temperatures remained within acceptable limits under hot conditions while also avoiding an excessive reduction in the cold case scenario. In particular, the radiators were designed to dissipate the excess heat generated on nodes 1, 2, 7, and 8, which, according to the implemented eclipse modelling and the Sun and Moon interaction profiles with the spacecraft, result as the hottest surfaces during the orbit. Following the LADEE architecture, the radiator surface was not modelled as body-mounted on the eight lateral faces but rather as an additional radiative area. In the actual mission, this corresponds to the top face of the octagon, requiring appropriate heat

transport mechanisms to transfer the excess heat from the hottest nodes to this surface. The final radiator area implemented in the model was  $A_{rad} = 4.75, m^2$ , which is closer to the actual radiator area used on the spacecraft, approximated as  $A_{rad,real} = 2.42, m^2$ , compared to the value obtained in the previous single-node analysis. The thermal analysis shows that the maximum temperature reached during the simulation is  $T_{max} = 309.07 K$  on node 7, while the minimum temperature recorded is  $T_{min} = 268.83 K$  on node 5. Note that the simulation also required the activation of a heater on this last node to prevent excessive cooling during parts of the orbit. Although this represents an early design iteration, the thermal performance achieved is satisfactory, with node temperatures remaining within the expected operational limits.

**Cold case scenario** As for the mononodal analysis, the cold scenario refers to Sun Safe Mode (SSM). The results are the following:

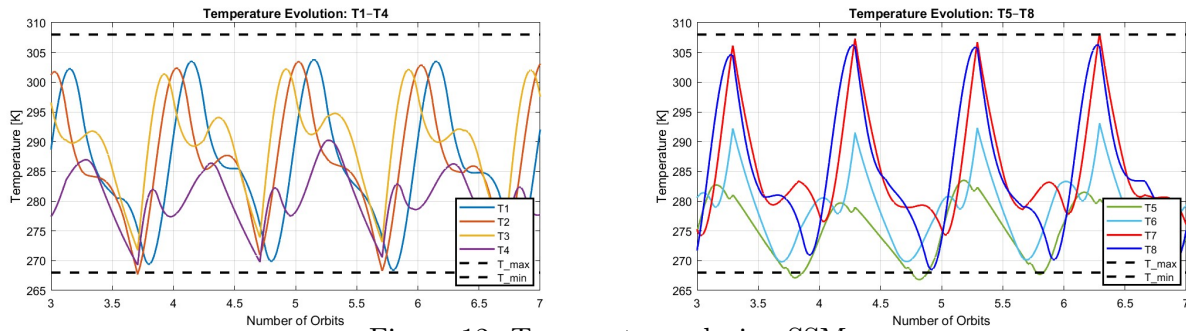


Figure 12: Temperatures during SSM.

To prevent temperatures from falling below the allowable limits, heaters were required on faces 2, 4, 5, and 7. This necessity arises from the modelled attitude dynamics and, in particular, the spacecraft's rotation about its own axis in lunar orbit relative to the Sun, which leaves these surfaces predominantly in shadow. Heater power levels were determined iteratively and configured to activate only when the surface temperature drops below a predefined threshold. The thermal simulations for the cold case yielded favourable results, with the maximum temperature recorded as  $T_{max} = 308.14 K$  and the minimum temperature as  $T_{min} = 267.73 K$ . However, the heater power consumption required to maintain these conditions was found to be  $Q_{heaters} = 275 W$ , which is clearly not compliant with the power availability of the spacecraft. Further investigation and optimization of the heater usage will be required in subsequent design iterations to ensure thermal limits are respected while remaining within the mission's power budget constraints.

#### 6.4 Mass, Power and Data budget

For the mass budget, only the radiator and the heaters are considered, and a margin of 20% is applied to consider the neglected components. The radiator was made of aluminum [60] and its mass was estimated based on the spacecraft geometry and assuming a uniform thickness of 1 mm. The estimated power budget is obtained by scaling down the total power obtained from sizing, which most likely does not reflect the actual power consumption as it refers to the whole spacecraft structure. For this reason, the required power of the heaters is set to 50 W and, considering an intermediate power to surface ratio and density from the datasheet [61], the overall mass of the heaters is computed.

Component	Power Consumption [W]	Mass [kg]
Radiator	—	6.53
Heaters	50	0.330
<b>Total with 20% margins</b>	<b>60</b>	<b>8.23</b>

Table 26: Mass and Power Budget.

For the data budget, the team considered every component to be monitored by a temperature sensor and the ability to communicate at least the temperature of the most critical ones, as listed in Table 24. The team assumed that each temperature sensor provides a 16-bit float data value, for a total of 352 bits required by TCS.

## 7 Electric Power Subsystem (EPS)

The LADEE's EPS is responsible for generating, distributing and storing energy for the spacecraft and its systems.

### 7.1 Architecture

The EPS prioritizes simplicity and fast integration, employing a Direct Energy Transfer (DET) architecture. Aside from the harness, it uses only Commercial Off-The-Shelf (COTS) or standard components, guiding the design, assembly, testing, and operations. All payloads and avionics units operate on an unregulated bus, with voltage following that of the battery; regulation and isolation are managed internally by each load [62]. The EPS follows the Single Point Ground (SPG) design philosophy, with all power returns isolated from the spacecraft body except at the single SPG point. All EPS functions are managed by the Integrated Avionics Unit (IAU) [63], developed by Moog Inc. [64].

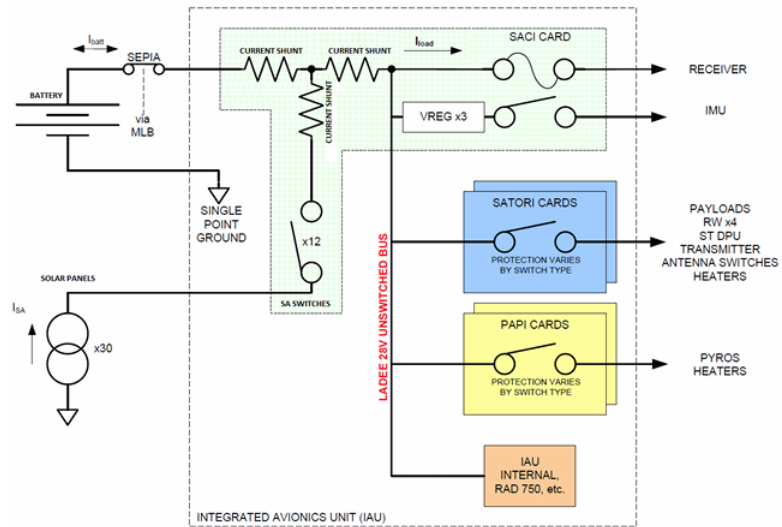


Figure 13: EPS architecture [62]

**Solar Panels:** The power generation on LADEE was performed by a body-fixed array of solar panels. It consists of 22 panels with  $22.3 \text{ cm}^2$  cells on the Payload Module, Extension Module and Single Stage Extension, and 8 panels on the bus module, each with  $27.5 \text{ cm}^2$  cells [7]. The system is capable of producing 295 Watts at 1 AU [12] and individually each panel generates about 1 A [62]. The gallium arsenide-based multi-junction solar cells [65] were made by EMCORE Corporation [66]. The cell datasheet is unavailable, so it is assumed to be the BTJ which has efficiency of 28.5% [53].

**Battery:** A lithium-ion battery, provided by ABSL Power Solutions Inc. [67], is configured in an 8S16P arrangement, with a capacity of 24 Ah, an energy content of 691 Wh, and a voltage range of 20 to 33.6 V, with a nominal voltage of 28 V [68]. The battery, with a mass of 6.8 kg , interfaces with the EPS through a component known as SEPIA.

**Power Distribution:** Within the IAU, three types of boards are dedicated to interfacing subsystems of the spacecraft and distributing the correct amount of power. In particular, the Solar Array and Charge control Interface (SACI) card interfaces the solar arrays with the battery, providing battery charge control and telemetry feedback capabilities. The SACI card measures  $112 \text{ mm} \times 218 \text{ mm} \times 36 \text{ mm}$  and has a mass of 0.32 kg [69]. It also includes the Solar Array (SA) switches, three current shunts and three voltage regulators, which are used to reduce the voltage for critical components such as the IMU [37]. Two Power-switching and Pyro Integration (PAPI) cards are used to power the heaters and the propulsion system. These cards are classified as Electronic Safe and Arm Devices (ESAD), meaning they are also designed to prevent accidental arming or firing of pyrotechnic devices by eliminating system sensitivities to environmental stimuli [70]. Finally, two SATORI boards power all the payloads and spacecraft operations, as well as the Command & Data Handling System [70].

**SA Switches:** The 30 solar panels are controlled by 12 SA switches. The SA switches can turn a set of solar panels ON or OFF to regulate the electrical current used to charge the battery [71].

**Current Shunts:** The LADEE spacecraft utilized current shunts in its EPS to measure onboard load, battery, and SA currents [62]. These low-resistance shunts measured voltage drops in order to determine the magnitude of currents. Furthermore, pairing the shunt resistors with controllable switches enables dynamic regulation of the power delivered to the bus, allowing the system to actively divert excess current when necessary.

## 7.2 Subsystem Rationale

The EPS of LADEE was designed with a strong emphasis on simplicity and reliability. It was prioritized the use of COTS wherever possible in order to reduce costs and minimize technical risks. The EPS was also intended to be modular and compatible with the MCSB, to allow the design to be repurposed in the future in similar small-scale missions. This brought to the selection of an unregulated power bus. This decision not only helped reduce costs but also facilitated the use of COTS components, since only a limited number of devices required precise voltage regulation. These specific needs were addressed separately, further reducing hardware complexity and associated costs. The nominal bus voltage of 28 V was selected as it was well suited to the total power requirements of the system, which remained far below 2 kW. Similar reasoning influenced the choice of a DET system over a more complex Peak Power Tracking approach. In this case, simplicity and cost-effectiveness were prioritized, with the understanding that additional power dissipation could be treated with thermal control. The spacecraft relied on body-mounted solar panels, avoiding additional deployment mechanisms and strict pointing requirements. This choice improved mechanical robustness and lowered the risk of mission failure due to moving parts. The solar panels were divided into 12 segments and connected to the switches so that a failure on a given switch cannot create a catastrophic failure in power generation. Although using 30 switches would have optimized reliability, the selection of a COTS IAU was the primary factor that limited this approach. For the same reason, only one current shunt was available for the entire SA string [62]. The placement of components within the spacecraft was primarily driven by thermal considerations. Located within the Radiator Module [10], both the IAU and the battery benefited from a thermally regulated environment.

## 7.3 Power per Phase and Mode

In this section is described power demand across mission phases to better highlight key events and related average powers.

**LEOP, Transfer, LOA:** Starting with detumbling, AOCS (84 W) worked continuously to reduce angular rates until a stable attitude was achieved, and solar generation could be relied upon. After the detumbling, payload testing (54 W) was carried out, and the TMTC radios (47 W) came online to transmit health-status telemetry and receive frequent telecommands to update the trajectory. Throughout detumbling and into transfer and LOA, the OBDH (15.8 W) remained active to handle telemetry, command sequencing and health monitoring, while the TCS (52.5 W) powered survival heaters when needed to mitigate temperature swings. During transfer and LOI, the AOCS continued providing precise attitude determination and corrections (43 W), whereas the OCS of the propulsion subsystem (26 W) executed sequential perigee manoeuvres and the Moon-approach insertion burn. Assuming estimated usage percentages relative to the duration of each phase, the average power consumption was calculated as 149 W, 119 W, and 113 W respectively.

**Commissioning, Science, Disposal:** during commissioning, the AOCS (43 W) ensured fine pointing for LLCD alignment to execute the high-power optical link tests (141 W). In the science phase, the alternation of NMS/LDEX (45 W) and UVS (14 W) was planned according to observation schedules, while specific time slots were allocated for TMTC (40.5 W in transmission, 7 W in receiving). During Disposal, the Propulsion System (67 W) performed the deorbit burn. Across all three phases, the OBDH (15 W) remained active for command and data handling. The TCS (52.5 W)

powered heaters when needed to maintain thermal control. The AOCS and PS also introduced moderate additional loads (84 W, 67 W) every few days due to reaction wheel desaturation and OMMs. Assuming phase-duration usage profiles, the average power consumption for Commissioning, Science, and Disposal was estimated as 219 W, 128 W, and 157 W, respectively.

The higher average of disposal with respect to science is related to a higher telecommand and propulsion subsystem usage due to the phase criticality and very low altitude. As expected, the most demanding phase is Commissioning, where the LLCD's high power requirements may necessitate a dedicated operational profile to ensure sufficient energy availability. The MAR-PWR-010 for single peak power per component and the MAR-PWR-040 for the average power were considered.

Regarding operational modes, a detailed power budget is presented in Sec.7.5.1. However, similar correlations of mode-specific and phase-specific power demands with the EPS architecture can be drawn. The maximum power generation capability of the body-mounted solar panels (295 W) [7] aligns with the estimated average and peak loads across mission phases/modes, confirming that, despite the limitations in panel area due to body-mounting, the architecture can support the expected loads with potential support from the onboard battery. Regarding the battery, it was likely treated as the primary power source during detumbling (Delta-H mode) and the initial portion of LEOP, when the spacecraft's attitude was uncertain and solar input could not be reliably guaranteed. Based on the estimated average power consumption of 162 W with margins and assuming a 60-minute duration, capacity needed for this period is 162 Wh, corresponding to a Depth of Discharge (DoD) of about 23%, consistent with operational limits considered. Following similar evaluation for eclipses (both in Commissioning and Science phase), a DoD of around 15% is estimated, which also in this case remains well within the system's limits. A final interconnection between power per phase/mode and EPS architecture is related to the unregulated bus, that is preferred when no frequent oscillations in terms of downstream power demands are expected.

## 7.4 Operational Profiles and Available Sources

Following a chronological perspective, specific operational profiles may be required in initial and science phase. In particular, as already mentioned, during the detumbling phase solar power generation is likely limited due to uncontrolled spacecraft orientation. Consequently, it is reasonable to assume that the battery acted as the primary power source during this period, either partially or fully. A similar energy management scheme applies during the sunlit–eclipse–sunlit orbital cycle. While SAs provide power during illuminated segments, the battery is required to sustain the spacecraft loads throughout eclipse periods. Subsequent recharging phases are essential to restore battery charge levels. Supporting this assumption, as stated in [3], a portion of the daily orbits was explicitly allocated to power regeneration activities.

In terms of available sources, a distinction can be made between primary and secondary. The primary source is the Sun, with LADEE operating at approximately 1 AU, implying a relatively stable solar irradiance. Therefore, variations in power generation are mainly due to eclipse periods and spacecraft attitude rather than distance. Thanks to the body-mounted configuration of the solar panels, aspect angle sensitivity is hugely reduced. Flexibility is higher around the pitch and yaw axes, while roll deviations could expose top/bottom faces, not provided of solar panels. However, pointing constraints along different modes and those adopted during power regeneration phases help mitigate this issue, making additional sun-pointing requirements unnecessary. The secondary source is the battery, which supports the power system whenever solar generation is unavailable or insufficient.

## 7.5 Subsystem Sizing

### 7.5.1 Average Power per Mode

The team evaluated the average power demanded for each operational mode. This was done by multiplying the component's power consumption by its operating time per orbit and dividing the result by the orbital period. Design maturity margins of 5%, 10%, and 20% were applied according

to European Cooperation for Space Standardization (ECSS) standards, depending on whether the components were COTS, modified COTS, or newly designed, respectively. The complete power budget was calculated for all possible modes and the most representative are presented in Table 27.

Comp.	Power	Margin	NOM	SSM	TCM (LLCD)	DeltaVM	TPC	Eclipse
P/Ls								
NMS	36 [7]	+10%	16.5	0.0	0.0	0.0	0.0	0
LDEX	5 [7]	+10%	5.5	0.0	0.0	0.0	0.0	0
UVS	13 [7]	+10%	2.7	0.0	0.0	0.0	0.0	0
LLCD	141 [7]	+20%	0.0	0.0	38.3	0.0	0.0	38.3
AOCS								
RWs	12 [48]	+5%	12.6	12.6	12.6	12.6	12.6	12.6
GYROS	4	+5%	4.2	4.2	4.2	0.0	4.2	4.2
STA	20 [35]	+5%	21.0	0.0	21.0	21.0	21.0	21.0
IMU	12 [37]	+5%	0.0	12.6	0.0	12.6	0.0	0.0
RCS	44 [14]	+5%	0.0	0.0	0.0	1.7	0.0	0
TMTC								
Rx	6.3 [27]	+20%	3.1	3.1	5.0	3.1	3.1	5.0
Tx	36.75 [27]	+20%	0	0	0	0	0	0
OBDH								
Avionics	15 [24]	+5%	15.8	15.8	15.8	15.8	15.8	15.8
PS								
OCS	9.8 [14]	+5%	0.0	0.0	0.0	0.4	0.0	0.0
Valves	7.7 - 37.7	+5%	8.0	8.0	8.0	9.2	8.0	8.0
TCS								
Heaters	50	+5%	0.0	0.0	0.0	0.0	0.0	17.8
TEC	9.5 [72]	+5%	5.9	5.9	6.6	5.9	5.9	0.0
TOT			95.2	62.2	111.5	82.2	70.6	122.7
+20% Margin			114.3	74.6	133.8	98.6	84.7	147.2

Table 27: Average Power Budget per Mode in [W]

It is important to note that the TCM is analysed only for the LLCD configuration, representing the worst-case scenario compared to MGA, and corresponding to the most demanding sunlight and eclipse conditions. This case serves as the baseline for power sizing with relative eclipse condition. Although the power-intensive PS and RCS subsystems have short operational durations (max burn: 252.6 s [7]), they do not significantly affect average power. However, associated valves also consume power, some draw constant power (8 W), while others only during actuation. The LLCD operates for maximum 30 minutes per orbit [7]; the NMS, about 45 minutes [7]. No exact durations are available for LDEX and UVS; based on mission data [21], LDEX is assumed nearly always active, while UVS is considered operational approximately 25% of the time. Additionally, the SACI and PAPI cards are part of the avionics subsystem [69]. As expected, SSM and TPC are the least power-demanding modes, with the former prioritizing efficiency and the latter thermal control.

### 7.5.2 Solar Panels Sizing

The preliminary sizing of the solar panels is realized considering the body-mounted SA to be present on the lateral surface of the spacecraft only, which is approximated as an octagonal prism. The solar panels must provide enough power during sunlight of one orbit to satisfy the request during the entirety of the same orbit, both at the beginning and end of life. The power that must be produced by the solar array is the following:

$$P_{SA} = \frac{\frac{P_{sunlight} T_{sunlight}}{X_{sunlight}} + \frac{P_{eclipse} T_{eclipse}}{X_{eclipse}}}{T_{sunlight}} \quad (15)$$

Where  $P_{sunlight}$  and  $P_{eclipse}$  are retrieved from Sec. 7.5.1 respectively 133.8 W and 147.2 W. The efficiencies of the DET architecture  $X_{sunlight}$  and  $X_{eclipse}$  are set to 0.85 and 0.65 respectively [24].

$T_{sunlight}$  and  $T_{eclipse}$  represent the time of the orbit of sunlight and eclipse. It is possible to compute the power flux at Beginning of Life (BOL) and End of Life (EOL):

$$P_{BOL} = \varepsilon P_0 I_d \cos(\theta) \quad [\text{W/m}^2] \quad ; \quad P_{EOL} = (1 - dpy)^{years} P_{BOL} \quad [\text{W/m}^2] \quad (16)$$

Where  $\varepsilon$  is the efficiency of the S/Cs, mentioned in Sec. 7.1,  $I_d$  is the degradation factor set to 0.7, the annual degradation  $dpy$  is 3% and  $P_0$  is the solar flux at 1 AU from the Sun [24]. This formulation refers to a flat plate, but the panels are placed along the faces of an octagon, where no more than four of the eight panels at the time are illuminated, each with a different solar aspect angle. For this reason, an equivalent solar aspect angle  $\theta_{eq}$  is introduced. The angle  $\theta_{eq}$  is defined such that a flat surface, equal in area to four panels and tilted by  $\theta_{eq}$ , would present the same effective area to the Sun as the four panels arranged in the octagonal configuration. The configuration that presents the smallest surface toward the Sun, and so the smallest power production, among all possible rotations of the octagon around its centre, was found to occur when one surface is directed toward the Sun and the two adjacent ones have a solar aspect angle of 45°. Hence, given the area of a single panel A, the equivalent angle is  $\theta_{eq} = \arccos\left(\frac{S_{seen\ from\ Sun}}{S_{tot}}\right) = \arccos\left(\frac{(1+\sqrt{2})A}{4A}\right) = 52.88^\circ$ . Hence, the area needed for the solar panels is computed as:  $A_{SA} = \frac{P_{SA}}{P_{EOL}}$ . Now a more in-depth sizing of the solar arrays can be realized, imposing that the nominal voltage of the bus of 28V [7] must be guaranteed, due to its unregulated nature. The number of S/C connected in series and parallel is computed as:

$$N_{SC} = \frac{A_{SA}}{A_{SC}} \quad N_{SC, series} = \left\lceil \frac{V_{bus}}{V_{SC, max}} \right\rceil \quad N_{SC, parallel} = \left\lceil \frac{N_{SC}}{N_{SC, series}} \right\rceil + 1 \quad (17)$$

Where the voltage of a single cell is 2.37 V [68] and  $N_{SC, parallel}$  is augmented by 1 to account for the single-string failure margin. So, now it is possible to compute the real solar array surface, the power produced at the beginning and end of life, and the total mass:

$$N_{SC, real} = N_{SC, series} N_{SC, parallel} \quad ; \quad A_{SA, real} = N_{SC, real} A_{SC} \quad ; \quad M_{SA} = \frac{P_{BOL} A_{SA, real}}{\text{Specific Power}} \quad (18)$$

Where the specific power of the array is assumed to be 90 W/kg, according to the literature [24, 73]. It is important to notice that, since this approach is valid for only four panels, the total number of cells, the solar array surface and mass are doubled to include the entire octagon.

### 7.5.3 Battery Sizing

The sizing of the lithium-ion battery must ensure that the total energy is enough to satisfy the power requirements during the eclipse:

$$E_{battery} = \frac{\frac{P_{eclipse} T_{eclipse}}{X_{eclipse}}}{DoD \cdot \eta} \quad (19)$$

Where the DoD for a mission like LADEE, with less than 2000 cycles, can be as high as 100%, but it is initially set to 80% to be more conservative. The efficiency of the battery is 80% [58, 74]. The number of Battery Cell (BC) connected in series and in parallel is retrieved as follows:

$$N_{BC, series} = \left\lceil \frac{V_{bus}}{V_{BC}} \right\rceil; \quad E_{string} = \mu C_{BC} (N_{BC, series} V_{BC}); \quad N_{BC, parallel} = \left\lceil \frac{E_{battery}}{E_{string}} \right\rceil + 1 \quad (20)$$

Where  $V_{BC} = 3.6$  V and  $C_{BC} = 1.5$  Ah are respectively the maximum voltage and the capacity of a single 18650HC(M) BC [73, 58];  $\mu = 0.8$  represents the packing energy factor [24]. Finally, a refinement can be made by considering the maximum peak power condition during LLCD operations, of around 380.8 W: noting that under the minimum bus voltage condition of 20 V [68], the required current  $i_{max, required}$  of 19.04 A exceeds the capability of the currently sized battery, 13.50 A, as each string of cell will grant maximum  $i_{max, BC}$ . To ensure the system can deliver this current, additional parallel strings are needed. The values of  $N_{BC, parallel}$  and  $N_{BC}$  are updated:

$$i_{max, required} = \frac{P_{max}}{V_{bus, min}}; \quad N_{BC, parallel} = \left\lceil \frac{i_{max, required}}{i_{BC, max}} \right\rceil + 1; \quad N_{BC, real} = N_{BC, series} N_{BC, parallel} \quad (21)$$

From this result, the energy and mass of the battery is computed, taking into account a specific energy of 133 Wh/kg, based on information on the 18650HC(M) battery cell [73].

$$E_{real} = E_{string} N_{BC,parallel} ; M_{battery} = \frac{E_{real}}{E_{sp,BC}} \quad (22)$$

From the incremented value of the battery capacity energy, a lower DoD is retrieved inverting eq 19.

## 7.6 Sizing results

Parameter	Value
$T_{orbit}$	2.21 h
$T_{eclipse}$	0.75 h
$T_{sunlight}$	1.46 h
$X_{sunlight}$	0.85
$X_{eclipse}$	0.65
$P_0$	1367.5 W/m <sup>2</sup>
$I_d$	0.7
$\theta_{eq}$	52.88°
$dpy$	0.49 y [7]
$d$	0.03 [24]
$V_{bus}$	28 V [7]
$P_{sp,SC}$	90 W/m <sup>2</sup> [58]
$E_{sp,BC}$	133 Wh/kg

Table 28: Data

Parameter	Value
$A_{SC}$	27.50 cm <sup>2</sup> [7]
$V_{SC,max}$	2.37 V [53]
$\varepsilon_{SC}$	0.285 [53]
$P_{SA}$	273.34 W
$P_{BOL}$	164.66 W/m <sup>2</sup>
$P_{EOL}$	162.20 W/m <sup>2</sup>
$N_{SC,series}$	12
$N_{SC,parallel}$	53
$N_{SC,real}$	1272
$A_{SA}$	3.67 m <sup>2</sup>
$P_{BOL}$	287.99 W
$P_{EOL}$	283.69 W
$M_{SA}$	6.40 kg

Table 29: Solar Array Data

Parameter	Value
$DOD$	43.75%
$\eta$	0.80 [58]
$\mu$	0.8 [58]
$V_{BC,battery}$	3.60 V [58]
$i_{BC,max}$	1.50 A
$C_{BC}$	1.50 Ah [73]
$N_{BC,series}$	8
$N_{BC,parallel}$	14
$N_{BC,real}$	112
$i_{max,required}$	19.04 A
$E_{battery,real}$	483.84 Wh
$M_{battery,real}$	3.64 kg
$V_{battery}$	1.61 L

Table 30: Battery Data

The results show that the power demand is consistent with the real mission, nominally 295 W. The computed solar array area takes into account a 5% margin for inert surfaces. The results are compliant with the actual array surface of LADEE, which is estimated to be roughly 3.8 m<sup>2</sup> and the total number of cells around 1300. As for the battery, the actual LADEE unit had 691 Wh of energy, 24 Ah capacity, and a mass of 6.8 kg, values notably higher than those derived in this analysis. This discrepancy likely stems from the full lunar eclipse experienced during the Extended Science phase, which prevented recharging for over 4 hours. Other possible reasons include the high power demand of the LLCD (in its first flight), and a design choice to ensure multiple orbits of autonomy for fault tolerance. As a COTS component, it likely met requirements with a good cost-performance trade-off, although performance were higher.

## 7.7 Mass, Power and Data budgets

A 25% margin on total mass is included to account for harnesses and cabling. For the data budget, voltage and current telemetry from all key EPS components is considered to ensure mission reliability. Current is monitored via shunt sensors on each solar array segment (see Sec. 7.1), as well as on the battery and main load bus, totalling 14 measurements. Voltage is measured at the same points, with an additional sensor on the unregulated bus to monitor critical levels for onboard systems. All values are transmitted as 32-bit floats, resulting in a total EPS data rate of about 928 bits/s.

Component	Mass [kg]	Power [W]
Solar Panels	6.40	-
Battery	6.8	-
IAU	0.98	15
<b>Total + 25% margin</b>	<b>17.73</b>	-

Table 31: Subsystem mass and power budget

## 8 OBDH

LADEE's OBDH has the task to gather, save and eventually protect both Engineering and Scientific Data but also to distribute instructions and operations scheduling along mission duration.

### 8.1 OBDH Architecture and Rationale

The OBDH subsystem has two main functionalities for LADEE: executing the Flight Software (FSW), which involved multiple internal operations, and managing communications to and from the ground [75]. Most of these operations are instructed directly from electronics components contained in the IAU, namely a Single Board Computer (SBC) card hosting a Rad750 Central Processing Unit (CPU), a SACI board, 2 PAPIs boards, 2 SATORI boards, a Digital Multi Operations Avionics Board (DMOAB), an Analog Multi Operations Avionics Board (AMOAB) and 1 spare slot as shown in Fig. 14.

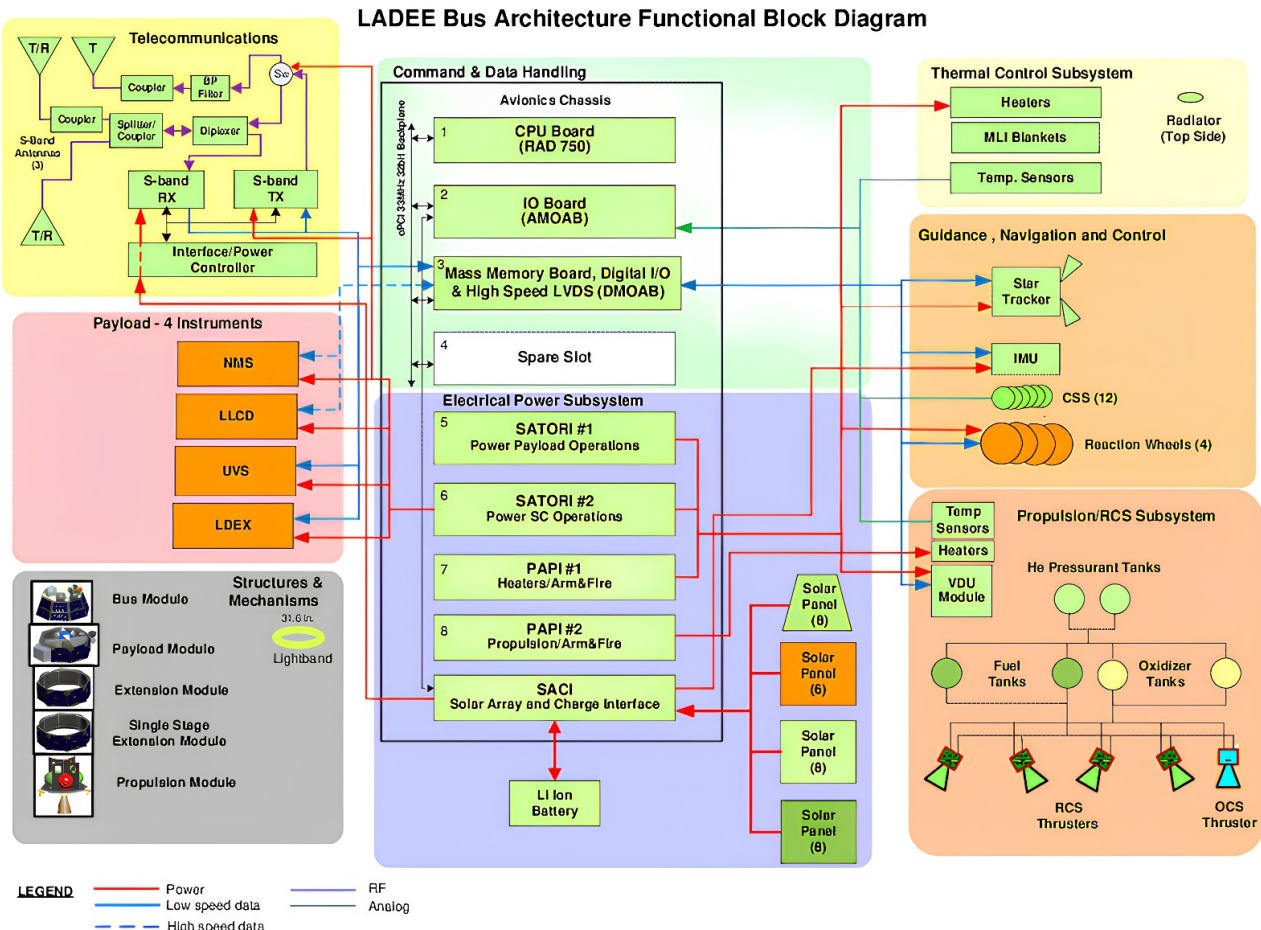


Figure 14: OBDH architecture [76]

**CPU:** The main CPU is the 3U RAD750, produced by BAE Systems Electronics. It was populated with a 128 MiB of SDRAM and supported error detection using Nibble detection, without the possibility of correction. The COTS On Board Computer (OBC) hosts the FSW and controls most of the spacecraft instructions, comprised AOCS related. The RAD750 was among the highest-performing microprocessors available at the time of the mission, delivering over 400 MIPS at 200 MHz. Moreover, it is a highly reliable component, with proven flight heritage from several other successful missions

and high radiation resistance of 1 Mrad. The choice of a very reliable COTS component with flight heritage results consistent with LADEE's safe design philosophy and low budget.

**I/O Interfaces and Memory:** Both the AMOAB and DMOAB could perform multiple functionalities and their flexibility was a driver for their selection [77]. The AMOAB interfaces' temperature sensors, which usually return an analog signals, substituting multiple local Analog to Digital Converters (ADCs) with the board. On the opposite, the DMOAB had the task to interface the CPUs to the remainder of the digital signals. Furthermore, both the Multi Operations Avionics Boards (MOABs) boards could cover the role of mass storage system, each with 12 GB of Flash memory [77], but, as expressed in Fig. 14, it is possible that only the DMOAB stored data [77]. This choice is most probably related to the higher need of saving digital data, both engineering and scientific, and that only one mass memory could grant enough data space for the whole satellite, as will be investigated in Sec. 8.2. The DMOAB was also protected following the Single-Error Correct Double-Error Detect (SECDED) algorithm for the SDRAM and SRAM and Triple Modular Redundancy (TMR), allowing safer data transmission and storage from single-bit errors.

The OBC interfaced with the EPS through the SACI, PAPI and SATORI boards, each of them comprised in the EPS had the task of controlling and distributing power each to specific subsystems or part of the spacecraft. It is worth noting that also the SACI board could distribute a limited number of instructions to PAPI and SATORI boards [69], showing the presence of a microprocessor. Again, the OBC interfaced the PS through the Valve Driver Unit (VDU) module, which controlled the valves of the subsystem.

**Payload electronics:** The NMS used a radiation-hardened, 32-bit Coldfire microprocessor with 2 MB of Static RAM (SRAM), 32 KB of Programmable ROM (PROM), for bootloader, and 1 MB of Electrically Erasable PROM (EEPROM), for flight software and scripts. It featured 2 high-precision 16-bit ADC for sensor data, 15 Digital-to-Analog Converters (DACs) to control elements like filaments and Radio Frequency (RF) systems.

The UVS used an embedded 8051 microcontroller integrated within a radiation-tolerant Actel RTAX2000S Field Programmable Gate Array (FPGA). It was supported by an external 32 KB PROM and included internal RAM with error correction. The FPGA handled timing, instrument control, and data coordination, using a First In First Out (FIFO) buffer to manage data flow and prevent loss during high-rate acquisition.

The LLCD used a Virtex-4 FPGA to handle both downlink (up to 622 Mbps) and uplink (20 Mbps) data processing, performing all encoding, decoding, and timing control within a single high-speed, reprogrammable chip.

The LDEX used an FPGA to handle all logic, data processing, and command execution. Though no microprocessor's name was found in literature, the FPGA managed 16-bit ADC inputs and stored data in SRAM [7, 78].

The payload OBDH design on LADEE was based on each instrument's needs. NMS used a Coldfire microprocessor for flexible control and scripting, while UVS used an 8051 microcontroller inside an FPGA for timing and data handling. LDEX and LLCD used FPGA to manage fast data processing without separate processors. These choices followed standard design logic: use local processing when performance is critical, and use FPGA for high-speed or specialized tasks. FPGA also allowed in-flight reconfiguration, which helped with fault recovery or updates during the mission.

**Data Flow Architecture:** All modules of the Command and Data Handling (C&DH) subsystem are interconnected via a compact PCI backplane bus operating at a clock speed of 33 MHz with a data width of 32 bit [76]. This bus is based on the Peripheral Component Interconnect (PCI) 2.1 standard, which implies that all data transfers occur synchronously, according to a system clock. Communication between the OBDH subsystem and other subsystems, such as telemetry and payload, is established through RS-422 bus interfaces. This is a protocol for serial data communication that uses two wires with a differential and point-to-point full duplex line with a maximum bit rate of 10 Mbps. However,

as illustrated in Fig. 14, the NMS and LLCD subsystems employ high-speed data links. While the NMS link also uses RS-422 since its data rate requirement, presented in the previous paragraph, is lower than the maximum, the LLCD requires data transfer rates up to 622 Mbps, exceeding the capabilities of RS-422. Consequently, a different communication system is utilized for the LLCD; however, no further details are available regarding this system [7]. This method of data handling suggests a centralized architecture, as all data originating from other subsystems are independently connected to the I/O boards. However, within the IAU, the cPCI is acting as a distributed bus for internal data management.

The decision to implement a centralized configuration is primarily driven by the high reliability it provides, while also allowing failures to impact only a single line without requiring excessive redundancy. The choice of a cPCI backplane is mainly due to the use of commercial off-the-shelf (COTS) components, which aligns well with the architecture as it connects all parts of the C&DH system and supports fast, high-speed data transfer. On the other hand, the use of the RS-422 serial interface simplified hardware development and reduced risk. It eliminated the need for additional wiring, complex cable routing, and the extra weight associated with modifying command or status connections during development [19]. Furthermore, the RS-422 standard uses differential signalling, where data is transmitted as the voltage difference between two wires, reducing noise and ensuring secure communication.

**Software (SW):** The FSW was developed using MATLAB Simulink and implemented in C for the spacecraft's main CPU, while BASIC is used for some peripheral microprocessors. The transition from Simulink models to C code was achieved through auto-coding, which help reduce reliance on highly experienced software engineers, albeit at the expense of lower SW efficiency. However, auto-coding facilitated easier debugging and faster implementation of modifications, contributing to overall cost savings.

## 8.2 OBDH Sizing

The objective of the OBDH sizing analysis is to determine the total volume of data generated on board during the scientific phase of the mission. For each subsystem, the equipment responsible for producing stored data is analysed. The number of values  $n$ , data type, bit size, and sampling frequency are identified for each relevant element, and the corresponding datarate is calculated as the product of these parameters. The only exception is the P/L, for which datarate values were directly obtained from literature sources [7]. Elements operating with event-based logic do not contribute to the overall datarate, as they lack a defined sampling frequency.

A conservative margin of 400% is applied to the total datarate. Finally, the required mass memory is estimated by multiplying the margined datarate by the maximum duration between downlink windows during the scientific phase, approximately 17 hours [3].

The result is a required mass memory of 8.65 GB, compared to the 12 GB of Flash memory actually installed on board, as mentioned in Section 8.1. This discrepancy may be explained by the fact that, during science-mode communications and the LLCD demonstration, a portion of the uplink data could also be stored in mass memory. This additional contribution may justify the larger memory installed, considering that the uplink datarate is 8 kbit/s for nominal communications and up to 20 Mbit/s for the LLCD, both non-negligible values compared to others listed in Table [7]. However, these contributions were not considered in this analysis, as the focus of this section is to size the data volume generated onboard. Another factor to consider is that the sizing refers strictly to the nominal scientific phase. It is possible that the commissioning phase may require additional memory, due to the high uplink datarate of the LLCD, despite the shorter intervals between communication windows.

Parameter name	n.	Data Type	Bit Size	Frequency [Hz]	Datarate [bps]
<b>EPS</b>					
Battery Temperature	2	sint16	16	0,5	16
Battery Current	1	sint16	16	1	16
Battery Voltage	1	sint16	16	1	16
Bus Voltage	1	sint16	16	1	16
Solar Arrays Current	30	sint16	16	1	480
Current Shunts Voltages (DET)	3	sint16	16	1	48
Voltage Regulators	3	sint16	16	1	48
SA temp sensors	30	sint16	16	1	480
SA switches	12	Boolean	1	event-based	0
<b>TCS</b>					
Heaters Voltage	12	sint16	16	1	192
TECs Voltage	1	sint16	16	1	16
<b>AOCS</b>					
STA	4	float32	32	1	128
CSS	12	sint16	16	2	384
IMU	6	float32	32	10	1920
MEMS gyro (in RW)	4	float32	32	10	1280
Control mode ID	1	uint8	8	event-based	0
Estimated quaternion	4	float32	32	10	1280
Estimated Sun vector	3	float32	32	2	192
Estimated angular rates	3	float32	32	10	960
IMU current	1	sint16	16	1	16
IMU voltage	1	sint16	16	1	16
IMU temperature	1	sint16	16	0,5	8
RW saturation flag	1	Boolean	1	event-based	0
Orbit Propagation	6	float32	32	1	192
<b>P/L</b>					
NMS	[ - ]	float32	32	[ - ]	3500
LDEX	[ - ]	uint16	16	[ - ]	200000
UVS	[ - ]	float32	32	[ - ]	14700
LLCD	[ - ]	float32	32	[ - ]	[ - ]
<b>PS</b>					
Latch valves	9	Boolean	1	1	9
Pyro Valves	1	Boolean	1	event-based	0
Tanks Temperature sensors	10	sint16	16	0,5	80
Tank pressure transducers	2	sint16	16	1	32
<b>TMTC</b>					
Transfer Switch	1	Boolean	1	event-based	0
Transponder voltage	1	sint16	16	1	16
Temperature sensor	1	sint16	16	0,5	8
<b>OBDH</b>					
OBC temp	1	sint16	16	0,5	8
OBC voltage	1	sint16	16	1	16
OBC current	1	sint16	16	1	16
Boot count	1	uint16	16	event-based	0
Boot cause	1	sint16	16	event-based	0

Parameter name	n.	Data Type	Bit Size	Frequency [Hz]	Datarate [bps]
Watchdog	1	uint16	16	1	16
On-Board-Time	1	uint16	16	1	16
Stored packed count	1	uint16	16	1	16
<b>TOT [bps]</b>					226137
<b>TOT WITH MARGIN [bps]</b>					1130685
<b>TOT [GB]</b>					8,65

## 9 LADEE Structure

The LADEE spacecraft bus derives from the MCSB, a small, low-cost spacecraft architecture. It consists of Radiator Module, which carries the avionics, electrical system and sensors; Bus Module; Payload Module, which carries the LLCD and NMS; two Extension Modules, which house the PS, and the Propulsion Module [7].

### 9.1 Primary Structure

The primary structure is the main that transmits loads to the base of the satellite and also defines its overall stiffness. The primary structure of LADEE consists of the five common spacecraft bus modules of the MCSB. The bus has a mass of  $191, 1\text{kg}$ , including the inert mass of the propulsion system [12]. The four main modules are interconnected to each other. Some of the modules are hollow, while others contain additional Cruciform crossbeam internal panels. The Cruciform improves the overall structural stability and resilience to external loads, and acts as an integral electrical and thermal conductor to the face sheets. The fifth module, the Propulsion Module, consists of the spacecraft bottom deck and the Thrust Cruciform and houses the tanks. Each module is structurally designed and interconnected to accommodate launch loads and provide attenuation of impact loads [63].

**Materials:** The main bus is constructed from lightweight carbon composite, primarily selected for its high strength-to-weight ratio and good resistance to fatigue and stress corrosion [63]. Although it has low erosion resistance, this is not a concern given the absence of atmospheric oxygen during the Moon phase, and the short duration of the Earth phase. These characteristics align well with the mission requirements, which demand a light structure capable of withstanding various mechanical loads. Furthermore, its mechanical properties are not significantly affected by rapid temperature changes [79], which is important considering the lunar environment. The main drawbacks of the material chosen are its anisotropy, high cost and poor electrical conductivity. The former is addressed by carefully aligning the fibers along expected load paths. Thin layers of pure aluminum foil, bonded to the composite with a strong, non-conductive adhesive, enhance the poor electrical conductivity [63]. Although cost may seem in contradiction with mission constraints, the unique advantages of the material make it a justified choice for key structural elements where strength, durability, and weight savings are essential. The propulsion housing is made of M55J carbon-cyanate fiber composite, which shares the same characteristics described above, but it also provides increased stiffness to prevent vibrations at natural frequencies [80].

### 9.2 Secondary structure

The secondary structure includes elements attached to the primary structure that locally improve the structural integrity, but contribute negligibly to the transfer of global loads.

**Radiator Deck:** It serves as the mounting platform for the avionics, battery, attitude sensors, the UVS, and the LDEX. It is located on top of the Bus Module [7], with the primary function of dissipating excess heat and ensure the stability of the instruments mounted on it. Hence, the panel must withstand the loads it encounters, but it is not considered a primary structural element due to its small contribution to the overall stiffness.

**Composite panels:** as mentioned in Sec 9.1, structural panels are present in the internal part of some faces of the MCSB. These panels act as additional structural elements and interfaces for electrical grounding [63]. As they serve to structurally reinforce only few internal faces areas, they are considered a secondary structural element.

**Body-Mounted Solar Arrays:** It is mounted over the entire lateral surface of the MCSB modules and is designed for both energy generation and thermal control. As a secondary structure, it must withstand some local loads; however, being body-mounted, they experience lower dynamic loads and higher reliability compared to deployable arrays. Each MCSB module includes provisions for interfacing with the solar panels, allowing them to be installed or removed at any time. This feature facilitates access to the spacecraft's interior [7, 63].

**Structural inserts and fittings:** Inserts are placed between the panels, with the scope of carrying part of the mechanical loads. The inserts are adhesively bonded into the panels by a high strength epoxy that acts also as an electrical insulator [63]. On the other hand, interface fittings connect and secure different parts of the spacecraft, in particular adjacent panels [80].

**Materials:** The radiator deck is a large, single piece of aluminum. This material is ideal due to its high strength-to-weight ratio, low cost, and excellent thermal and electrical conductivity [81]. These properties justify the selection of aluminum considering the mission requirements described in Sec. 9.1. However, while aluminum's high thermal conductivity helps distribute heat evenly, its low emissivity is a drawback. Although the specific aluminum type is unknown, it likely received a surface treatment to increase emissivity, which is common practice.

The panels material is T300 carbon fiber reinforced with TenCate RS-3C epoxy resin, which shares the same performances of the main bus discussed in Sec. 9.1. In addition, it has low thermal distortion, ensuring the pointing accuracies of observational instruments [80]. The inserts and fittings are made of bonded aluminum and machined titanium, respectively [80]. Aluminum is used to support loads and increase conductivity, while titanium provides high strength where needed.

### 9.3 Tertiary structure

The tertiary structure refers to those appendages and items specifically designed to hold equipment with low natural frequencies, which interact with the dynamics of the satellite. LADEE, like many spacecraft, contains a variety of small metallic components, such as clips for securing wire harnesses or support brackets for holding firmly some electronic parts, payloads and sensors [7, 63].

**Materials:** Those structures are mainly made of sheet metal or machined aluminum, balancing strength and weight [80].

### 9.4 Subsystem mass

To evaluate the subsystem mass, a preliminary calculation is performed. In the absence of specific data on panel thickness, a uniform thickness of 1 cm is assumed. While the density of each component is available from datasheet, the volume is estimated. The main structure is modelled as a hollow cylinder with an octagonal base, and a 60% margin is applied to account for holes in the panels. The propulsion module is represented as the bottom deck and two panels supporting the tanks, with a 65% margin introduced to consider tank cutouts. Finally, an additional 25% is added to the total mass to account for brackets, inserts, and fittings, resulting in an overall margin of 33% on the currently estimated mass, in line with literature recommendations [80].

	MCSB	PS module	Panels	Radiator	Solar array	Total	Total +33%
Density [ $kg/m^3$ ]	1760	1910	1760	2700	-	-	-
Volume [ $m^3$ ]	0,03089	0,02025	0,01579	0,0024	-	-	-
Mass [ $kg$ ]	54,37	38,67	27,79	6,53	6,4	133,77	178,36

Table 33: LADEE Structure Mass

### 9.5 Launcher interface and limitations

The Minotaur V Payload Adapter Module (PAM) can adapt from the 92 inch outer mold line down to a standard 38 inch adapter [82]. However, to accommodate the LADEE dimensions, a Payload Attach Fitting (PAF) was used, attached to the PAM through a shock and vibration isolation system. The PAF was then connected to the spacecraft via a separation system responsible for detaching the spacecraft at the programmed time. Regarding the spacecraft interface, it was achieved through a 31 inch ring adapter situated around the propulsion system, allowing the OCS to be housed inside the PAF, conserving internal volume inside the launcher [83].

Although not stated explicitly in literature, positioning the structural interface near the spacecraft's central axis is a standard engineering approach that helps transfer launch loads axially through

the spacecraft's strongest structural line, minimizing bending moments and enhancing load-bearing efficiency. Combined with the shock-isolated PAF, this setup mitigated high-frequency vibrations [82] and enabled a low tip-off separation, supporting LADEE's required deployment orientation [83].

Although the payload fairing envelope and launcher environment did not impose strict configuration constraints, LADEE's overall dimensions had to conform to the available fairing volume. To ensure a compact and versatile geometry, LADEE was designed with an octagonal cross-section. This configuration not only optimized internal packaging efficiency, but also increased the available surface area for power generation via body-mounted solar panels. Furthermore, the inward inclination of the upper section of the S/C was likely implemented to ensure proper accommodation within the narrowing geometry of the bi-conic fairing.

The absence of deployable appendages was driven both by the limited fairing volume and an early design choice to prioritize simplicity and reliability; it also eliminated the need for complex mechanism, except for the launcher separation one.

Launcher-imposed dynamic requirements that in particular influenced the internal and external layout, particularly in the placing of high mass components, were allowable COM offset relative to the launch vehicle centerline and limits on the spacecraft's moments of inertia [82].

Additionally, load distribution was a key consideration for configuration. High-load regions near the launch vehicle adapter were reserved for robust structural members, while sensitive subsystems and payloads were strategically placed in zones with lower expected loads. This ensured the preservation of both mechanical integrity and mission-critical functionality throughout the launch phase.

## 10 LADEE Configuration

The objective of this section is to analyse the positioning of the instrumentation and components on board of LADEE, especially referring to their physical, mechanical or operational interactions.

### 10.1 External Components Configuration

**Payload:** The NMS was laterally positioned on the payload module to enable atmospheric gas sampling aligned with the spacecraft's velocity vector (RAM mode) and, by rotating 180°, to perform background measurements in the anti-RAM orientation. The LDEX, mounted on the radiator module, required similar alignment direction to measure high-velocity dust grain impacts. This relative configuration NMS-LDEX ensured both instruments operated concurrently, sharing the same general pointing requirement without mutual interference, thus optimizing

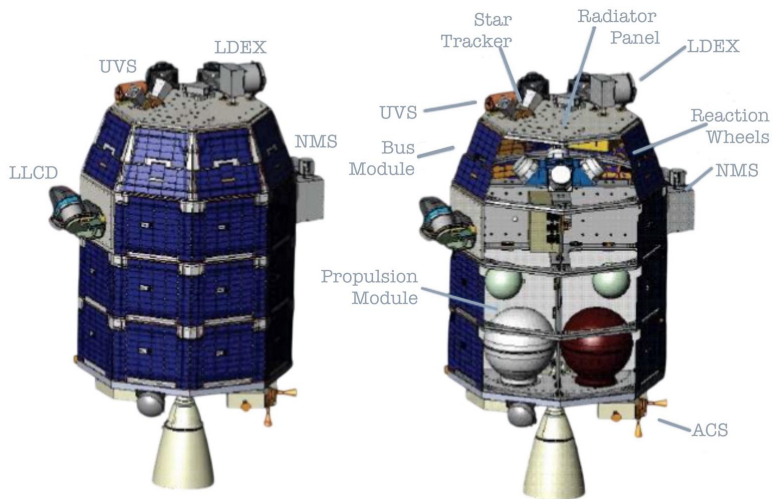


Figure 15: LADEE Config [84]

data collection in RAM mode. The LLCD was co-aligned with the medium-gain antenna allowing the usage of the two in the same attitude configuration, while the UVS, also on the radiator deck, leveraged thermal stability and an unobstructed view for limb and nadir observations (specific configurations for this instrument). The relative positioning of the UVS and LDEX, as well as with other radiator-panel components, minimized mutual interference in their fields of view. Finally, the two larger instruments, NMS and LLCD, were further arranged on opposite sides of the payload module to balance the centre of mass [7].

**Antennas:** The MGA was mounted on the upper portion of the radiator module, ensuring an unobstructed FOV towards Earth during TCM. The two LGAs were mounted on opposite sides of the spacecraft structure, one oriented upward and the other downward along the spacecraft's longitudinal axis. This configuration provided near-omnidirectional coverage, ensuring reliable reception of uplink commands regardless of the spacecraft's attitude [7], differently from the high pointing accuracy required by the MGA.

**Sensors:** Twelve CSSs were evenly distributed to ensure Sun direction knowledge in any spacecraft orientation. The two star trackers were mounted on the upper portion of the spacecraft, each oriented in slightly different directions with an offset of approximately 30–45° from the radiator panel. This configuration maximized the field of view and minimized potential occlusions, while the hot redundancy setup ensured continuous fine-pointing capability throughout the mission.

**Actuators:** Four RCS thrusters were mounted on the spacecraft bottom deck at 45° to the Z-axis to achieve full three-axis control. Their placement was chosen to maintain a safe distance from the radiator and payload modules, where critical components could be affected by plume impingement and thermal loads. Following the same rationale, the main engine OCS was centrally positioned on the bottom deck, with its nozzle extending below the primary structure to provide an unobstructed plume path for efficient thrust generation during orbital manoeuvres. This central alignment also helped to minimize unwanted torques during firing, contributing to stable and predictable spacecraft control.

**Solar Panels:** 30 solar panels were distributed around the central spacecraft body, a configuration that aimed to maximize exposure to sunlight regardless of the spacecraft's attitude or orbital position around the Moon. Minor shadowing from instruments like the LLCD and NMS was not critical due to their relatively small size compared to the overall area of the solar panels and the spacecraft body.

## 10.2 Internal Components Configuration

**PS:** It is reasonable to assume that the configuration design for the PS started by positioning the OCS nozzle centred in the Bottom Deck. After that, other PS components have been placed in the adjacent Propulsion module to minimize the cabling needed and the pressure losses. The six tanks, two each for fuel, oxidizer, and pressurant, were positioned symmetrically with respect to the body Z-axis in order to minimize COM excursion in the XY plane and to maintain nearly constant inertia axes.

**RWs:** LADEE's RWs were positioned in the centre of the Payload Module following a pyramidal configuration with the +Z body axis as its vertex. This orientation maximized torque about the Z-axis, which serves as the spacecraft's primary spin axis in most modes. Although mounting the RWs directly on the Radiator Panel would ease their thermal management, the resulting vibrations could compromise the measurements of the instruments or excite the panels' natural frequencies. A strong and separate structural component, a cruciform, has been preferred, as shown in Figure 15.

**Radiator Assembly:** The internal surface of the Radiator Panel houses the IAU, the battery and other components. This configuration offers partial shielding from external radiation while allowing passive thermal dissipation. Although both the battery and the IAU are mounted beneath the Radiator Panel, they are spaced apart, as both are significant heat sources.

Ultimately, modular design offers a significant advantage by enabling greater flexibility in both designing and sourcing components, as well as in their integration. In fact, it reduces the dependence on the spatial and functional constraints imposed by other subsystems. The PS serves as a clear example of this approach: the entire Extension Module is dedicated to it, with minimal interference from or to other subsystems.

## 11 Mass Budget

### 11.1 Values found in literature

Item	Mass [kg]	Margin	Mass with Margin [kg]
P/L	49.70	—	—
PS	25.14	—	—
TTMTC	4.56	—	—
AOCS	12.28	—	—
TCS	6.53	—	—
EPS	13.20	—	—
OBDH	11.01	—	—
STRUCT	118.37	—	—
<b>Total Dry Mass (w/o adapter)</b>	<b>240.70</b>	—	—
Propellant Mass	134.8	—	—
<b>Total Wet Mass (w/o adapter)</b>	<b>375.50</b>	—	—
Adapter mass	18.78	—	—
<b>Total launch mass (w/ adapter)</b>	<b>394.28</b>	—	—
<b>Maximum launchable mass</b>	<b>342.00</b>	—	—

Table 34: Mass budget for LADEE mission based on literature sources.

## 11.2 Values computed from reverse engineering

Item	Mass [kg]	Margin	Mass with Margin [kg]
P/L	49.70	0%	49.70
PS	12.19	20.75 %	14.71
TTMTC	12.07	6.49 %	12.85
AOCS	14.00	17.07 %	16.39
TCS	6.86	9.76 %	7.53
EPS	10.04	35.23 %	13.58
OBDH	10.00	20.00 %	12.00
STRUCT	120.84	33.00 %	160.71
<b>Total Dry Mass (w/o adapter)</b>	235.70	—	237.78
System margin (w/o adapter)	—	20%	
<b>Total Dry Mass with margin (w/o adapter)</b>	—	—	344.98
Propellant Mass	133.74	—	—
<b>Total wet mass (w/o adapter)</b>	369.44	—	478.72
Adapter mass	18.47	—	23.94
<b>Total launch mass (w/ adapter)</b>	387.91	—	502.66
<b>Maximum launchable mass</b>	—	—	342.00

Table 35: Mass budget for LADEE mission based on reverse engineering estimations

### 11.3 Comments

The team reconstructed the LADEE mass budget by analysing each subsystem individually, taking into account both literature values and reverse-engineered estimates, along with the corresponding margins, for each of their components. The following outlines the rationale behind the team's approach:

**Margins adopted:** The margin values reported in Table 35 represent the total mass margin applied to each subsystem, resulting from the aggregation of margins applied to its individual components.

**Payload:** For the payloads, the values reported in the literature were used in both tables. This approach is justified by the fact that payload mass is typically specified by the client and is therefore considered deterministic; as such, no margin was applied.

**PS:** The team retrieved from literature the masses of the OCS and RCS, reported in both tables. The tank masses were retrieved from literature [13] and from reverse sizing which, as already stated, hugely underestimates them. A 5 % margin has been applied over all components as they are all COTS and a further 15 % is applied over the total mass to account for harness.

**TMTC:** In order to reverse-engineer the subsystem, the team extrapolated mass budgets of similar subsystems from non directly related literature sources [24]. Most literature values are known [19, 27] except for the amplifier, whose mass was assumed to match the reverse-engineered estimate. The mass of the transponder is considerably lower in the literature-based assessment [27] compared to the value obtained from system-level estimates in [24]. The diplexer/filter mass contribution is explicitly included in the reverse engineering analysis but is already integrated within the transponder mass in the actual LADEE configuration, creating further discrepancy.

**AOCS:** The AOCS comprises the masses of the CSSs, the STA, the IMU and the RWs. Literature data are available from the datasheets [48, 35, 37, 33]. The reverse engineering of the AOCS is realized assuming reasonable mass values for each sensor and actuator from typical ranges found in literature [24] which result to be very close estimates.

**TCS:** Only the radiator panel and heaters have been considered, with the masses of other components deemed negligible and/or complex to accurately estimate. The radiator panel mass, estimated during the reverse engineering analysis, has also been adopted for the literature-based assessment. This approach ensures consistency and traceability in the mass estimation process when data on high-mass components are not directly available.

**EPS:** The EPS mass budget includes the secondary lithium battery and the body-mounted solar array. The mass of the solar array is not available in the literature, so the same value as the reverse engineering sizing was assumed. A conservative margin of 25% is used to account for the harness mass.

**OBDH:** OBDH literature mass budget has been retrieved from upper estimates of the masses of the multiple boards and components [69, 77, 37]. For the reverse engineering, the team extrapolated the whole subsystem mass from literature values of similar OBDH architecture [24], resulting in around 10 kg and applied a 20% margin for harness.

**STRUCT:** The structural mass comprises the MCSB, the propulsion module, and the composite panel set. In accordance with literature guidelines [80], a 33% margin is applied to account for structural inserts and fittings. The resulting estimated mass shows good agreement with values reported in the literature. These reference values were obtained by subtracting the masses of all individual subsystem components and payloads from the value of the dry mass found in literature [7].

**Maximum launchable mass:** It can be observed that the maximum launchable mass for a trans-lunar injection [82] is lower than the total mass of LADEE. This discrepancy is the primary reason why the spacecraft was initially deployed into a Low Earth Orbit, with the subsequent lunar injection manoeuvre carried out using the onboard propulsion system. Since the adapter mass was not specified in the Minotaur V user's guide, it is conservatively estimated as 5% of the total wet mass.

## References

- [1] Mihaly Horanyi et al. “The lunar dust experiment (LDEX) onboard the lunar atmosphere and dust environment explorer (LADEE) mission”. In: *The Lunar Atmosphere and Dust Environment Explorer Mission (LADEE)* (2015).
- [2] eoPortal. *LADEE (Lunar Atmosphere and Dust Environment Explorer)*. Accessed: 2025-03-04. 2012. URL: <https://www.eoportal.org/satellite-missions/ladee#ladee-lunar-atmosphere-and-dust-environment-explorer>.
- [3] Matthew V. D’Ortenzio et al. “Operating LADEE: Mission architecture, challenges, anomalies, and successes”. In: *2015 IEEE Aerospace Conference*. 2015, pp. 1–23. DOI: [10.1109/AERO.2015.7118961](https://doi.org/10.1109/AERO.2015.7118961).
- [4] Richard C. Elphic and Christopher T. Russell, eds. *The Lunar Atmosphere and Dust Environment Explorer Mission (LADEE)*. Springer International Publishing, 2015. ISBN: 9783319187174. DOI: [10.1007/978-3-319-18717-4](https://doi.org/10.1007/978-3-319-18717-4). URL: <http://dx.doi.org/10.1007/978-3-319-18717-4>.
- [5] Arlen Kam et al. *LADEE FLIGHT DYNAMICS: OVERVIEW OF MISSION DESIGN AND OPERATIONS*. Jan. 2015.
- [6] Butler et al. “The Lunar Atmosphere and Dust Environment Explorer Mission (LADEE) Mission”. In: *National Aeronautics and Space Administration* (2010). URL: <https://ntrs.nasa.gov/api/citations/20100021423/downloads/20100021423.pdf>.
- [7] Richard C. Elphic and Christopher T. Russell, eds. *The Lunar Atmosphere and Dust Environment Explorer Mission (LADEE)*. Springer International Publishing, 2015. ISBN: 9783319187174. DOI: [10.1007/978-3-319-18717-4](https://doi.org/10.1007/978-3-319-18717-4). URL: <http://dx.doi.org/10.1007/978-3-319-18717-4>.
- [8] NASA’s Technology Transfer Program. *General Mission Analysis Tool (GMAT) v.R2016a*. <https://software.nasa.gov/software/GSC-17177-1>. 2016.
- [9] Arlen Kam Alisa Hawkins and John Carrico. “LADEE Maneuver Planning and Performance”. In: *Proceedings of the AAS/AIAA Astrodynamics Specialist Conference* (2015).
- [10] NASA. *LADEE PDS Spacecraft Description*. Tech. rep. National Aeronautics and Space Administration (NASA), Mar. 2013. URL: [https://web.archive.org/web/20150504231834/https://prod.nais.nasa.gov/eps/eps\\_data/137365-SOL-001-003.doc](https://web.archive.org/web/20150504231834/https://prod.nais.nasa.gov/eps/eps_data/137365-SOL-001-003.doc).
- [11] M Muhalim and Subramaniam Krishnan. “Design of Nitrogen-Tetroxide/Monomethyl Hydrazine thruster for upper stage application”. In: *Monomethyl Hydrazine thruster for upper stage application* (2010).
- [12] NASA. *LADEE Press Kit*. Tech. rep. National Aeronautics and Space Administration (NASA), Aug. 2013. URL: <https://www.nasa.gov/content/ladee-press-kit>.
- [13] Andrew S. Gundersen et al. *Lunar Mission Tanks Using Surface Tension Propellant Management Devices for Propellant Acquisition and Supply (CoM = Center of Mass; GEO = Geosynchronous Orbit; LADEE = Lunar Atmosphere Dust Environment Explorer)*. [https://www.researchgate.net/publication/350871752\\_Lunar\\_Mission\\_Tanks\\_Using\\_Surface\\_Tension\\_Propellant\\_Management\\_Devices\\_for\\_Propellant\\_Acquisition\\_and\\_Supply\\_CoM\\_Center\\_of\\_Mass\\_GEO\\_Geosynchronous\\_Orbit\\_LADEE\\_Lunar\\_Atmosphere\\_Dust\\_Environment\\_Explor](https://www.researchgate.net/publication/350871752_Lunar_Mission_Tanks_Using_Surface_Tension_Propellant_Management_Devices_for_Propellant_Acquisition_and_Supply_CoM_Center_of_Mass_GEO_Geosynchronous_Orbit_LADEE_Lunar_Atmosphere_Dust_Environment_Explor). Accessed: 2025-07-05. 2021.
- [14] Aerojet Rocketdyne. *In-Space Data Sheets 4.8.20*. <https://www.satcatalog.com/component/r-4d-15-hipat-445n-high-performance-300-to-1/>.
- [15] George P. Sutton and Oscar Biblarz. *Rocket Propulsion Elements*. 9th. John Wiley & Sons, 2016. ISBN: 978-1-118-75265-2.

- [16] Wikipedia contributors. *Monomethylhydrazine — Wikipedia, The Free Encyclopedia*. Accessed: 2025-07-05. 2024. URL: <https://en.wikipedia.org/wiki/Monomethylhydrazine> (visited on 07/05/2025).
- [17] Wikipedia contributors. *Dinitrogen tetroxide — Wikipedia, The Free Encyclopedia*. Accessed: 2025-07-05. 2024. URL: [https://en.wikipedia.org/wiki/Dinitrogen\\_tetroxide](https://en.wikipedia.org/wiki/Dinitrogen_tetroxide) (visited on 07/05/2025).
- [18] The Lee Company. *Piloting Dual-Coil Solenoid Valve*. <https://www.theleeco.com/product/piloting-dual-coil-solenoid-valve/>.
- [19] Vanessa Kuroda et al. “Comm for Small Sats: The Lunar Atmosphere and Dust Environment Explorer (LADEE) Communications Subsystem”. In: *28th Annual AIAA/USU Conference on Small Satellites*. SSC14-XII-4. AIAA/USU. Logan, Utah, 2014.
- [20] Lisa Policastri, J Carrico, and Craig Nickel. “Pre-launch orbit determination design and analysis for the LADEE mission”. In: *Proceedings of the 25th AAS/AIAA Space Flight Mechanics Meeting, Williamsburg, VA*. 2015, pp. 11–15.
- [21] Mark Medeiros et al. *Communications System Architecture Supporting the LADEE Mission*. Tech. rep. NASA/TP-2016-07047. Accessed April 2025. NASA Goddard Space Flight Center, 2016. URL: <https://ntrs.nasa.gov/api/citations/20160007047/downloads/20160007047.pdf>.
- [22] Bryan Butler et al. *The Lunar Atmosphere and Dust Environment Explorer Mission*. Tech. rep. NASA/2015-20455. NASA, 2015. URL: <https://ntrs.nasa.gov/api/citations/20150020455/downloads/20150020455.pdf>.
- [23] Butler Hine et al. *The Lunar Atmosphere and Dust Environment Explorer (LADEE) Mission*. Tech. rep. NASA Technical Reports Server, 2010. URL: <https://ntrs.nasa.gov/api/citations/20100021423/downloads/20100021423.pdf>.
- [24] James R. Wertz Wiley J. Larson. *Space Mission Analysis and Design*. 3rd. Wiley J. Larson, James R. Wertz, 1992. ISBN: 978-1881883104.
- [25] NASA. *Exploring the Moon: A Teacher’s Guide with Activities*. <https://science.nasa.gov/wp-content/uploads/2024/01/exploring-the-moon-teachers-guide.pdf>. NASA EG-1997-10-116-HQ. Washington, D.C., 1997.
- [26] Jason D. Lohn et al. “Automated Synthesis of a Lunar Satellite Antenna System”. In: *IEEE Transactions on Antennas and Propagation* 63.4 (Apr. 2015), pp. 1436–1444. DOI: 10.1109/TAP.2015.2404332.
- [27] Space Micro.  *$\mu$ SGLS-100 S-Band Transponder Datasheet*. <https://www.spacemicro.com>. Rev6. 15378 Avenue of Science, Suite 200, San Diego, CA 92128, Mar. 2017.
- [28] Deepa Kumari and Madan Saini. “Design and Performance Analysis of Convolutional Encoder and Viterbi Decoder for Various Generator Polynomials”. In: (May 2016), pp. 67–71.
- [29] Winner Olabiyi. “Performance Comparison of OFDM Systems with Different Modulation Schemes”. In: (Nov. 2024).
- [30] Jet Propulsion Laboratory, California Institute of Technology. *Deep Space Network Services Catalog*. Tech. rep. 820-100, Rev. H. Approved by Jeff Berner, Bradford Arnold, Timothy Pham, and Sami Asmar. Pasadena, California: Jet Propulsion Laboratory, California Institute of Technology, June 2022. URL: <https://epdm.jpl.nasa.gov>.

- [31] Steve Slobin. *Module 302E: Antenna Positioning*. <https://deepspace.jpl.nasa.gov/dsndocs/810-005/ground-station-properties/>. Version 302E. Deep Space Network Telecommunications Link Design Handbook (810-005), Jet Propulsion Laboratory, California Institute of Technology. May 2024.
- [32] Max B. Reid. “The Deep Space Network”. In: *Deep Space Telecommunications Systems Engineering*. Ed. by Neil J. Cornish. DESCANSO Design and Performance Summary Series. Jet Propulsion Laboratory, California Institute of Technology, 2000. Chap. 2, pp. 21–53. URL: [https://descanso.jpl.nasa.gov/monograph/series10/02\\_Reid\\_chapt2.pdf](https://descanso.jpl.nasa.gov/monograph/series10/02_Reid_chapt2.pdf).
- [33] Redwire Space. *Redwire Space Coarse Analog Sun Sensor (CASS)*. Online. Accessed: 2025-04-24. United States, Nov. 2021. URL: [https://satsearch.co/products/redwirespace-coarse-analog-sun-sensor?utm\\_source=chatgpt.com](https://satsearch.co/products/redwirespace-coarse-analog-sun-sensor?utm_source=chatgpt.com).
- [34] Jeff Foust. *LADEE Sends Its First Images of the Moon Back to Earth*. Accessed: 2025-04-22. 2013. URL: <https://spacenews.com/ladee-sends-its-first-images-of-the-moon-back-to-earth/>.
- [35] Leonardo S.p.a. *AUTONOMOUS STAR TRACKERS: The A-STR and AA-STR*. Tech. rep. Document code: MM07786 1-17. Via delle Officine Galileo, 1 - 50013 Campi Bisenzio (FI), Italy: Leonardo S.p.a., 2017. URL: <https://www.leonardocompany.com>.
- [36] Northrop Grumman. *Northrop Grumman Official Website*. <https://www.northropgrumman.com/> [Accessed: 2025-04-24]. 2025.
- [37] Northrop Grumman Corporation. *LN-200S and LN-200HPS Inertial Measurement Unit (IMU) Datasheet*. <https://cdn.northropgrumman.com/-/media/Project/Northrop-Grumman/ngc/what-we-do/space/ln-200s-1n-200hps-imu/LN-200S-LN-200HPS-inertial-measurement-unit-imu-datasheet.pdf>. Approved for Public Release; Distribution is Unlimited; #21-0865; Dated 06/09/21. 2021.
- [38] Jesse C. Fusco, Sean S. M. Swei, and Robert H. Nakamura. “Sun Safe Mode Controller Design for LADEE”. In: *AIAA Guidance, Navigation, and Control Conference*. NASA’s Ames Research Center, AIAA 2015. American Institute of Aeronautics and Astronautics. Moffett Field, CA, 2015. URL: <https://ntrs.nasa.gov/api/citations/20150020455/downloads/20150020455.pdf>.
- [39] Microsat Systems Canada Inc. (MSCI). *MSCI MicroWheel 1000: High Performance Attitude Control for Mini and Microsatellites*. Technical Datasheet. MSCK-MK-DD-002 Rev B. 2-6877 Goreway Drive, Mississauga, Ontario, Canada L4V 1L9, n.d. URL: <mailto:info@mscinc.ca>.
- [40] MSC Inc. *MSC Inc. – Automation, Robotics, and System Integration*. Accessed: 2025-04-25. 2025. URL: <https://www.mscinc.ca/>.
- [41] John L. Bresina. “Activity Planning for a Lunar Orbital Mission”. In: *Proceedings of the Twenty-Seventh Conference on Innovative Applications of Artificial Intelligence*. NASA Ames Research Center. Association for the Advancement of Artificial Intelligence. Palo Alto, CA: AAAI Press, 2021, pp. 3887–3895.
- [42] Ken Galal, Craig Nickel, and Ryan Sherman. “Attitude Design for the LADEE Mission”. In: *Special Session on Flight Dynamics Aspects of the LADEE Mission*. 20150018791. NASA Ames Research Center and Goddard Space Flight Center. 2015.
- [43] Philip A. Ferguson. “On-Orbit Spacecraft Inertia and Rate Sensor Scale Factor Estimation for Microsatellites”. In: *22nd Annual AIAA/USU Conference on Small Satellites*. Discusses estimation techniques using rate sensors and justifies the inclusion of both high-accuracy IMUs and MEMS gyros to balance precision and cost in microsatellites like MOST. Microsat Systems Canada Incorporated. Logan, Utah, 2008.

- [44] Howard Cannon. *Flight Software for the LADEE Mission*. Aerospace Control and Guidance Systems Committee Meeting #116. Oct. 2015. URL: <https://ntrs.nasa.gov/api/citations/20160000569/downloads/20160000569.pdf>.
- [45] Brandon D. Owens and Alan R. Crocker. “SimSup’s Loop: A Control Theory Approach to Spacecraft Operator Training”. In: *Proceedings of the IEEE Aerospace Conference*. U.S. Government work not protected by U.S. copyright. IEEE. Big Sky, MT, USA, 2020.
- [46] V. N. Zharkov and A. P. Trubitsyn. “Lunar Mascons”. In: *The Soviet-American Conference on Cosmochemistry of the Moon and Planets, Part 1*. NASA Technical Report 19780005007. Washington, DC: NASA, 1977. URL: <https://ntrs.nasa.gov/api/citations/19780005007/downloads/19780005007.pdf>.
- [47] Thomas J. Kelly. *Apollo Experience Report - Development of the Lunar Module Landing Gear*. Tech. rep. NASA-TN-D-7080. NASA, 1969. URL: <https://ntrs.nasa.gov/citations/19690020961>.
- [48] Microsat Systems Canada Inc. *MicroWheel 1000*. Accessed: Apr. 27, 2025. 2025. URL: <https://www.reactionwheel.ca/products/MicroWheel-1000.pdf>.
- [49] Butler Hine, Stevan Spremo, and Mark Turner. *The Lunar Atmosphere and Dust Environment Explorer (LADEE) Mission*. Tech. rep. NASA/TP-2010-21423. NASA Ames Research Center, 2010. URL: <https://ntrs.nasa.gov/api/citations/20100021423/downloads/20100021423.pdf>.
- [50] Consultative Committee for Space Data Systems (CCSDS). *CCSDS Publications Directory*. <https://public.ccsds.org/Pubs/Forms/AllItems.aspx>. Accessed: April 28, 2025. 2024.
- [51] The Providence Journal. “Dunmore aerospace materials protect LADEE robotic lunar explorer”. In: *The Providence Journal* (2013). Accessed: 2025-05-07. URL: <https://eu.providencejournal.com/story/news/2013/09/09/20130909-dunmore-aerospace-materials-protect-ladee-robotic-lunar-explorer-ece/35395528007/>.
- [52] SpaceNews Staff. *EMCORE Awarded Solar Panel Manufacturing Contract for NASA’s Lunar Atmosphere and Dust Environment Explorer (LADEE) Mission*. Accessed: 2025-05-09. Oct. 2011. URL: <https://spacenews.com/emcore-awarded-solar-panel-manufacturing-contract-for-nasas-lunar-atmosphere-and-dust-environment-explorer-ladee-mission/>.
- [53] EMCORE Corporation. *BTJ Photovoltaic Cell: Advanced Triple-Junction Solar Cell for Space Applications*. <http://www.emcore.com>. Datasheet. EMCORE Corporation, Sept. 2012. URL: <http://www.emcore.com>.
- [54] Richard H. Hoffman. *Spaceflight Performance of Silver Coated FEP Teflon as a Thermal Control Surface on the IMP-I Spacecraft*. Tech. rep. X-762-73-113. NASA Technical Report, Document ID: 19740012426. Greenbelt, Maryland: NASA Goddard Space Flight Center, Apr. 1973.
- [55] Gregory T. Delory. *LADEE PDS Spacecraft Description*. Tech. rep. DES-11.LADEE.PDSSD Rev. 1.2. NASA Ames Research Center, Mar. 2013. URL: [https://sbnarchive.psi.edu/pds4/lindex/laddee\\_lindex\\_20161118/document/laddee\\_spacecraft\\_rev1\\_2.pdf](https://sbnarchive.psi.edu/pds4/lindex/laddee_lindex_20161118/document/laddee_spacecraft_rev1_2.pdf).
- [56] John H. Henninger. *Solar Absorptance and Thermal Emittance of Some Common Spacecraft Thermal-Control Coatings*. Tech. rep. NASA RP-1121. NASA Reference Publication 1121. Greenbelt, Maryland: NASA Goddard Space Flight Center, Dec. 1984. URL: <https://ntrs.nasa.gov/api/citations/19840015630/downloads/19840015630.pdf>.

- [57] Hume Peabody et al. “Early Operations Flight Correlation of the Lunar Laser Communications Demonstration (LLCD) on the Lunar Atmosphere and Dust Environment Explorer (LADEE)”. In: *Thermal and Fluids Analysis Workshop (TFAWS)*. NASA Thermal and Fluids Analysis Workshop 2015, GSFC. NASA Goddard Space Flight Center. 2015. URL: <https://ntrs.nasa.gov/api/citations/20150022058/downloads/20150022058.pdf>.
- [58] Sasha V. Weston et al. *2023 State-of-the-Art Small Spacecraft Technology*. NASA Technical Publication TP-20250000142. NASA Ames Research Center, 2024. URL: [https://ntrs.nasa.gov/api/citations/20250000142/downloads/2023%20SOA\\_final.pdf](https://ntrs.nasa.gov/api/citations/20250000142/downloads/2023%20SOA_final.pdf).
- [59] John H. Henninger. *Solar Absorptance and Thermal Emittance of Some Common Spacecraft Thermal-Control Coatings*. NASA Reference Publication NASA-RP-1121. Greenbelt, MD: NASA Goddard Space Flight Center, 1984. URL: <https://ntrs.nasa.gov/api/citations/19840015630/downloads/19840015630.pdf>.
- [60] Collier Aerospace. *Optimization Software Improves Small Satellite Design*. <https://collier aerospace.com/2013/06/04/optimization-software-improves-small-satellite-design/>. Accessed: 2025-05-11. 2013. URL: <https://collier aerospace.com/2013/06/04/optimization-software-improves-small-satellite-design/>.
- [61] NASA Ames Research Center, Small Spacecraft Systems Virtual Institute. *State-of-the-Art Small Spacecraft Technology*. Tech. rep. NASA/TP—2024-10001462. Accessed from: <http://www.nasa.gov/smallsat-institute/sst-soa>. Ames Research Center, Moffett Field, California: National Aeronautics and Space Administration (NASA), Feb. 2024.
- [62] Joshua B Forgione et al. “Low-cost, risk-reduction testing of class D spacecraft photovoltaic systems”. In: *2014 IEEE Aerospace Conference*. 2014, pp. 1–12. DOI: 10.1109/AERO.2014.6836459.
- [63] James A. Lukash and Earl Daley. “Design and Development of an Equipotential Voltage Reference (Grounding) System for a Low-Cost Rapid-Development Modular Spacecraft Architecture”. In: *Proceedings of the 2010 IEEE Aerospace Conference*. IEEE. Big Sky, MT: IEEE, 2010. URL: <https://ntrs.nasa.gov/citations/20110015461>.
- [64] Moog Inc. *Moog Inc. – Precision Motion Control Solutions*. Accessed: 2025-05-16. 2025. URL: <https://www.moog.com/>.
- [65] Compound Semiconductor. *Emcore GaAs panels to go into orbit in NASA’s LADEE mission*. Accessed: 2025-05-14. Nov. 2011. URL: [https://compoundsemiconductor.net/article/88698/Emcore\\_GaAs\\_panels\\_to\\_go\\_into\\_orbit\\_in\\_NASAs\\_LADEE\\_mission](https://compoundsemiconductor.net/article/88698/Emcore_GaAs_panels_to_go_into_orbit_in_NASAs_LADEE_mission).
- [66] EMCORE Corporation. *EMCORE Corporation*. Accessed: 2025-05-14. 2025. URL: <https://www.emcore.com/>.
- [67] ADS Group. *ABSL Power Solutions Ltd*. <https://www.adsgroup.org.uk/members/absl-power-solutions-ltd-2/>. Accessed: 2025-05-18. 2025.
- [68] EnerSys. *Li-ion Rechargeable Battery ABSL 8s16p 28V 24Ah*. <https://en.sekorm.com/doc/3664100.html>. Datasheet published on Sekorm. Mar. 2020.
- [69] Moog Inc. *SACI, PAPI, McLASI Boards Datasheet*. Tech. rep. Form 500-1113 1019. Accessed: 2025-05-16. Moog Inc., 2019. URL: <https://www.moog.com/content/dam/moog/literature/sdg/space/avionics/moog-saci-papi-mclasi-boards-datasheet.pdf>.
- [70] Gautam Biswas et al. “An Approach To Mode and Anomaly Detection With Spacecraft Telemetry Data”. In: *International Journal of Prognostics and Health Management* 7.4 (2016). Open-access article under Creative Commons Attribution 3.0 License, p. 033. DOI: 10.36001/ijphm.2016.v7i4.2467. URL: <https://www.researchgate.net/publication/311513578>.

- [71] Nathaniel Benz, Danilo Viazza, and Karen Gundy-Burlet. “Multi-Purpose Spacecraft Simulator for LADEE”. In: *2015 IEEE Aerospace Conference*. U.S. Government work not protected by U.S. copyright. IEEE. 2015. DOI: 10.1109/AERO.2015.7118996. URL: <https://ieeexplore.ieee.org/document/7118996>.
- [72] Tark Solutions. *Thermoelectric Handbook*. Accessed May 18, 2025. 2022. URL: [https://tark-solutions.com/sites/default/files/fields/media.file.field\\_media\\_file/2022-12/Thermoelectric-Handbook-060222.pdf](https://tark-solutions.com/sites/default/files/fields/media.file.field_media_file/2022-12/Thermoelectric-Handbook-060222.pdf).
- [73] Rachel Buckle and Sam Roberts. “Review of Commercial Cells for Space Applications”. In: *Proceedings of the European Space Power Conference (ESPC 2016)*. Vol. 17006. EDP Sciences. EDP Sciences, 2017. DOI: 10.1051/e3sconf/20171617006. URL: <https://doi.org/10.1051/e3sconf/20171617006>.
- [74] Ignacio F. Acero et al. “A Method for Validating CubeSat Satellite EPS Through Power Budget Analysis Aligned With Mission Requirements”. In: *IEEE Access* 11 (2023). Open Access, pp. 43316–43330. DOI: 10.1109/ACCESS.2023.3271596. URL: <https://doi.org/10.1109/ACCESS.2023.3271596>.
- [75] Elisabeth Eitel. “How Thrusters and Controls on NASA’s LADEE Work”. In: *Machine Design* (Mar. 2014). URL: <https://www.machinedesign.com/markets/defense/article/21833626/how-thrusters-and-controls-on-nasas-ladee-work>.
- [76] Gautam Biswas et al. “An Approach To Mode and Anomaly Detection with Spacecraft Telemetry Data”. In: *International Journal of Prognostics and Health Management* 7.1 (2016). Open access under Creative Commons Attribution 3.0 License, p. 033. ISSN: 2153-2648. URL: [https://www.nasa.gov/mission\\_pages/ladee/main/index.html](https://www.nasa.gov/mission_pages/ladee/main/index.html).
- [77] Moog Inc. *MOAB Series of Boards Datasheet*. <https://www.moog.com/content/dam/moog/literature/sdg/space/avionics/moog-moab-series-of-boards-datasheet.pdf>. Accessed: May 27, 2025. 2023.
- [78] Don M. Boroson et al. “The Lunar Laser Communications Demonstration (LLCD)”. In: *2009 Third IEEE International Conference on Space Mission Challenges for Information Technology (SMC-IT)*. IEEE, Aug. 2009, pp. 23–28.
- [79] Sharun Hegde, B. Satish Shenoy, and K.N. Chethan. “Review on carbon fiber reinforced polymer (CFRP) and their mechanical performance”. In: *Materials Today: Proceedings* 19 (2019), pp. 658–662. DOI: 10.1016/j.matpr.2019.07.749.
- [80] Elisabeth Eitel. “Software lets spacecraft carry heavier loads”. In: *Machine Design* (2013). Accessed: 2025-06-01. URL: <https://www.machinedesign.com/3d-printing-cad/article/21833288/software-lets-spacecraft-carry-heavier-loads>.
- [81] U.S. General Services Administration. *Aluminum: Characteristics, Uses and Problems*. Accessed: 2025-06-01. 2023. URL: <https://www.gsa.gov/real-estate/historic-preservation/historic-preservation-policy-tools/preservation-tools-resources/technical-procedures/aluminum-characteristics-uses-and-problems>.
- [82] Northrop Grumman. *Minotaur IV, V, VI User’s Guide*. Tech. rep. TM-17589E. Approved for public release; distribution unlimited. Dulles, VA: Northrop Grumman, 2020. URL: <https://docslib.org/doc/1194471/minotaur-user-guide-3-pdf>.
- [83] William Graham. “Orbital’s Minotaur V launches LADEE mission to the Moon”. In: *NASASpaceFlight.com* (Sept. 2013). Accessed: 2025-06-01. URL: <https://www.nasaspacelight.com/2013/09/orbital-s-minotaur-v-launch-ladee-mission-moon/>.

- [84] Brian M. Cudnik and Brian H. Day. “Ground Based Observations of Lunar Meteoroid Phenomena in Support of the LADEE Mission”. In: *Unpublished article on ResearchGate* (Mar. 2013). Accessed via ResearchGate. URL: [https://www.researchgate.net/publication/258803197\\_Ground\\_Based\\_Observations\\_of\\_Lunar\\_Meteoroid\\_Phenomena\\_in\\_Support\\_of\\_the\\_LADEE\\_Mission](https://www.researchgate.net/publication/258803197_Ground_Based_Observations_of_Lunar_Meteoroid_Phenomena_in_Support_of_the_LADEE_Mission).